Iterative Receiver for MIMO-OFDM System with ICI Cancellation and Channel Estimation

Rui Li

A thesis submitted in fulfilment of
requirements for the degree of Master of Philosophy (Research)

School of Electrical & Information Engineering
The University of Sydney

March 2008

To my parents

Abstract

As a multi-carrier modulation scheme, Orthogonal Frequency Division Multiplexing (OFDM) technique can achieve high data rate in frequency-selective fading channels by splitting a broadband signal into a number of narrowband signals over a number of subcarriers, where each subcarrier is more robust to multipath. The wireless communication system with multiple antennas at both the transmitter and receiver, known as multiple-input multiple-output (MIMO) system, achieves high capacity by transmitting independent information over different antennas simultaneously. The combination of OFDM with multiple antennas has been considered as one of most promising techniques for future wireless communication systems.

The challenge in the detection of a space-time signal is to design a low-complexity detector, which can efficiently remove interference resulted from channel variations and approach the interference-free bound. The application of iterative parallel interference canceller (PIC) with joint detection and decoding has been a promising approach. However, the decision statistics of a linear PIC is biased toward the decision boundary after the first cancellation stage. In this thesis, we employ an iterative receiver with a decoder metric, which considerably reduces the bias effect in the second iteration, which is critical for the performance of the iterative algorithm.

Channel state information is required in a MIMO-OFDM system signal detection at the receiver. Its accuracy directly affects the overall performance of MIMO-OFDM systems. In order to estimate the channel in high-delay-spread environments, pilot symbols should be inserted among subcarriers before transmission. To estimate the channel over all the subcarriers, various types of interpolators can be used. In this thesis, a linear interpolator and a trigonometric interpolator are compared. Then we propose a new interpolator called the multi-tap method, which has a much better system performance.

In MIMO-OFDM systems, the time-varying fading channels can destroy the orthogonality of subcarriers. This causes serious intercarrier interference (ICI), thus leading to significant system performance degradation, which becomes more severe as the normalized Doppler frequency increases. In this thesis, we propose a low-complexity iterative receiver with joint frequency-domain ICI cancellation and pilot-assisted channel estimation to minimize the effect of time-varying fading channels. At the first stage of receiver, the interference between adjacent subcarriers is subtracted from received OFDM symbols. The parallel interference cancellation detection with decision statistics combining (DSC) is then performed to suppress the interference from other antennas. By restricting the interference to a limited number of neighboring subcarriers, the computational complexity of the proposed receiver can be significantly reduced.

In order to construct the time variant channel matrix in the frequency domain, channel estimation is required. However, an accurate estimation requiring complete knowledge of channel time variations for each block, cannot be obtained. For time-varying frequency-selective fading channels, the placement of pilot tones also has a significant impact on the quality of the channel estimates. Under the assumption that channel variations can be approximated by a linear model, we can derive channel state information (CSI) in the frequency domain and estimate time-domain channel parameters. In this thesis, an iterative low-complexity channel estimation method is proposed to improve the system performance. Pilot symbols are inserted in the transmitted OFDM symbols to mitigate the effect of ICI and the channel estimates are used to update the results of both the frequency domain equalizer and the PIC-DSC detector in each iteration. The complexity of this algorithm can be reduced because the matrices are precalculated and stored in the receiver when the placement of pilots symbols is fixed in OFDM symbols before transmission.

Finally, simulation results show that the proposed MIMO-OFDM iterative receiver can effectively mitigate the effect of ICI and approach the ICI-free performance over time-varying frequency-selective fading channels.

Acknowledgements

This thesis is by far the most significant accomplishment in my life, and it would have been impossible without people who supported me and believed in me.

Most of all, I would like to express my sincere gratitude to my supervisor, Professor Branka Vucetic, for her offering me such an invaluable chance to study at the University of Sydney, for her being a constant source of research ideas, insightful discussions and inspiring words in times of needs and for her unique attitude of being strict with academic research which will shape my career forever. Although heavily loaded with administrative work and being busy, she manages to make herself available for the meeting with me every week. She is always friendly and approachable even for unscheduled consultations. My experiences in the Telecommunications Laboratory under Professor Vucetic are the most valuable times in my career and life.

I sincerely thank my co-supervisor, Dr Yonghui Li, for his intensive guidance and encouragement. Learning from him has been a very fruitful and enjoyable experience. The discussions on my research topic with him often led to new ideas, taking research to new directions with successful results.

I would like to sincerely thank Dr Zhendong Zhou for his valuable remarks and comments, which had made significant contributions to improving the quality of my papers. I would also like to thank my former and current colleagues in Telecommunications Laboratory, including Dr Yang Tang, Dr Zhuo Chen, Dr Lixiang Xiong, Wibowo Hardjawana and Kun Pang for their helpful discussions and encouragement.

I am very grateful to my fiancee, Ruina Liu, for her intense support, endless patience and great devotion. Without her unconditional support and sacrifice, I could never have made it

this far.

Last but by no means least, I would like to thank my parents for their continued support, encouragement and sacrifice throughout the years, and I will be forever indebted to them for all that they have done.

Statement of Originality

All material presented in this thesis is the original work of the author, unless otherwise stated. The content of this thesis has not been previously submitted for examination as part of any academic qualifications. Most of the results contained herein have been accepted for publication, or submitted for publication, in journal or conference of international standing. The author's contribution in terms of published material is listed in next section "Publications", and is referenced throughout using alphabetical-numerical citations. Numerical citations refer to the references listed in the bibliography.

The original motivation to pursue research in this field was provided by thesis supervisor Professor Branka Vucetic and co-supervisor Dr Yonghui Li at the School of Electrical and Information Engineering, the University of Sydney, Australia.

Rui Li
Telecommunication Laboratory
School of of Electrical and Information Engineering
The University of Sydney
New South Wales, Australia
March 2008

Publications

Conference Paper

[C1] Rui Li, Yonghui Li and Branka Vucetic, "Iterative Receiver for MIMO-OFDM Systems with Joint ICI Cancellation and Channel Estimation," *IEEE WCNC 2008*, Las Vegas, USA, 31 March-3 April, pp. 7-12.

Contents

List of Figures

List of Tables

List of Acronyms

1-D	One-Dimensional
4G	Fourth Generation
ADSL	Asymmetric Digital Subscriber Line
APP	A Posteriori Probability
AWGN	Additive White Gaussian Noise
BER	Bit Error Rate
BPSK	Binary Phase-Shift Keying
CSI	Channel State Information
DAB	Digital Audio Broadcasting
DFT	Discrete Fourier Transform
DSC	Decision Statistic Combiner
DS-CDMA	Direct Sequence Code Division Multiple Access
DVB-T	Terrestrial Digital Video Broadcasting
EIR	Extrinsic Information Ratio
FFT	Fast Fourier Transform
FSK	Frequency-Shift Keying
ICI	Intercarrier Interference
IDFT	Inverse Discrete Fourier Transform
IFFT	Inverse Fast Fourier Transform
ISI	Inter Symbol Interference
LLR	Log-Likelihood Ratio
LMS	Least-Mean Square
LS	Least Square
MAP	Maximum a Posteriori Probability
MBWA	Mobile Broadband Wireless Access
MIMO	Multiple-Input Multiple-Output

ML	Maximum Likelihood
MLD	Maximum Likelihood Decoding
MLSE	Maximum Likelihood Sequence Estimation
MMSE	Minimum Mean-Square Error
MPSK	Multiple Phase-Shift Keying
MSE	Mean-Square Error
OFDM	Orthogonal Frequency Division Multiplexing
PAPR	Peak-to-average Power Ratio
PIC	Parallel Interference Canceler
PIC-DSC	Parallel Interference Canceler with Decision Statistic Combiner
PIC-STD	Standard Parallel Interference Canceler
PSK	Phase-Shift Keying
QAM	Quadrature Amplitude Modulation
QoS	Quality of Service
RSC	Systematic Convolutional Codes
SC	Strongest Competitor
SER	Symbol Error Rate
SINR	Signal-to-Inter-carrier-Interference-plus-Noise Ratio
SISO	Soft-Input Soft-Output
SNR	Signal-to-Noise Ratio
SOVA	Soft Output Viterbi Algorithm
SQAM	Staggered Quadrature Amplitude Modulation
SUI	Stanford University Interim
VA	Viterbi Algorithm
WiMax	Worldwide Interoperability for Microwave Access
WLAN	Wireless Local Area Network
WMAN	Wireless Metropolitan Area Network
WPAN	Wireless Personal Area Network
WRAN	Wireless Regional Area Network
WSS	Wide Sense Stationary

List of Mathematical Terms

c	speed of light
D	threshold of frequency-domain equalizer
f_c	carrier frequency
f_d	Doppler frequency
Δf	spacing between subcarriers
$\mathbf{F}$	FFT matrix
G	guard interval
h	fading channel in time domain
$\mathbf{H}$	fading channel in frequency domain
$\mathbf{H}_a$	time-invariant circular matrix of fading channel
$\mathbf{H}_v$	time-variant circular channel matrix of fading channel
$\mathcal{H}_{diag}$	diagonal matrix
$\mathcal{H}_{ICI}$	ICI interference matrix
$\mathbf{I}$	identity matrix
$I_0(\cdot)$	modified zero-order Bessel function of the first kind
$J_0(\cdot)$	zero-order Bessel function of the first kind
K	Rician factor
L	number of discrete paths of multipath fading channel
m_a	mean value
M_R	number of receive antennas
M_R	number of transmit antennas
N	number of subcarriers
$\mathbf{P}$	orthogonal matrix used as pilot symbols
$\mathbf{r}$	received sequence
T	time duration of one OFDM symbol
T_s	sampling period

$\mathbf{u}$	information sequence
v	vehicle speed
$\mathbf{v}$	encoder output sequence
$\mathbf{W}$	AWGN in frequency domain
$\mathbf{x}$	transmitted sequence
$\mathbf{X}$	information symbol in frequency domain
$\mathbf{y}$	received OFDM symbol in time domain
$\mathbf{Y}$	received OFDM symbol in frequency domain
λ	log-likelihood ratio
Λ	a posteriori log-likelihood ratio
σ^2	variance
ω	AWGN in time domain
μ	path metric
ρ	correlation coefficient
θ	incident angle
τ	time delay
τ_d	root mean square delay spread of the channel
$\widehat{\Phi_{p,q}}$	estimate of the channel vector
^{T}	transposition
^{H}	conjugate transposition
†	Moore-Penrose pseudo inversion

Chapter 1

Introduction

1.1 Motivation

In recent years, the rapid growth of wireless communications has resulted in an increasing demand for high data rate communications in many applications, such as wireless local area networks (WLANs), and worldwide interoperability for microwave access (WiMax). The main challenge of all these applications is to support high data rate with limited bandwidth and restricted power consumption.

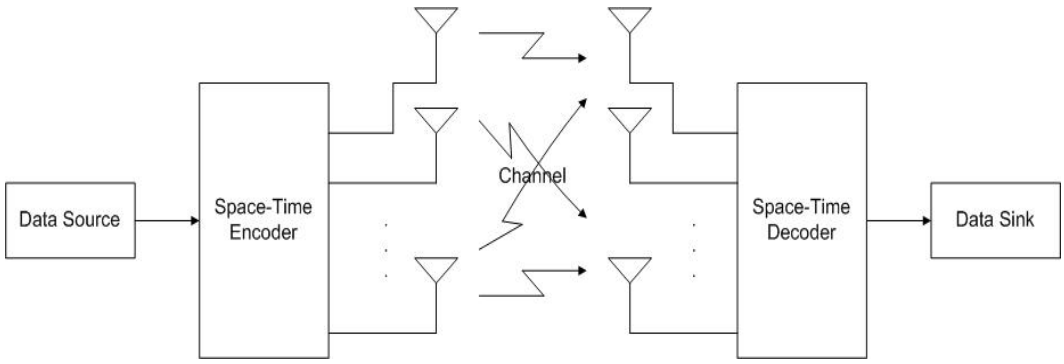

Figure 1.1: Block diagram of a MIMO system

The block diagram of a wireless communication system with multiple antennas at both the transmitter and receiver, known as a multiple-input multiple-output (MIMO) system,

is shown in Figure 1.1. It has been proven that the use of multiple antennas at both ends of a wireless system has the potential of drastically achieve a high capacity through spatial multiplexing technique [1] [2]. If the perfect channel-state information (CSI) is available at the receiver, the average capacity grows linearly with the smaller number of transmit and receive antennas.

However, the system with high data rates in mobile communications typically is affected by higher delay spread relative to the symbol duration. Moreover, a high Doppler spread resulted from time-varying channels or mobile environments makes the data transmission less reliable. In conventional single-carrier communication systems, multipath fading of wireless channels leads to inter-symbol interference (ISI), which requires complex equalizers as the data rate increases.

Multi-carrier modulation is one of the transmission schemes that is less sensitive to time dispersion of the channel. A basic multi-carrier transmitter diagram is shown in Figure 1.2. In multi-carrier systems, the transmission bandwidth is divided into several narrow sub-channels and data is transmitted parallel in these sub-channels. Data in each sub-channel is modulated at a relatively low rate so that the delay spread of the channel does not cause any degradation as each of the sub-channels will experience a flat response in the frequency domain. Although the principles have been known since the early 1960s [3] [4], multi-carrier modulation techniques, especially Orthogonal Frequency Division Multiplexing (OFDM), have gained more attention in the last ten years, due to the increased powerful techniques of digital signal processing. The basic idea of OFDM is to turn the wideband frequency-selective wireless channel into a set of frequency-flat narrowband channels. As a consequence, the complexity of the equalization technique reduces considerably. Hence, the design of the receiver is simplified significantly. Also, multi-carrier systems efficiently exploit the transmission spectrum because they allow a spectral overlap among the subcarriers.

OFDM, as a multi-carrier modulation technique, overcomes the main problem arising from high-data-rate communications, known as time dispersion. In OFDM systems, the subcarrier frequencies are chosen in such a way that there is no influence on other subcarriers in the detection of the information in a particular subcarrier, when the orthogonality of the subcarriers is maintained. The data-bearing symbol stream is split into several lower-rate streams and these streams are transmitted on different subcarriers. Since this increases the symbol period by the number of overlapping subcarriers, multipath echoes will affect only a small

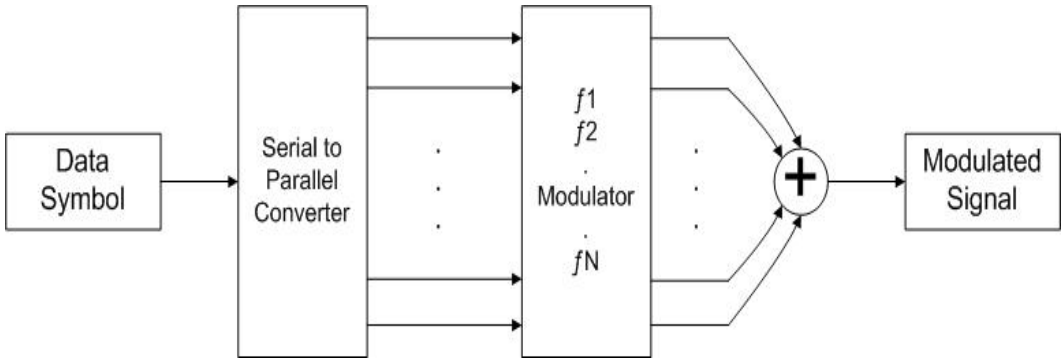

Figure 1.2: Block diagram of basic multi-carrier transmitter

portion of the neighboring symbols. Remaining ISI can be removed by cyclically extending the OFDM symbol. The length of the cyclic extension should be at least as long as the maximum delay spread of the channel. In this way, OFDM reduces the effect of multipath propagation encountered with high data rates, and avoids the need for complex equalizers.

Although OFDM has proved itself as an efficient modulation technique, it has its own challenges. Sensitivity to frequency offsets, caused when a receiver's oscillator does not run at exactly the same frequency as the transmitter's oscillator, is one of the major problems. This offset perturbs the orthogonality of the sub-carriers, degrading the system performance. Another problem is the large Peak-to-average Power Ratio (PAPR) of the OFDM signal, which requires power amplifiers with large linear ranges. Hence, power amplifiers require more back-off which, in turn, reduces the power efficiency. Some other problems include phase distortion, Doppler spread and intercarrier interference.

Most standards employing OFDM do not utilize the available resources effectively. Most of the time, systems are designed for the worst transmission scenarios. The length of the cyclic prefix, for example, is chosen in such a way that it is larger than the maximum expected delay spread of the channel, which introduces a considerable amount of overhead to the system. However, if the maximum excess delay of the channel is known, the length of the cyclic prefix can be changed adaptively according to the channel conditions, instead of setting it for the worst case. The information about the frequency selectivity of the channel can also be very useful for improving the performance of the wireless radio receivers through transmitter and receiver adaptation.

OFDM is used as the modulation method for Digital Audio Broadcasting (DAB) [5] and

Terrestrial Digital Video Broadcasting (DVB-T) [6] in Europe, and in Asymmetric Digital Subscriber Line (ADSL) [7]. Wireless Local Area Networks use OFDM as their physical layer transmission technique. Different WLAN standards have been developed in Europe, USA, and Japan, such as the European standard ETSI HiperLAN/2 [8], and the American standard IEEE 802.11a/g [9]; each has similar physical layer specifications based on OFDM. The combination of MIMO and OFDM improves the quality of service (QoS) and data rate of the system by exploiting the multiplexing gain and the diversity gain. Evolving wireless standards, such as the mobile Wi-Fi (IEEE 802.11n) and WiMax (IEEE 802.16e), employ multiple transmit and receive antennas with OFDM technique for increased spectral efficiency and improvement of performance.

1.2 Research Problems and Contributions

OFDM has many good properties that make it an attractive modulation scheme for high data rate transmission. However, it also has some inherent disadvantages. One of its disadvantages is that the OFDM system is very sensitive to Doppler spread. Since the subcarriers are closely spaced and the bandwidth of each subcarrier is very narrow, the orthogonality among the subcarriers can be easily destroyed by time variation of fading channels. This causes severe inter-carrier interference (ICI) with the increase of the normalized Doppler frequency and symbol duration. ISI and ICI are dual to each other occurring at different domains; one in the time domain and the other in the frequency-domain. ISI can be easily removed by cyclically extending the OFDM symbol as long as the length of the cyclic prefix is larger than the maximum delay spread of the channel. However, ICI caused by time-varying fading channels results in an error floor if it is not compensated for [10]. As a major problem in multi-carrier systems, ICI cancellation needs to be taken into account when designing OFDM systems.

In references [11] and [12], authors analyzed the effect of ICI and obtained exact expressions for the ICI of an OFDM signal caused by Doppler spread. With the initial assumption that the channel is known with a fixed number of paths for a sufficiently large number of subcarriers N, the ICI can be modeled as a Gaussian random process according to the central limit theorem.

The issue of ICI cancellation has been widely studied in digital communication systems. Receiver antenna diversity based techniques were proposed in [12] and [13] to mitigate the ICI and reduce the error floor. However, sensitivity analysis in [14] has shown that a huge performance degradation will occur for Doppler frequencies of the order of 10% of the subcarrier spacing, therefore limiting the benefits of multiple receiver antennas. As normalized Doppler spread increases, the diversity equalization techniques are less effective in mitigating ICI in OFDM mobile systems.

Jeon [15] has proposed a frequency-domain equalization technique to reduce the time-variation effect of a multipath fading channel by assuming that the channel impulse response varies in a linear fashion during a block period. However, they assumed that some of the coefficients of the channel matrix are negligible. For a channel with two non-zero power-delay profile samples, the simulation results show that performance improvement only under a normalized Doppler spread of up to 2.72% and delay spread of $2\mu s$. This indicates that the performance is improved only under low Doppler and delay spread environments. The delay spread can be much longer and the normalized Doppler frequency can be as high as 10% in high mobility scenarios. This method also relies on the information from adjacent OFDM symbols for channel estimation, which increases the complexity of the OFDM system.

Some other ICI cancellation schemes have been proposed. In [16], the same data symbols are modulated on adjacent subcarriers. In [17], a polynomial cancellation coding was proposed for OFDM systems. Instead of modulating the individual subcarrier, the data symbols are grouped and modulated with various weights at the transmitter and maximal ratio combining these copies at the receiver. Simulation results of both methods show that the ICI can be significantly mitigated. Although these two methods have a much better signal to ICI ratio than an ordinary OFDM system, they imply a substantial reduction of spectral efficiency and require some modifications to the conventional OFDM transmitter and receiver, making them inapplicable to real systems.

In this thesis, an ICI cancellation algorithm is proposed in the frequency domain to reduce the effect of time-varying fading, based on the general expression of ICI power for OFDM systems. It will be shown to be highly effective in combating ICI with a low complexity.

The OFDM receiver in the proposed algorithm consists of a two stage parallel interference canceler (PIC) with iterative detection and decoding. At the first stage, the matrix of inter-

carrier interference caused by time-varying channels is calculated, and then subtracted from received OFDM symbols. At the second stage, the interference from different antennas is suppressed by a parallel interference canceler and decision statistics combiner (DSC) technique. The decision statistics of each stage are updated by soft outputs generated from each decoder and used to improve the system performance in the following iterations. In order to reduce the complexity of the proposed iterative receiver, a simplified ICI cancellation method is proposed by setting a threshold when calculating the interference matrix, based on the fact that most interference energy is concentrated in the neighborhood of the desired component.

When the channel state information is known at the receiver, simulation results show that the proposed methods can effectively mitigate for the effect of intercarrier interference and can approach ICI-free performance even under the high Doppler frequencies of time-varying fading channels.

Furthermore, the system performance relies on the knowledge of CSI at the receiver. Perfect channel estimates can be obtained only if the channel is noiseless and time invariant. Although some methods have been proposed for the estimation and tracking of time-varying channels [15, 18–23], they require extensive computations or simply ignore the ICI to reduce the complexity. However, ICI considerably affects the channel estimation [24]. For the time-varying channel, the ICI should be accounted for in the channel estimation process. Conventional channel estimation algorithms treat ICI as part of the additive white Gaussian noise and these algorithms perform poorly when ICI is significant.

In pilot-tone insertion techniques, the channel estimation can be performed by either block-type or comb-type. The block-type channel estimation, based on inserting pilot tones into all of the OFDM subcarriers, has been developed under the assumption of a slow fading channel [25]. The channel estimation for this block-type pilot arrangement can be based on the Least Square (LS) or Minimum Mean-Square Error (MMSE). The MMSE estimate has been shown to give $10 \sim 15$ dB gain in signal-to-noise ratio (SNR) for the same mean-square error of channel estimation over the LS estimate [26]. In [27], a low-rank approximation is applied to the linear MMSE by using the frequency correlation of the channel to reduce the complexity of MMSE. The comb-type pilot based channel estimation, has been introduced to satisfy the need for equalizing when the channel changes even in one OFDM block. The comb-type pilot based channel estimation consists of algorithms to estimate the channel at pilot frequencies and to interpolate the channel. The estimation of the channel at the

pilot frequencies for comb-type based channel estimation can be based on LS, MMSE or Least Mean-Square (LMS). MMSE has been shown to perform much better than LS. In [28], the complexity of MMSE is reduced by deriving an optimal low-rank estimator with singular-value decomposition. Other comb-type based channel estimations were proposed for multipath fading channel, such as linear interpolation, second-order interpolation, low-pass interpolation, spline cubic interpolation, and time domain interpolation. In [28], second-order interpolation has been shown to perform better than the linear interpolation. In [29], time-domain interpolation has been proven to give a lower bit-error rate (BER) than linear interpolation.

Unlike conventional channel estimation techniques, where ICI is treated as part of the noise, the proposed approach takes the effect of ICI into account in channel estimation. In the proposed approach for OFDM systems with severe ICI, pilot tones are placed not far apart from each other, but grouped together periodically to mitigate the effects of ICI. Based on this insertion, a simplified channel estimation method is proposed in this thesis. Based on the assumption that the channel can be approximated to vary in a linear fashion in an OFDM block, the channel estimation method can estimate channel parameters in time domain directly, which also includes the impact of ICI on the results of channel estimates. The channel estimation matrices in the proposed method can be precalculated and stored in the receiver when the position of pilots tones are fixed in the OFDM symbols. The results from this estimation can be used to update the performance of the PIC-DSC technique and the ICI cancellation algorithm. For the high Doppler frequencies, the assumption that the CSI varies linearly no longer holds and gives rise to an error floor. A more effective channel estimation method dealt with high Doppler frequencies will be investigated in the future.

1.3 Thesis Outline

This thesis consists of six chapters, the rest of which are organized as follows:

Chapter 2 introduces the convolutional codes and optimum decoding. A maximum likelihood (ML) and a maximum a posteriori probability (MAP) are introduced for a convolutional code example. Moreover, the turbo codes and iterative decoding principle are described with an example of a parallel turbo code consisting of two recursive systematic convolutional

codes.

Chapter 3 gives the descriptions of wireless fading channels, including multipath propagation, Doppler shift, time-invariant and time-variant fading channels. The basic OFDM principles and several concepts, such as cyclic prefix, modulation, equalization and channel estimation, are analyzed. Then, two iterative MIMO-OFDM receiver models are presented, a standard parallel interference canceler (PIC-STD) and its improved version known as PIC with decision statistics combiner (PIC-DSC). The performance comparisons of both systems are shown through simulation results.

Chapter 4 discusses pilot-assisted channel estimation in MIMO-OFDM systems for time-invariant multipath channels. Various frequency-domain interpolators that estimate the time-invariant channel are analyzed: a linear interpolator and a trigonometric interpolator. A new algorithm, called the multi-tap method, is proposed for estimation of a time-invariant multipath channel. Simulation results show that our proposed method achieves the best system performance compared to other known interpolators.

Chapter 5 proposes a new algorithm for intercarrier interference cancellation in mobile scenarios. A simplified method is proposed to reduce the computation complexity in the frequency-domain equalizer. Furthermore, in time-variant scenarios, a pilot-assisted channel estimation method is proposed under the assumption that the channel can be approximated by a linear model. The estimated channel will be used to update the frequency-domain equalizer and parallel interference canceler in the proposed iterative MIMO-OFDM receiver. Simulation results show that the proposed equalization algorithm can mitigate the effect of ICI effectively.

Chapter 6 concludes this thesis by providing a summary of major contributions and suggests potential future work.

Chapter 2

Iterative Decoding Principles

This chapter is devoted to reviewing the optimal decoding of convolutional codes and the iterative maximum a posteriori probability (MAP) decoding principles. Convolutional codes and turbo codes are chosen as they are used in the current and proposed next generation of cellular mobile communication standards. In this review of maximum likelihood (ML) decoding and iterative MAP decoding, we adapt most of the material from [30–33].

2.1 System Model

We consider the simple model of a single user coded system as shown in Figure 2.1. A digital information source generates information bearing messages to be transmitted. The output of the information source is converted to a sequence $\mathbf{u}$ consisting of N binary digits. The channel encoder converts the information sequence $\mathbf{u}$ into an encoded sequence $\mathbf{v}$. The encoding process introduces controlled redundancy into the information sequence to combat thermal noise and some other deleterious factors during the transmissions through the channel. At the receiver, the decoder performs the inverse operation resulting in an estimate of the information sequence $\mathbf{u}$, which is denoted by $\hat{\mathbf{u}}$. The modulator will transform the output of the encoder into appropriate electrical waveforms suitable for transmission over the channel based on the channel characteristics. The modulated sequence $\mathbf{x}$ will then be sent into the channel for transmission. The channel is the physical medium between the transmitter and

the receiver, which might be wired lines, optical fiber cables or wireless links. In the process of transmission, noise is inevitably introduced by various mechanisms ranging from additive thermal noise generated by electronic devices, to atmospheric noise. The channel is modeled as an additive white Gaussian noise channel. At the receiver the demodulator processes the received waveforms and produces the discrete time output with an infinite number of quantization levels. The demodulator output sequence is called the received sequence and denoted by $\mathbf{r}$. The channel decoder attempts to recover the information sequence $\mathbf{u}$. It produces an estimated sequence $\hat{\mathbf{u}}$ which, ideally, is a replica of $\mathbf{u}$.

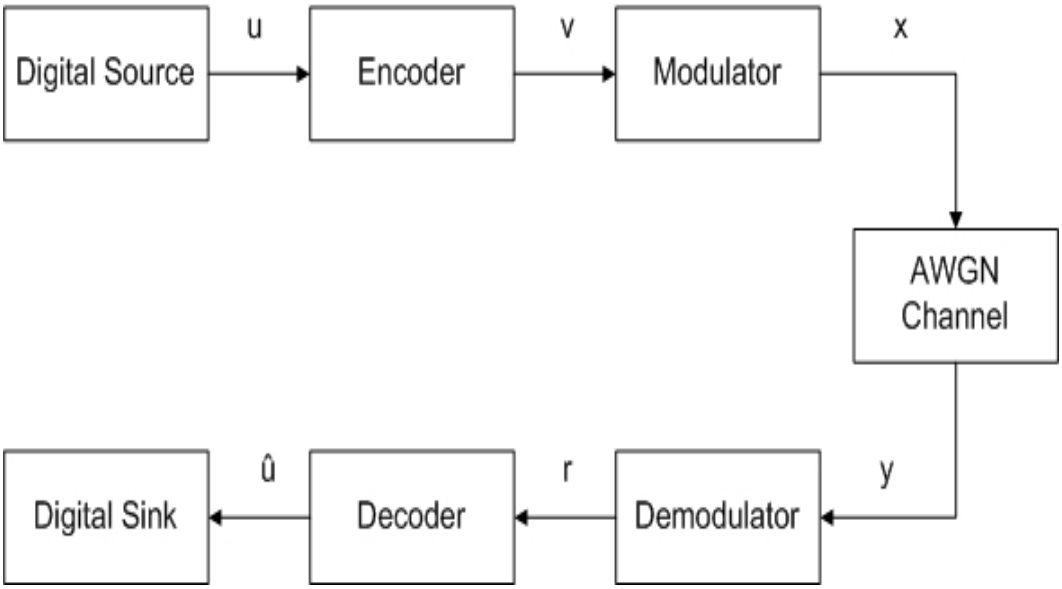

Figure 2.1: Single user coded system model

2.1.1 Convolutional Codes and Optimum Decoding

Convolutional codes have been widely used in applications such as space and satellite communications, cellular mobiles, digital video broadcasting, etc. Its popularity stems from simple structure and availability of easily implementable maximum likelihood soft decision decoding methods.

The (n, k, m) convolutional code can be implemented as a k input and n $(n > k)$ output linear circuit with input memory m. The structure introduced to the signal by a convolutional code is defined by the generator polynomials which describe the connections between the

encoder inputs and outputs. The performance of the code depends on a code rate, defined as $R = \frac{k}{n}$, and a code memory m. Figure 2.2 shows the encoder for the example of a binary $(2, 1, 2)$ code with generator polynomials $(5_8, 7_8)$. The encoding equations can be written as

$$\mathbf{v}^1 = \mathbf{u} * \mathbf{g}^{(1)} \qquad \mathbf{v}^2 = \mathbf{u} * \mathbf{g}^{(2)} \tag{2.1}$$

where $*$ denotes the convolution and all operations are modulo-2.

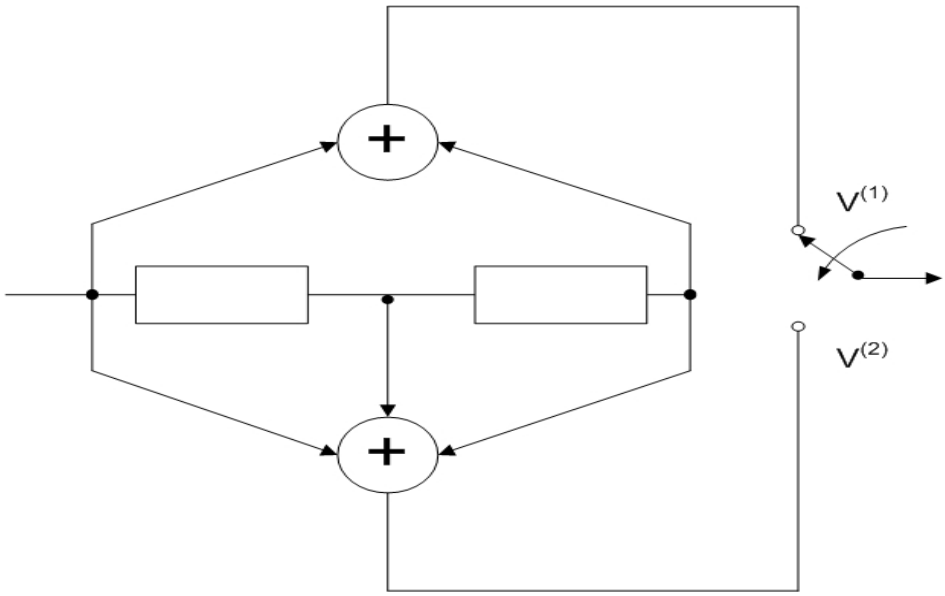

Figure 2.2: Encoder for a binary (2,1,2) convolutional code

A convenient and common way of describing encoding and decoding operations is using trellis diagrams. A trellis stage for an input at time t for a binary $(2, 1, 2)$ code is shown in Figure 2.3. A trellis diagram consists of N such stages, where N is the number of input words, each consisting of k input data bits. The state of the encoder is defined as the content of its shift register. For the encoder with a total memory K, the number of states is 2^K. Each new block of k inputs causes the transition to a new state. That is, there are 2^k branches leaving each state. Each branch is labeled by the k inputs causing the transition at time unit t, denoted by $\mathbf{u}_t = (u_{t,0}, \cdots, u_{t,k-1})$, and n corresponding outputs, denoted by $\mathbf{v}_t = (v_{t,0}, \cdots, v_{t,n-1})$.

Given that $\mathbf{r}$ is received, the conditional error probability of the decoder is defined as

$$P(E|\mathbf{r}) = P(\hat{\mathbf{u}} \neq \mathbf{u}) = P(\hat{\mathbf{v}} \neq \mathbf{v}) \tag{2.2}$$

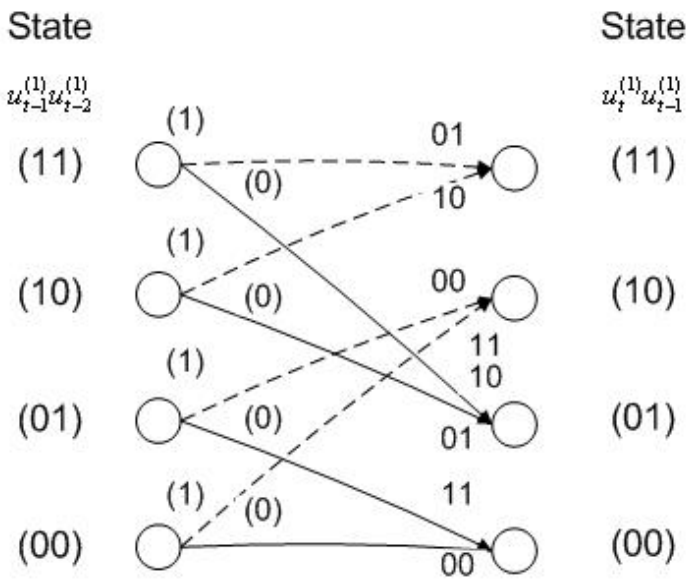

Figure 2.3: One stage in a trellis diagram for a binary (2,1,2) convolutional code

The probability of error in the decoder is then given by

$$P(E) = \sum_{r} P(E|\mathbf{r})P(\mathbf{r}) \tag{2.3}$$

The term $P(\mathbf{r})$ is independent of the decoding algorithm, so the minimum probability of error in Eqn. 2.3 is achieved by minimizing $P(E|\mathbf{r}) = P(\hat{\mathbf{v}} \neq \mathbf{v}|\mathbf{r})$ for all $\mathbf{r}$. This is equivalent to maximizing $P(\hat{\mathbf{v}} = \mathbf{v}|\mathbf{r})$. That is, the decoder searches for $\hat{\mathbf{v}}$ which maximizes

$$P(\hat{\mathbf{v}} = \mathbf{v}|\mathbf{r}) = \frac{P(\mathbf{r}|\mathbf{v})P(\mathbf{v})}{P(\mathbf{r})} \tag{2.4}$$

If the coded sequences are all equally likely, then for a discrete memory channel the optimal decoding maximizes

$$P(\mathbf{r}|\mathbf{v}) = \prod_{i} P(r_i|v_i) \tag{2.5}$$

It is convenient to consider the logarithm of the expression in Eqn. 2.5. As $log(x)$ is a monotonically increasing function, maximizing the expression in Eqn. 2.5 is equivalent to maximizing

$$\log P(\mathbf{r}|\mathbf{v}) = \sum_{i} \log P(r_i|v_i) \tag{2.6}$$

The function $logP(\mathbf{r}|\mathbf{v})$ is known as log-likelihood function and the decoding algorithm that maximizes this function is known as the maximum likelihood (ML) decoding algorithm.

2.1.2 Viterbi Algorithm

In 1967 Viterbi proposed an efficient algorithm for the decoding of convolutional codes. This algorithm can achieve maximum likelihood decoding performance, which minimizes the probability of error in the decoding of the whole received sequence, when the binary information bits are statistically independent and equally likely.

The following describes the principles of the Viterbi algorithm. For simplicity, we assume a binary code, $k = 1$ and consider BPSK modulation. The data sequence $\mathbf{u} = (u_1, \cdots, u_t, \cdots, u_N)$ is encoded by a convolutional $(n, 1, m)$ encoder. The trellis diagram has a total number of $M = 2^m$ distinct states, indexed by integer l, $l = 0, 1, \cdots, M-1$. The state of the trellis S_t represents the encoder register content at time t. The state in a trellis diagram, from time t to t', is denoted by

$$\mathbf{S}_t^{t'} = (S_t, S_{t+1}, \cdots, S_{t'}) \tag{2.7}$$

The corresponding encoder output sequence is

$$\mathbf{v}_t^{t'} = (\mathbf{v}_t, \mathbf{v}_{t+1}, \cdots, \mathbf{v}_{t'}) \tag{2.8}$$

where $\mathbf{v}_t = (v_{t,0}, v_{t,1}, \cdots, v_{t,n-1})$ and n is the codeword length. The encoded sequence is BPSK modulated generating the sequence

$$\mathbf{x}_t^{t'} = (\mathbf{x}_t, \mathbf{x}_{t+1}, \cdots, \mathbf{x}_{t'}) \tag{2.9}$$

where $\mathbf{x}_t = (x_{t,0}, x_{t,1}, \cdots, x_{t,n-1})$. The received bit corresponding to the transmitted bit $x_{t,i}$ is a sum of the transmitted bit and additive white Gaussian noise (AWGN)

$$r_{t,i} = x_{t,i} + n_{t,i}, \quad i = 0, 1, \cdots, n-1 \tag{2.10}$$

where $n_{t,i}$ is a zero mean Gaussian random variable with variance σ^2. The received sequence for a block of information bits from time t to time t' is denoted by

$$\mathbf{r}_t^{t'} = (\mathbf{r}_t, \mathbf{r}_{t+1}, \cdots, \mathbf{r}_{t'}) \tag{2.11}$$

where $\mathbf{r}_t = (r_{t,0}, r_{t,1}, \cdots, r_{t,n-1})$.

The Viterbi (ML) decoder selects the word $x = x_1^N$ that maximizes the likelihood function

$$\log P(\mathbf{r}|\mathbf{x}) = \sum_{t=1}^{N} \log P(\mathbf{r}_t|\mathbf{x}_t) = \sum_{t=1}^{N} \sum_{j=0}^{n-1} \log P(r_{t,j}|x_{t,j}) \tag{2.12}$$

For the Gaussian channel this becomes

$$\log P(\mathbf{r}|\mathbf{x}) = -nN \log \sqrt{2\pi}\sigma - \sum_{t=1}^{N} \sum_{j=0}^{n-1} \frac{(r_{t,j} - x_{t,j})^2}{2\sigma^2} \tag{2.13}$$

From Eqn. 2.13 we notice that maximizing the log-likelihood function is equivalent to minimizing the Euclidean distance between the received sequence $\mathbf{r} = \mathbf{r}_1^N$ and modulated sequence $\mathbf{x} = \mathbf{x}_1^N$ in the trellis diagram. The Euclidean distance is given by

$$Ed(\mathbf{r}, \mathbf{x}) = \sum_{t=1}^{N} \sum_{j=0}^{n-1} \frac{(r_{t,j} - x_{t,j})^2}{2\sigma^2} \tag{2.14}$$

For the procedures in the Viterbi algorithm it is convenient to define the branch and path metrics as

$$\nu_t^{(\mathbf{x}_t)} = \sum_{j=0}^{n-1} \frac{(r_{t,j} - x_{t,j})^2}{2\sigma^2} \;\; and \;\; \mu_M = \sum_{t=1}^{M} \nu_t^{(\mathbf{x}_t)} \;\; \text{respectively} \tag{2.15}$$

The Viterbi algorithm is equivalent to using dynamic programming for finding the shortest path through a weighted graph. The objective of the algorithm is to find a maximum likelihood path in the trellis, that is, a path with a minimum path metric (also referred to as the minimum distance path or shortest path). The search for the maximum likelihood path is performed in a recursive manner. At each time t, the path consisting of t branches with a minimum metric is selected and stored for each state. This shortest partial path for a particular state is called the survivor. The decision on the data bit u_t is made with a delay τ . The minimum path metric at time $t + \tau$ is computed as the minimum metric path among the M survivor path metrics, one for each of the M trellis states. The survivor path metric for state S_t is computed as

$$\mu_t = \min_{\mathbf{x}_t} [\mu_{t-1} + \nu_t^{(\mathbf{x}_t)}] \tag{2.16}$$

where μ_{t-1} is the survivor metric for the state S_{t-1} which is connected with the state S_t by a branch associated with a codeword $\mathbf{x}_t$.

If the minimum path metric $\mu_{N,min}$ corresponds to path $\hat{\mathbf{x}}$, then the decoder selects the binary symbol on this path at time t, namely $\hat{u}_t$, and delivers it as a hard estimate of the transmitted symbol u_t.

In the concatenated schemes where the output of the decoder is fed into another decoder or another soft-input module, it is of interest that the decoder produces the bits' a posteriori probability estimates rather than the bits' hard estimates.

The Viterbi algorithm can be modified to generate soft outputs by considering both the maximum likelihood path and the strongest competitor (SC) path. The strongest competitor path is the minimum path metric for the path obtained when the trellis symbol on the maximum likelihood path at time t is replaced by its complementary symbol. If we denote the metric of the ML and SC paths containing the data bit u_t by M_t^{ml} and M_t^{sc} , respectively, then the a posteriori log-likelihood ratio for the data bit at time t is estimated as

$$\Lambda(u_t) = \log \frac{P(u_t = 1|\mathbf{r})}{P(u_t = 0|\mathbf{r})} = \log \frac{e^{-M_t^{ml}}}{e^{-M_t^{sc}}} \tag{2.17}$$

if the bit on a ML path is $u_t = 1$, or as

$$\Lambda(u_t) = \log \frac{P(u_t = 1|\mathbf{r})}{P(u_t = 0|\mathbf{r})} = \log \frac{e^{-M_t^{sc}}}{e^{-M_t^{ml}}} \tag{2.18}$$

if the bit on a ML path is $u_t = 0$.

The a posteriori probabilities of the data bit can be calculated from Eqn. 2.17 as

$$P(u_t = 1|\mathbf{r}) = \frac{e^{\Lambda_t}}{1 + e^{\Lambda_t}} \tag{2.19}$$

$$P(u_t = 0|\mathbf{r}) = \frac{1}{1 + e^{\Lambda_t}} \tag{2.20}$$

If the decision is made on a finite block length, then the proposed algorithm can be implemented as a bi-directional recursive method with forward and backward recursions.

2.1.3 MAP Decoding Algorithm

The maximum a posteriori probability (MAP) algorithm uses a decoding criteria that minimizes the bit-error probability, whereas the Viterbi algorithm minimizes the sequence-error probability. The MAP algorithm is computationally more complex that the Viterbi algorithm and requires knowledge of noise variance. However, MAP considers all possible paths in a trellis as opposed to the soft output Viterbi algorithm (SOVA) which considers only the ML and SC paths. This becomes a very important advantage of the MAP algorithm for the iterative decoding algorithms.

The soft-output MAP decoder calculates the a posteriori log-likelihood ratio for the data bit u_t as

$$\Lambda(u_t) = \log \frac{P\{u_t = 1|\mathbf{r}\}}{P\{u_t = 0|\mathbf{r}\}} \tag{2.21}$$

where $P\{u_t = i|\mathbf{r}\}$, $i = 0, 1$ is the a posteriori probability (APP) of the data bit u_t. The decoder makes the hard decision by comparing $\Lambda(u_t)$ to zero

$$u_t = \begin{cases} 1 & if \;\; \Lambda(u_t) > 0 \\ 0 & otherwise \end{cases} \tag{2.22}$$

The APPs in Eqn. 2.21 can be computed from a trellis diagram as

$$P(u_t = 0|\mathbf{r}) = \sum_{(m',m)\in B_t^0} P\{S_{t-1} = m', S_t = m|\mathbf{r}\} \tag{2.23}$$

$$P(u_t = 1|\mathbf{r}) = \sum_{(m',m)\in B_t^1} P\{S_{t-1} = m', S_t = m|\mathbf{r}\} \tag{2.24}$$

where S_{t-1} and S_t are the encoder states at time $t-1$ and t, respectively, and B_t^0 and B_t^1 are set of transitions from state m' to state m caused by $u_t = 0$ and $u_t = 1$, respectively. Eqn. 2.23 and Eqn. 2.24 can be written as

$$P(u_t = 0|\mathbf{r}) = \sum_{(m',m)\in B_t^0} \frac{P\{S_{t-1} = m', S_t = m, \mathbf{r}\}}{P\{\mathbf{r}\}} \tag{2.25}$$

$$P(u_t = 1|\mathbf{r}) = \sum_{(m',m)\in B_t^1} \frac{P\{S_{t-1} = m', S_t = m, \mathbf{r}_1^N\}}{P\{\mathbf{r}\}} \tag{2.26}$$

where the $P\{\mathbf{r}\}$ is a constant. Since it does not affect the maximization, it will be dropped in further derivations.

In order to efficiently calculate the information bits' APPs, the following probability functions are defined [30]

$$\alpha_t(m) = P\{S_t = m, \mathbf{r}_1^t\} \tag{2.27}$$

$$\beta_t(m) = P\{\mathbf{r}_{t+1}^N|S_t = m\} \tag{2.28}$$

$$\gamma_t^i(m, m') = P\{u_t = i, S_t = m, \mathbf{r}_t|S_{t-1} = m'\} \tag{2.29}$$

where

$$\mathbf{r}_t = (r_{t,0}, \cdots, r_{t,i}, \cdots, r_{t,n-1}) \tag{2.30}$$

$$\mathbf{r}_t^k = (\mathbf{r}_t, \mathbf{r}_{t+1}, \cdots, \mathbf{r}_k) \tag{2.31}$$

The joint transition probability $P\{S_{t-1} = m', S_t = m, \mathbf{r}\}$ can be expressed as

$$P\{S_{t-1} = m', S_t = m, \mathbf{r}\} = \alpha_{t-1}(m') \sum_{i \in 0,1} \gamma_t^i(m', m)\beta_t(m) \tag{2.32}$$

where $\alpha_t(m)$ and $\beta_t(m)$ are obtained recursively as

$$\alpha_t(m) = \sum_{m'} \alpha_{t-1}(m') \sum_{i \in 0,1} \gamma_t^i(m', m) \tag{2.33}$$

$$\beta_t(m) = \sum_{m'} \beta_{t+1}(m') \sum_{i \in 0,1} \gamma_t^i(m, m') \tag{2.34}$$

and $\gamma_t^i(m, m')$ is a channel transition probability weighted by the information bit a priori probability $p_t(u_t = i), i = 0, 1$, where u_t is the information symbol associated with the transition $S_{t-1} = m' \rightarrow S_t = m$. Coefficient $\gamma_t^i(m', m)$ can be written as

$$\gamma_t^i(m', m) = p_t(u_t = i) \prod_{j=0}^{j=n-1} P\{r_{t,j}|x_{t,j}\} \tag{2.35}$$

$$P\{r_{t,j}|x_{t,j}\} = \frac{1}{\sqrt{2\pi}\sigma} e^{-\frac{(r_{t,j}-x_{t,j})^2}{2\sigma^2}} \tag{2.36}$$

where $x_{t,j}, j = 0, \cdots, n-1$ is a BPSK modulated symbol in a codeword associated with transition $S_{t-1} = m' \rightarrow S_t = m$.

If we assume that the encoder starts and ends in a zero state, the boundary conditions are

$$\alpha_0(0) = 1, \quad \alpha_0(m) = 0 \quad for \quad m \neq 0 \tag{2.37}$$

$$\beta_N(0) = 1, \quad \beta_N(m) = 0 \quad for \quad m \neq 0 \tag{2.38}$$

The log-likelihood ratio $\Lambda(u_t)$ can be written as

$$\Lambda(u_t) = \log \frac{\sum_{m', m \in B^1} \alpha_{t-1}(m')\gamma_t^1(m', m)\beta_t(m)}{\sum_{m', m \in B^0} \alpha_{t-1}(m')\gamma_t^0(m', m)\beta_t(m)} \tag{2.39}$$

The above algorithm is usually referred to as forward/backward algorithm, since the coefficients $\alpha_t(m)$ are calculated recursively starting from the beginning of the trellis (forward recursion), and the $\beta_t(m)$ coefficients are calculated recursively starting from the end of the trellis (backward recursion).

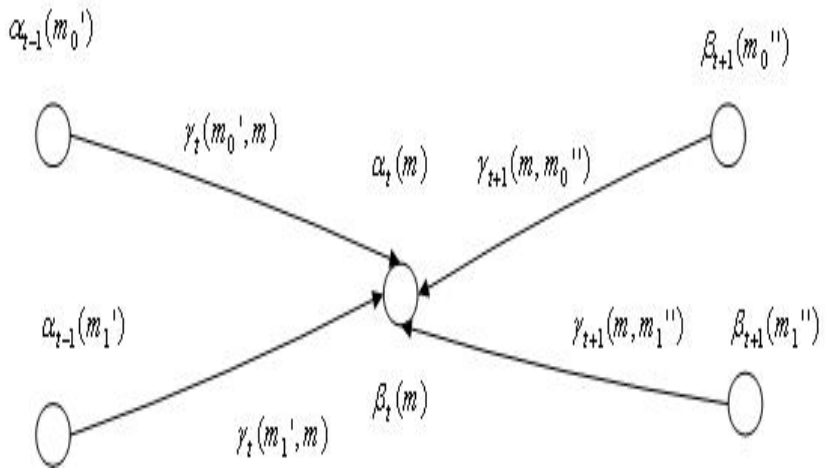

Figure 2.4: Graphic representation of the forward and backward recursions

Figure 2.4 shows the graphical representation of the forward and backward recursions. In this figure $\alpha_{t-1}(m_i')$ represents the α coefficient for state m_i' in the $(t-1)$th stage which is connected with a state m in the tth trellis stage and where transition $S_{t-1} = m_i' \rightarrow S_t = m$ is caused by the information bit $u_t = i, i = 0, 1$. Similarly, the $\beta_{t+1}(m_i'')$ denotes the β coefficient for state m_i'' in the $(t+1)$th trellis stage which is connected with a state m in tth trellis stage and where the transition $S_t = m \rightarrow S_{t+1} = m_i''$ is caused by the information bit $u_t = i, i = 0, 1$.

The a posteriori probabilities of the information bits can be calculated as

$$P\{u_t = 1|\mathbf{r}\} = \frac{e^{\Lambda(u_t)}}{1 + e^{\Lambda(u_t)}} \tag{2.40}$$

$$P\{u_t = 0|\mathbf{r}\} = \frac{1}{1 + e^{\Lambda(u_t)}} \tag{2.41}$$

The a posteriori probabilities of the transmitted bits can be calculated by adding the probabilities of the codewords that contain a particular transmitted bit. That is

$$P\{x_{t,j} = 1|\mathbf{r}\} = \sum_{u_t = i, x_{t,j} = 1} P\{u_t = i|\mathbf{r}\} \tag{2.42}$$

$$P\{x_{t,j} = -1|\mathbf{r}\} = \sum_{u_t=i, x_{t,j}=-1} P\{u_t = i|\mathbf{r}\} \tag{2.43}$$

2.1.4 Turbo Codes and an Iterative Decoding Principle

Turbo codes belong to the class of codes obtained by serial or parallel concatenation of recursive systematic convolutional codes [30]. These codes have gained a lot of attention since they can be decoded iteratively with a decoding performance that approaches the capacity limit. Furthermore, the iterative (turbo) decoding principle has been successfully applied in some other applications, such as joint decoding and detection of users in the direct sequence code division multiple access (DS-CDMA) system. In order to describe the iterative decoding principle, we consider an example of a parallel turbo code consisting of two $1/2$ rate recursive systematic convolutional codes (RSC). Turbo codes employ RSC codes since these have a weight distribution which results in a better bit error performance at low SNR than the equivalent nonsystematic feed-forward codes [30].

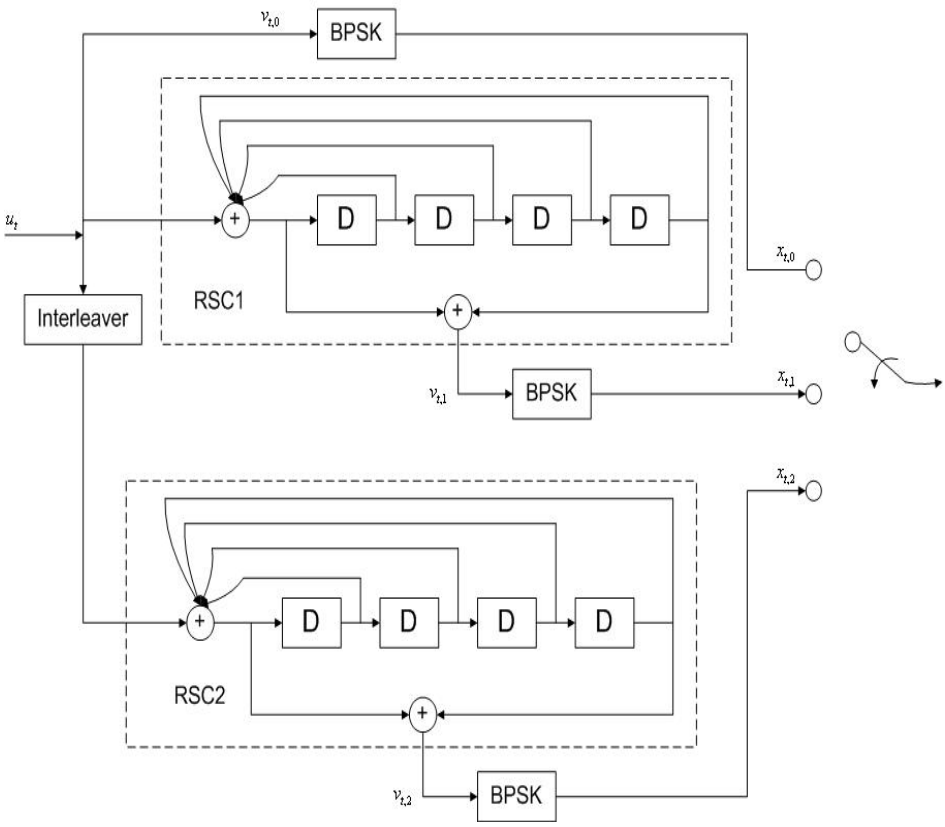

Figure 2.5: Turbo encoder with the two (2,1,4) RSC component codes

The turbo-encoder for this example is shown in Figure 2.5. It consists of two $(2, 1, 4)$ encoders operating on the same block of information bits. The first encoder directly encodes the information sequence $\mathbf{u}$, while the second encoder encodes the interleaved version of the information sequence. The interleaver is very important and both its size its design largely influence the performance. Its role is to generate a long block code from the small memory convolutional codes and to decorrelate the information which gets iteratively exchanged between the decoders in a turbo decoding process [30].

The overall rate of the turbo decoder for this example is $1/3$ and the encoder output for each input data bit consists of an information bit followed by the two parity check bits generated by the RSC encoders.

For large interleaver sizes the complexity of the optimal maximum likelihood sequence estimation (MLSE) or MAP decoding becomes very high. The practical importance of the turbo codes comes from the existence of an efficient iterative decoding algorithm.

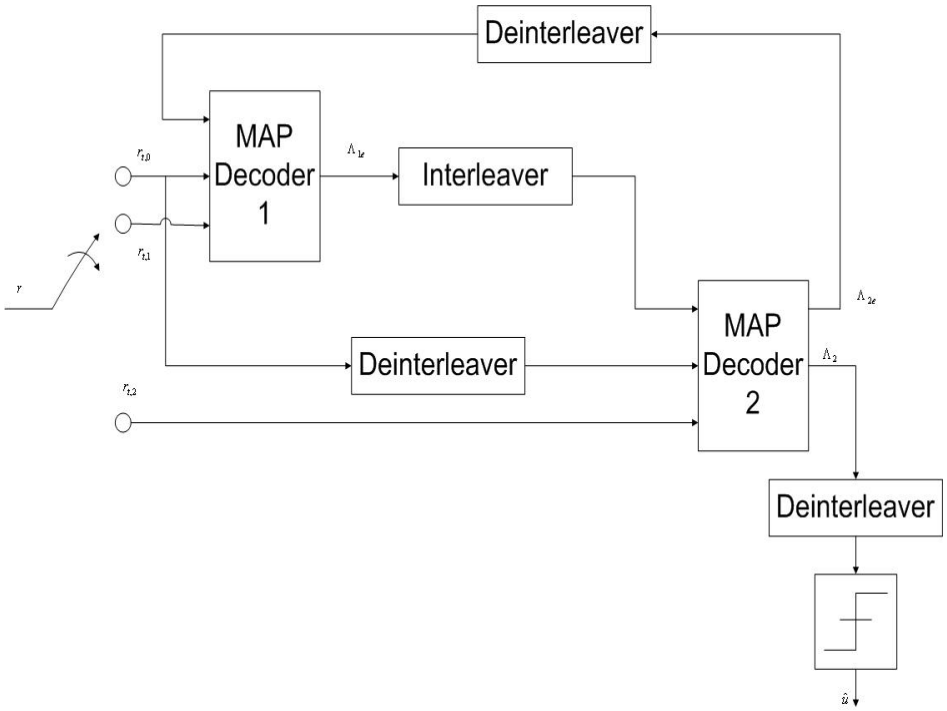

Figure 2.6: Turbo encoder with MAP decoding of the composed codes

The block diagram of the iterative (turbo) decoder is shown in Figure 2.6. In the turbo decoder each component code is decoded separately by the soft output decoding algorithm. The

ith, $i = 1, 2$ decoder calculates the a posteriori log-likelihood ratio (LLR) of the information bit as

$$\Lambda^i(u_t) = \log \frac{\sum_{(m',m)\in B^1} \alpha_{t-1}(m') p_t^i(1) \exp(\frac{-\sum_{j=0}^{n}(r_{t,j} - x_{t,j})^2}{2\sigma^2}) \beta_t(m)}{\sum_{(m',m)\in B^0} \alpha_{t-1}(m') p_t^i(0) \exp(\frac{-\sum_{j=0}^{n}(r_{t,j} - x_{t,j})^2}{2\sigma^2}) \beta_t(m)} \tag{2.44}$$

where α and β are given by Eqn. 2.34 and the a priori probability that bit $u_t = j$, $j = 0, 1$ is denoted by $p_t^i(j)$, for the decoder i, $i = 1, 2$.

From the log-likelihood ratio (LLR) for the data bit u_t, the decoder extracts a part of it that is not directly dependent on the a priori information or a systematic bit for the same data bit u_t. This information, referred to as extrinsic information, is then passed to the other decoder. The extrinsic information ratio (EIR) is given by

$$\Lambda_e^i(u_t) = \Lambda_i(u_t) - \log \frac{p_t^i(1)}{p_t^i(0)} + \frac{2}{\sigma^2} r_{t,0} \tag{2.45}$$

where $\log \frac{p_t^i(1)}{p_t^i(0)}$ is the a priori information ratio calculated in the jth decoder $j \neq i$ in the previous iteration, and $\frac{2}{\sigma^2} r_{t,0}$ is the systematic bit contribution.

The decoder for one component code takes as input extrinsic information supplied by the other decoder and uses it as the data bit a priori information in the MAP or SOVA decoding process.

The extrinsic information ratio (EIR) can be directly calculated by the forward/backward algorithm by excluding from Eqn. 2.44 terms that contain bit a priori probabilities $p_t^i(j)$ and the systematic bit $r_{t,0}$. That is, in terms of the forward/backward coefficients, the EIR is

given by

$$\Lambda_e^i(u_t) = \log \frac{\sum_{(m',m)\in B^1} \alpha_{t-1}(m') \exp(\frac{-\sum_{j=0}^{n}(r_{t,j} - x_{t,j})^2}{2\sigma^2})\beta_t(m)}{\sum_{(m',m)\in B^0} \alpha_{t-1}(m') \exp(\frac{-\sum_{j=0}^{n}(r_{t,j} - x_{t,j})^2}{2\sigma^2})\beta_t(m)} \tag{2.46}$$

The iterative exchange of information between decoders results in improvement of the individual decoder estimates. After a certain number of iterations the decoders stop producing further improvements. In the last stage of the decoding, hard decisions are made in the second decoder according to the Eqn. 2.22.

2.2 Summary

This chapter first introduced the convolutional codes with the example of a binary $(2, 1, 2)$ code with generator polynomials and forward error correcting schemes. Furthermore, the principles of turbo codes were introduced, and illustrated by an example. For the examples of convolutional codes and turbo codes, Viterbi, MAP and turbo decoding principles were discussed. Since MAP is optimal trellis-based iterative decoding method, in the following Chapters, $(15, 17)$ convolutional code and MAP decoder will be applied in the proposed MIMO-OFDM systems.

Chapter 3

Iterative Receiver for MIMO-OFDM System

For many real links such as radio, satellite and mobile channels, transmission error are mainly caused by variations of fading in received signal strength [33], which severely degrades the transmission performance. In this chapter, we first discuss the basic concepts of fading channel models, including multipath propagation and Doppler shift. Two fading models, Rayleigh fading and Rician fading, will be introduced to describe signal variations statistically. Then, we will analyze the principles of OFDM systems with a simple transceiver, and analyze the advantages of the OFDM technique by mathematical formulae. A MIMO-OFDM system model is proposed with an iterative receiver. The performance comparison of a standard parallel interference canceler (PIC-STD) and its improved version known as PIC with decision statistics combiner (PIC-DSC) is shown in simulation results.

3.1 Fading Channel Models

3.1.1 Multipath Propagation

In a cellular mobile radio environment, the surrounding objects, such as houses, buildings or trees, act as reflectors of radio waves. These obstacles produce reflected waves with attenuated amplitudes and phases. If a modulated signal is transmitted, multiple reflected waves of the transmitted signal will arrive at the receiving antenna from different directions with different propagation delays. These reflected waves are known as multipath waves [34]. Due to the different arrival angles and times, the multipath waves at the receiver site have different phases. When they are collected by the receive antenna at any point in space, they may combine either in a constructive or a destructive way, depending on the random phases. The sum of these multipath components forms a spatially varying standing wave field. The mobile unit moving through the multipath field will receive a signal which can vary widely in amplitude and phase. When the mobile unit is stationary, the amplitude variations in the received signal are due to the movement of surrounding objects in the radio channel. The amplitude fluctuation of the received signal, known as signal fading, is caused by the time-variant multipath characteristics of the channel [33].

3.1.2 Doppler Shift

Due to the relative motion between the transmitter and the receiver, each multipath wave is subject to a shift in frequency. The frequency shift of the received signal caused by the relative motion is the Doppler shift. It is proportional to the speed of the mobile unit. Consider a situation when only a single tone of frequency f_c is transmitted and a received signal consists of only one wave coming at an incident angle θ with respect to the direction of the vehicle motion. The Doppler shift of the received signal, denoted by f_d, is given by

$$f_d = \frac{v f_c}{c} \cos\theta \tag{3.1}$$

where v is the vehicle speed and c is the speed of light. The Doppler shift in a multipath propagation environment spreads the bandwidth of the multipath waves within the range of

$f_c \pm f_{d_{max}}$, where $f_{d_{max}}$ is the maximum Doppler shift, given by

$$f_{d_{max}} = \frac{v f_c}{c} \tag{3.2}$$

The maximum Doppler shift is also referred as the maximum fade rate. As a result, a single tone transmitted gives rise to a received signal with a spectrum of nonzero width. This phenomenon is known as frequency dispersion of the channel.

3.1.3 Time-invariant Fading Channels

Because of the multiplicity of factors involved in propagation in a cellular mobile environment, it is convenient to apply statistical techniques to describe signal variations.

In a narrowband system, the transmitted signals usually occupy a bandwidth smaller than the channel's coherence bandwidth, which is defined as the frequency range over which the channel fading process is correlated. That is, all spectral components of the transmitted signal are subject to the same fading attenuation. This type of fading is referred to as frequency nonselective or frequency flat. On the other hand, if the transmitted signal bandwidth is greater than the channel coherence bandwidth, the spectral components of the transmitted signal with a frequency separation larger than the coherence bandwidth are faded independently. The received signal spectrum becomes distorted, since the relationships between various spectral components are not the same as in the transmitted signal. This phenomenon is known as frequency selective fading. In wideband systems, the transmitted signals usually undergo frequency selective fading.

In this section we first introduce Rayleigh and Rician fading models to describe signal variations in a narrowband multipath environment. Then, the frequency-selective fading models for a wideband system are addressed.

3.1.3.1 Rayleigh Fading

We consider the transmission of a single tone with a constant amplitude. In a typical land mobile radio channel, we may assume that the direct wave is obstructed and the mobile unit

receives only reflected waves. When the number of reflected waves is large, according to the central limit theorem, two quadrature components of the received signal are uncorrelated Gaussian random processes with a zero mean and variance σ_s^2. As a result, the envelope of the received signal at any time instant undergoes a Rayleigh probability distribution and its phase obeys a uniform distribution between $-\pi$ and π. The probability density function (pdf) of the Rayleigh distribution is given by

$$p(a) = \begin{cases} \frac{a}{\sigma_s^2} e^{-a^2/2\sigma_s^2} & a \geq 0 \\ 0 & a < 0 \end{cases} \tag{3.3}$$

The mean value, denoted by m_a, and the variance, denoted by σ_a^2, of the Rayleigh distributed random variable are given by

$$\begin{cases} m_a & = \sqrt{\frac{\pi}{2}} \cdot \sigma_s = 1.2533\sigma_s \\ \sigma_a^2 & = (2 - \frac{\pi}{2})\sigma_s^2 = 0.4292\sigma_s^2 \end{cases} \tag{3.4}$$

If the probability density function in Eqn. 3.3 is normalized, so that the average signal power $(E[a^2])$ is unity, then the normalized Rayleigh distribution becomes

$$p(a) = \begin{cases} 2ae^{-a^2} & a \geq 0 \\ 0 & a < 0 \end{cases} \tag{3.5}$$

The mean value and the variance are

$$\begin{cases} m_a & = 0.8862 \\ \sigma_a^2 & = 0.2146 \end{cases} \tag{3.6}$$

The pdf for a normalized Rayleigh distribution is shown in Figure 3.1.

In fading channels with a maximum Doppler shift of $f_{d_{max}}$, the received signal experiences a form of frequency spreading and is band-limited between $f_c \pm f_{d_{max}}$. Assuming an omni-directional antenna with waves arriving in the horizontal plane, a large number of reflected waves and a uniform received power over incident angles, the power spectral density of the faded amplitude, denoted by $|P(f)|$, is given by

$$|P(f)| = \begin{cases} \frac{1}{2\pi\sqrt{f_{d_{max}}^2 - f^2}} & if |P(f)| \leq |f_{d_{max}}| \\ 0 & otherwise \end{cases} \tag{3.7}$$

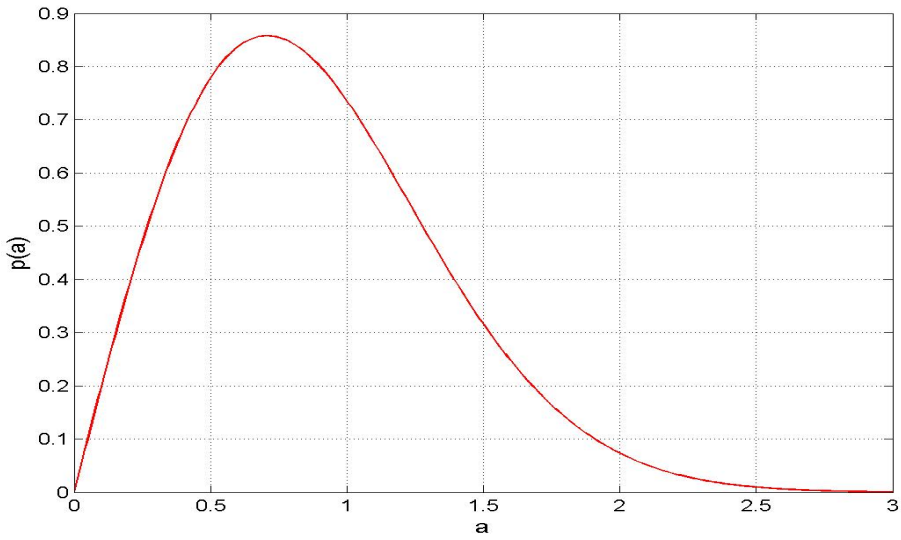

Figure 3.1: The pdf of Rayleigh distribution

where f is the frequency and $f_{d_{max}}$ is the maximum fade rate. The value of $f_{d_{max}}T_s$ is the maximum fade rate normalized by the symbol rate. It serves as a measure of the channel memory. For correlated fading channels this parameter is in the range $0 < f_{d_{max}}T_s < 1$, indicating a finite channel memory. The autocorrelation function of the fading process is given by

$$R(\tau) = J_0(2\pi f_{d_{max}}\tau) \tag{3.8}$$

where J_0 is the zero-order Bessel function of the first kind.

3.1.3.2 Rician Fading

In some propagation scenarios, such as satellite or microcellular mobile radio channels, there are essentially no obstacles on the line-of-sight path. The received signal consists of a direct wave and a number of reflected waves. The direct wave is a stationary non-fading signal with a constant amplitude. The reflected waves are independent random signals. Their sum is known as the scattered component of the received signal.

When the number of reflected waves is large, the quadrature components of the scattered signal can be characterized as a Gaussian random process with a zero mean and variance σ_s^2. The envelope of the scattered component has a Rayleigh probability distribution.

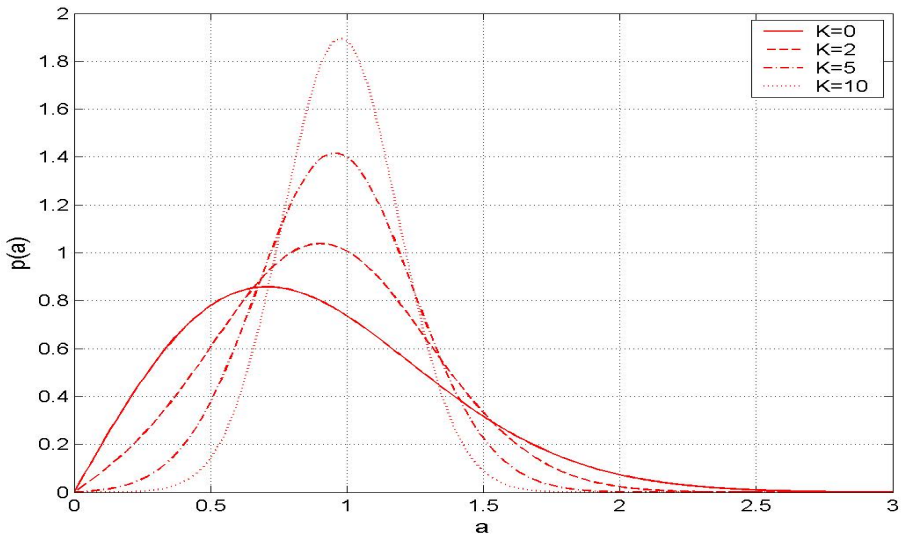

Figure 3.2: The pdf of Rician distributions with various K

The sum of a constant amplitude direct signal and a Rayleigh distributed scattered signal results in a signal with a Rician envelope distribution. The pdf of the Rician distribution is given by

$$p(a) = \begin{cases} \frac{a}{\sigma_s^2} e^{-\frac{(a^2+D^2)}{2\sigma_s^2}} I_0(\frac{aD}{\sigma_s^2}) & a \geq 0 \\ 0 & a < 0 \end{cases} \tag{3.9}$$

where D^2 is the direct signal power and $I_0(\cdot)$ is the modified Bessel function of the first kind and zero-order.

Assuming that the total average signal power is normalized to unity, the pdf in Eqn. 3.9 becomes

$$p(a) = \begin{cases} 2a(1+K)e^{-K-(1+K)a^2} I_0(2a\sqrt{K(K+1)}) & a \geq 0 \\ 0 & a < 0 \end{cases} \tag{3.10}$$

where K is the Rician factor, denoting the power ratio of the direct and the scattered signal components. The Rician factor is given by

$$K = \frac{D^2}{2\sigma_s^2} \tag{3.11}$$

The mean and the variance of the Rician distributed random variable are given by

$$\begin{cases} m_a & = \frac{1}{2}\sqrt{\frac{\pi}{1+K}} e^{-\frac{K}{2}[(1+K)I_0(\frac{K}{2})+KI_1(\frac{K}{2})]} \\ \sigma_a^2 & = 1 - m_a^2 \end{cases} \tag{3.12}$$

where $I_1(\cdot)$ is the first order modified Bessel function of the first kind. Small values of K indicate a severely faded channel. For $K = 0$, there is no direct signal component and the Rician pdf becomes a Rayleigh pdf. On the other hand, large values of K indicate a slightly faded channel. For K approaching infinity, there is no fading at all resulting in an AWGN channel. The Rician distributions with various K are shown in Figure 3.2.

These two models can be applied to describe the received signal amplitude variations when the signal bandwidth is much smaller than the coherence bandwidth.

3.1.3.3 Frequency Selective Fading

Frequency-selective fading channels can be modeled by a tapped-delay line. For a multipath fading channel with L different paths, the time-variant impulse response at time t to an impulse applied at time $t - \tau$ is expressed as [34]

$$h(t;\tau) = \sum_{l=1}^{L} h^{t,l}\delta(\tau - \tau_l) \tag{3.13}$$

where τ_l represents the time delay of the l-th path and $h^{t,l}$ represents the complex amplitude of the l-th path.

Without loss of generality, we assume that $h(t;\tau)$ is wide-sense stationary, which means that the mean value of the channel random process is independent of time and the autocorrelation of the random process depends only on the time difference [34]. Then, $h^{t,l}$ can be modeled by narrowband complex Gaussian processes, which are independent for different paths. The autocorrelation function of $h(t;\tau)$ is given by

$$\phi_h(\Delta t;\tau_i,\tau_j) = \frac{1}{2}E[h^*(t,\tau_i)h(t+\Delta t,\tau_j)] \tag{3.14}$$

where Δt denotes the observation time difference. If we let $\Delta t = 0$, the resulting autocorrelation function, denoted by $\phi_h(\tau_i,\tau_j)$, is a function of the time delays τ_i and τ_j. Due to the fact that scattering at two different paths is uncorrelated in most radio transmissions, we have

$$\phi_h(\tau_i,\tau_j) = \phi_h(\tau_i)\delta(\tau_i - \tau_j) \tag{3.15}$$

where $\phi_h(\tau_i)$ represents the average channel output power as a function of the time delay τ_i.

We can further assume that the L different paths have the same normalized autocorrelation function, but different average powers. Let us denote the average power for the l-th path by $P(\tau_l)$. Then we have

$$P(\tau_l) = \phi_h(\tau_l) = \frac{1}{2}E[h^*(t,\tau_l)h(t,\tau_l)] \tag{3.16}$$

Here, $P(\tau_l)$, $l = 1, 2, \cdots, L$, represents the *power delay profile* of the channel.

The root mean square (rms) delay spread of the channel is defined as [35]

$$\tau_d = \sqrt{\frac{\sum_{l=1}^{L} P(\tau_l)\tau_l^2}{\sum_{l=1}^{L} P(\tau_l)} - [\frac{\sum_{l=1}^{L} P(\tau_l)\tau_l}{\sum_{l=1}^{L} P(\tau_l)}]^2} \tag{3.17}$$

In wireless communication environments, the channel power delay profile can be Gaussian, exponential or two-ray equal-gain [36]. For example, the two-ray equal-gain profile can be represented by

$$P(\tau) = \frac{1}{2}(\delta(\tau) + \delta(\tau - 2\tau_d)) \tag{3.18}$$

where $2\tau_d$ is the delay difference between the two paths and τ_d is the rms delay spread. We can further denote the delay spread normalized by the symbol duration T_s by $\bar{\tau}_d = \frac{\tau_d}{T_s}$.

3.1.4 Time-variant Fading Channels

3.1.4.1 Correlation Function of Wireless Channels

We briefly describe the wireless channel statistics, emphasizing the separation property of the spaced-time and spaced-frequency correlation function of a wireless channel. The complex baseband representation of a wireless channel impulse response has the form [37] [38]

$$h(l,t,\tau) = \sum_{l=0}^{L-1} a_l(t)\delta(\tau - \tau_l) \tag{3.19}$$

where L is the number of paths, τ_l is the delay of the lth path, and $a_l(t)$ is a wide-sense stationary (WSS) narrowband complex Gaussian process, which is independent for different paths. We assume that $a_l(t)$ has the same normalized correlation function $r_t(\Delta t)$ for all l. Hence, the autocorrelation function of the amplitude is

$$r_{a_l}(\Delta t) = \frac{1}{2}E\{a_l(t+\Delta t)a_l^*(t)\} = \sigma_l^2 \tilde{r}_t(\Delta t) \tag{3.20}$$

where σ_l^2 is the average power of the lth path and the superscript $*$ denotes the complex conjugate. From Eqn. 3.19, we can get the frequency response of the time-varying channel

$$H(t,f) = \int_{-\infty}^{+\infty} h(l,t,\tau)e^{-j2\pi f\tau}d\tau = \sum_{l=0}^{L-1} a_l(t)e^{-j2\pi f\tau_l} \tag{3.21}$$

Then, the correlation function of the channel frequency response is given by

$$\begin{aligned}
\tilde{r}_H(\Delta t, \Delta f) &= \frac{1}{2}E\{H(t+\Delta t, f+\Delta f)H^*(t,f)\} \\
&= \sum_{k=0}^{L-1}\sum_{l=0}^{L-1}\frac{1}{2}E\{a_l(t+\Delta t)a_l^*(t)\}e^{-j2\pi(f+\Delta f)\tau_k}e^{j2\pi f\tau_l} \\
&= \sum_{l=0}^{L-1} r_{c_l}(\Delta t)e^{-j2\pi\Delta f\tau_l} \\
&= \tilde{r}_t(\Delta t)(\sum_{l=0}^{L-1}\sigma_l^2 e^{-j2\pi\Delta f\tau_l}) \\
&= \tilde{r}_t(\Delta t)\cdot\tilde{r}_f(\Delta f)
\end{aligned} \tag{3.22}$$

where

$$\tilde{r}_f(\Delta f) = \sum_{l=0}^{L-1}\sigma_l^2 e^{-j2\pi\Delta f\tau_l} \tag{3.23}$$

where $\Delta f = 1/(NT)$ is the spacing between subcarriers, N and T are the number of subcarriers and the symbol duration of a sub-channel respectively. From Eqn. 3.22, we can see that the correlation function of $H(t,f)$ can be separated into product of the time-domain correlation $\tilde{r}_t(\Delta t)$ and frequency-domain correlation $\tilde{r}_f(\Delta f)$. The correlation in frequency domain depends on the multipath delay spread while the correlation in the time-domain depends on the velocity of a vehicle or, equivalently the Doppler spread.

If the wireless channel is time variant during an OFDM symbol period, the discrete correlation function for different blocks and tones can be written as

$$r_H(n,k) = r_t(n)\cdot r_f(k) \tag{3.24}$$

where

$$r_t(n) = \tilde{r}_t(nT_s) = J_0(2\pi f_{d,max}T_s n) \tag{3.25}$$

$$r_f(k) = \tilde{r}_f(k\Delta f) = \sum_{l=0}^{L-1}\sigma_l^2 e^{-j2\pi k\Delta fTl} \tag{3.26}$$

n and k denote the sample positions on the time and frequency domain respectively, $T_s = (K+G)T$ is the OFDM symbol period, $G(\geq L)$ are the length of guard interval, $f_{d,max}$ is the maximum Doppler frequency, $J_0(\cdot)$ is the zeroth-order Bessel function of the first kind, and the Fourier transform of the zeroth-order Bessel function is given by

$$P(f) = \begin{cases} \frac{1}{2\pi f_{d,max}} \cdot \frac{1}{\sqrt{1-(f/f_{d,max})^2}} & |f| < f_{d,max} \\ 0 & otherwise \end{cases} \tag{3.27}$$

where f_d is the Doppler frequency which is related to the velocity of a vehicle v and the carrier frequency f_c

$$f_d = \frac{v f_c}{c} \tag{3.28}$$

where c is the speed of the light.

3.1.4.2 Jakes' Model

The Jakes' model has been widely used to approximate isotropic scattering environments, which implements the channel as a superposition of a finite number of sinusoids. Consider a frequency-nonselective fading channel comprised of N propagation paths; the low-pass fading process is given by [39] and [40]

$$g(t) = E_0 \sum_{n=1}^{N} C_n exp[j(\omega_m t \cos\alpha_n + \phi_n)] \tag{3.29}$$

where E_0 is a scaling constant, C_n is the random path gain, α_n and ϕ_n are two independent random variables uniformly distributed between $[0, 2\pi)$, representing the angle of the incoming wave and initial phase associated with the nth propagation path, and ω_m is the radian Doppler frequency given by $\omega_m = 2\pi f_m$.

Assuming that C_n is real valued, Eqn. 3.29 can be written as

$$g(t) = g_c(t) + j g_s(t) \tag{3.30}$$

$$g_c(t) = E_0 \sum_{n=1}^{N} C_n \cos(\omega_m t \cos\alpha_n + \phi_n) \tag{3.31}$$

$$g_s(t) = E_0 \sum_{n=1}^{N} C_n \sin(\omega_m t \cos\alpha_n + \phi_n) \tag{3.32}$$

The central limit theorem justifies that $g_c(t)$ and $g_s(t)$ can be approximated as Gaussian random processes for large N.

Based on Clarke's model in Eqn. 3.30, Eqn. 3.31 and Eqn. 3.32, Jakes derived his well-known simulation model for Rayleigh fading channels [40] to reduce the number of distinct Doppler frequency shifts, by selecting

$$E_0 = \sqrt{2} \tag{3.33}$$

$$C_n = \frac{1}{\sqrt{N}} \tag{3.34}$$

$$\alpha_n = \frac{2\pi n}{N}, \quad n = 1, 2, \cdots, N \tag{3.35}$$

$$\phi_n = 0 \tag{3.36}$$

$$N_o = \frac{N-2}{4} \tag{3.37}$$

Thus the base-band equivalent fading channel can be constructed through only $(N_o + 1)$ low frequency oscillators. The output signal of Jakes' model in terms of quadrature components can be expressed as

$$g(t) = g_c(t) + j g_s(t) \tag{3.38}$$

where

$$g_c(t) = \frac{2}{\sqrt{2}} \cos(\omega_m t + \phi_{N_o+1}) \cos(\alpha) + 2 \sum_{n=1}^{N_o} \cos(\omega_n t + \phi_n) \cos(\beta_n) \tag{3.39}$$

and

$$g_s(t) = \frac{2}{\sqrt{2}} \cos(\omega_m t + \phi_{N_o+1}) \sin(\alpha) + 2 \sum_{n=1}^{N_o} \cos(\omega_n t + \phi_n) \sin(\beta_n) \tag{3.40}$$

where, $f_n = f_m \cos(2\pi n/N)$, $n = 1, 2, \cdots, N_o$ represents the Doppler shift of the nth component, $\omega_n = 2\pi f_n$, $\omega_m = 2\pi f_m$, $\alpha = 0$ or $\pi/4$ and $\beta_n = \pi n/(N_o + 1)$, $n = 1, 2, \cdots, N_o$.

3.2 Orthogonal Frequency Division Multiplexing

3.2.1 An Overview of OFDM

It is well known that Chang proposed the original OFDM principles in 1966 [41]. In OFDM systems, subcarriers overlap with neighbourhood subcarriers, and orthogonality can still be

preserved through the staggered QAM (SQAM) technique. As more subcarriers are required, the modulation, synchronization, and coherent demodulation become complex resulting in additional hardware cost. In 1971, Weinstein and Ebert proposed a modified OFDM system in which the discrete Fourier transform (DFT) was applied to generate the orthogonal subcarriers' waveforms [4]. Their scheme reduced the implementation complexity significantly, by making use of the IDFT modules and the digital-to-analog converters. In their proposed model, baseband signals were modulated by the inverse DFT (IDFT) in the transmitter and then demodulated by DFT in the receiver. Therefore, all the subcarriers were overlapped with each other in the frequency domain, while the DFT modulation still assured their orthogonality. Moreover, the windowing technique was introduced in this paper to mitigate the ISI and ICI problems.

The cyclic prefix (CP) or cyclic extension was first introduced by Peled and Ruiz in 1980 for OFDM systems [42]. In this scheme, a conventional null guard interval, which is used for combating the ISI, is substituted by a cyclic extension, in which the OFDM symbol is cyclically extended in the guard time. With the sacrifice of the transmitting energy efficiency, this scheme can result in the ISI reduction. Hence it has been adopted by the current IEEE standards, such as IEEE 802.16n. In 1980, Hirosaki [43] introduced an equalization algorithm to suppress both ISI and ICI, which may have resulted from a channel distortion, synchronization errors, or phase errors. In the meantime, Hirosaki also applied QAM modulation, pilot tone, and trellis coding techniques in his high-speed OFDM system, which operated in voice-band spectrum. In 1985, Cimini [44] introduced a pilot-based method to reduce the interference emanating from the multipath and co-channels. In 1989, Kalet [45] suggested a subcarrier-selective allocating scheme. He allocated more data to subcarriers near the center of the transmission frequency band; these subcarriers will suffer less channel distortion. In the 1990s, OFDM systems have been applied for high data rate communications.

In OFDM systems, a high rate data stream is divided into a number of lower rate data streams that are transmitted simultaneously over a number of subcarriers. Because the symbol duration increases for the lower-rate parallel subcarriers, the relative amount of dispersion in time caused by multipath delay spread is decreased. Inter-symbol interference is eliminated almost completely by introducing a guard time in every OFDM symbol. Thus, OFDM is resilient to frequency selective fading. OFDM has been adopted in several wireless standards and services, such as the Wi-Fi /IEEE 802.11 wireless local area network (WLAN) standard, the Wi-MAX/IEEE 802.16 wireless metropolitan area network (WMAN) standard, the

IEEE 802.20 mobile broadband wireless access (MBWA) standard, the IEEE 802.22 wireless regional area network (WRAN) standard, the 3GPP and 3GPP2 Long Term Evolution. In the IEEE 802.11 standard, the carrier frequency can go up as high as 2.4 GHz or 5 GHz. Researchers tend to pursue OFDM operating at even higher frequencies nowadays. For example, the IEEE 802.16 standard proposes carrier frequencies ranging from 10 GHz to 60 GHz.

3.2.2 An OFDM System Model

The system performance of high data rate wireless communication suffers from multipath propagation. The multipath fading introduces the frequency selectivity, which occurs when the signal bandwidth is larger than the coherence bandwidth of a channel. The multiple replicas of distorted transmitted signals result in ISI at a receiver. To overcome this effect, a parallel transmission system, such as OFDM, alleviates the ISI experienced with serial systems. In such systems, the spectrum of an individual data element occupies only a small portion of the available bandwidth, called a sub-channel. In parallel data systems, the total signal bandwidth is divided into N overlapping frequency sub-channels. These systems are less sensitive to delay spread. Furthermore, the parallel transmission system does not require complex channel estimation or equalization algorithms for frequency-selective channels because a frequency-selective channel is converted into a number of frequency non-selective sub-channels. For this reason, OFDM is a promising technique for high data rate wireless communications due to its robustness against frequency-selectivity and its better spectral efficiency.

Figure 3.3 shows the transmitter and receiver of an OFDM system model. An OFDM symbol consists of a sum of subcarriers that are modulated by using phase-shift keying (PSK) or quadrature amplitude modulation (QAM). The available bandwidth is divided into N sub-channels. After MPSK/QAM modulation, the coded information symbol on the kth subcarrier, denoted by $X(k)$, is sent to OFDM modulator, and $x'(n)$ represents the transmitted data on the nth time slot. The OFDM signals $x'(n)$ is given by

$$x'(n) = \mathit{IFFT}\{X(k)\} = \sum_{k=0}^{N-1} X(k) e^{\frac{j2\pi nk}{N}}, \qquad 0 \leq k \leq N-1 \tag{3.41}$$

In this thesis, we assume that the guard interval G is larger than the maximum expected delay

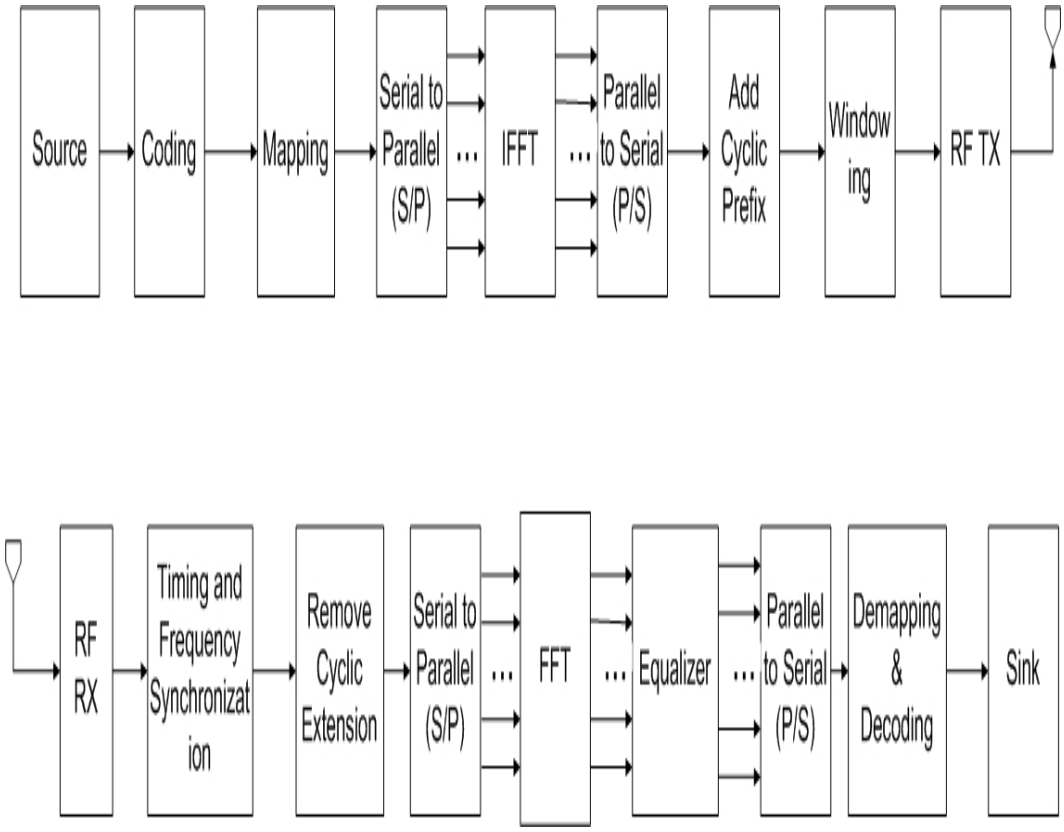

Figure 3.3: Block diagram of an OFDM transceiver

spread, such that multipath components from the previous symbol cannot interfere with the next symbol. Moreover, the guard interval should be chosen as the replica of the data at the end of the OFDM symbol. This ensures that the entire OFDM symbol with delayed replicas is always within the FFT interval, as long as the delay spread is smaller than the guard time. As a result, multipath signals with delays smaller than the guard time cannot cause ISI. x is the transmitted symbol with cyclic prefix vector of length G, given by

$$x(n) = \begin{cases} x'(n-G+N) & 0 \leq n \leq G-1 \\ x'(n-G) & G \leq n \leq N+G-1 \end{cases} \tag{3.42}$$

$T_s = \frac{T}{N+G}$ is the sampling period where T is the time duration of one OFDM symbol after inserting the guard interval. Assuming the multipath fading channel consists of L discrete paths, let $h(n,l)$ represent the nth sample of the lth channel path, and the received signal can

be written as

$$\begin{aligned} y(n) &= \sum_{l=0}^{L-1} h(n,l)x(n-l) + \omega(n) \\ &= h(n,0)x(n) + \cdots + h(n,L-1)x(n-L+1) + \omega(n) \end{aligned} \tag{3.43}$$

where $\omega(n)$ represents the additive white Gaussian noise (AWGN) at time n. If the channel is constant during the OFDM symbol period, $Y(k)$, the FFT of received symbol $y(n)$, can be written as

$$\begin{aligned} Y(k) &= \mathit{FFT}\{y(n)\} \\ &= \sum_{n=0}^{N-1}\{\sum_{l=0}^{L-1} h(l)x(n-l)\}e^{\frac{j2\pi nk}{N}} + + \sum_{n=0}^{N-1} \omega(n)e^{\frac{j2\pi nk}{N}} \\ &= H(k)X(k) + W(k) \end{aligned} \tag{3.44}$$

where $H(k)$ and $W(k)$ denote the FFT of $h(n,l)$ and $\omega(n)$. As can be seen from this equation, the convolution between transmitted symbol and the channel results in the simple multiplication relationship when processing the received OFDM symbol due to the cyclic prefix. The effect of the delay spread appears as a multiplication in the frequency domain according to the convolution theorem. This feature is very attractive for high delay spread applications as it removes the need to perform complex time-domain equalization.

3.3 Iterative Detection in MIMO-OFDM Systems

The block diagram of a MIMO-OFDM system transmitter is shown in Figure 3.4. In this part, the mathematical description of each step is given for both transmitter and receiver. At the transmitter side, the source bitstreams are first encoded by encoders and then mapped to a symbol stream by the digital MPSK/QAM modulator. Spatial multiplexing is a MIMO technique in which independent multiple symbol streams are transmitted at the same frequency band over different spatial channels. Pilot symbols for channel estimation are inserted in the frequency domain before OFDM modulation. The modulation of OFDM could be efficiently implemented by using IFFT. A cyclic prefix is usually appended to each OFDM symbol to avoid ISI due to the effect of multipath delay spread. Finally the symbol streams are converted from parallel to serial form and allocated to corresponding transmitters for transmission.

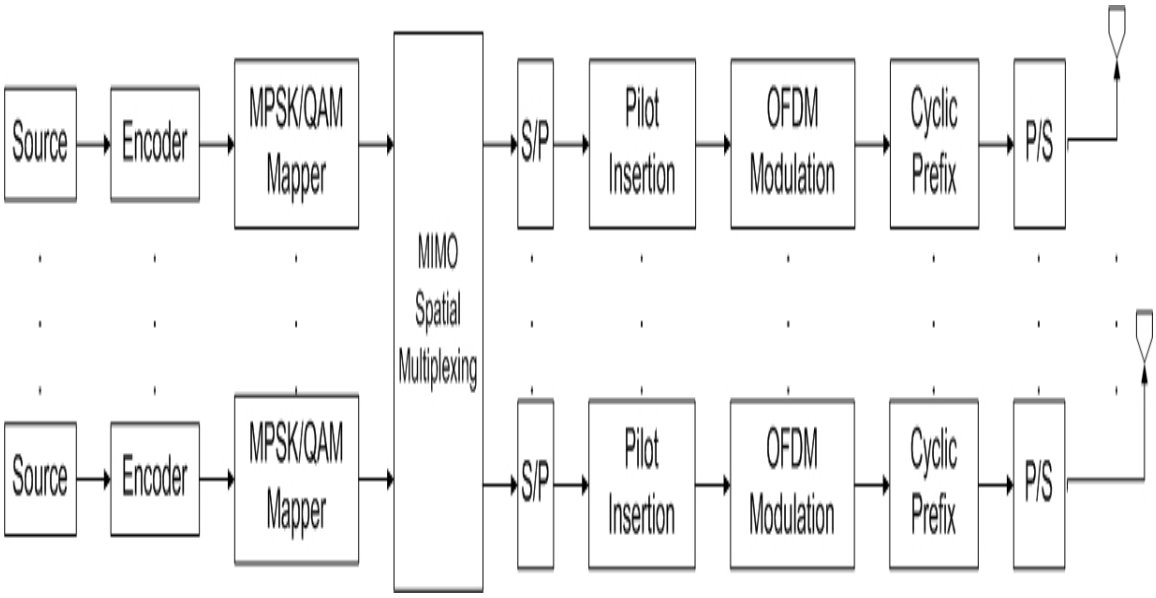

Figure 3.4: Block diagram of a MIMO-OFDM transmitter

Now we consider the MIMO-OFDM system with M_T transmit antennas and M_R receive antennas. The information signals from the sources are encoded by encoders, and then modulated into MPSK or QAM symbols. After the spatial interleaving [33], pilot tone signals are inserted into each symbol for channel estimation before OFDM modulation. $X_p(n)$ denote the information symbol sent by the pth transmit antenna at the nth subcarrier, given by

$$\mathbf{X}_p = [X_p(0), X_p(1), \ldots, X_p(N-1)]^T \tag{3.45}$$

where N is the number of subcarriers for one OFDM symbol.

After performing the inverse Fast Fourier Transform (IFFT) on each transmit antenna, the modulated signal on the pth transmit antenna can be expressed as follows

$$\mathbf{x}'_p = \mathbf{F}^H \mathbf{X}_p = [x'_p(0), x'_p(1), \ldots, x'_p(N-1)]^T \tag{3.46}$$

where $\mathbf{F}$ is $N \times N$ FFT matrix, given by

$$\mathbf{F} = \begin{bmatrix} 1 & 1 & \cdots & 1 \\ 1 & e^{-j\frac{2\pi}{N}} & \cdots & e^{-j\frac{2\pi(N-1)}{N}} \\ \vdots & \vdots & \ddots & \vdots \\ 1 & e^{-j\frac{2\pi(N-1)}{N}} & \cdots & e^{-j\frac{2\pi(N-1)(N-1)}{N}} \end{bmatrix} \tag{3.47}$$

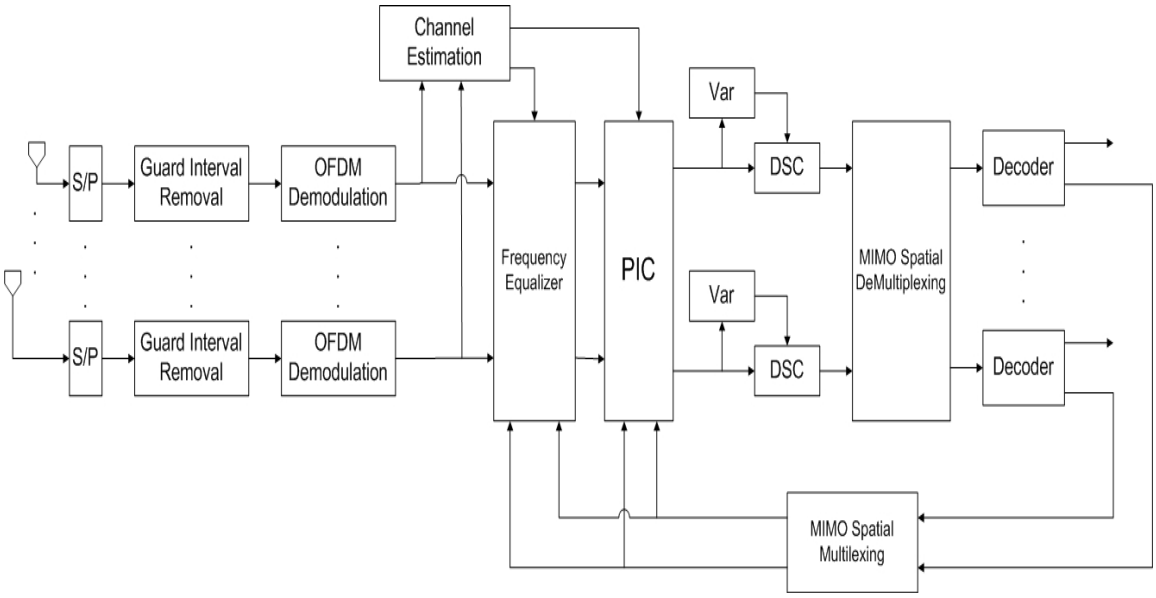

Figure 3.5: Block diagram of a MIMO-OFDM iterative receiver

In order to combat ISI resulted form the multipath delay of the channel, a guard interval G, which is greater than the expected maximum time delay ν, is inserted in each OFDM symbol:

$$x_p(n) = \begin{cases} x'_p(n-G+N) & 0 \leq n \leq G-1 \\ x'_p(n-G) & G \leq n \leq N+G-1 \end{cases} \tag{3.48}$$

Then, the entire OFDM symbols are transmitted through the fading channels. In this Chapter, we assume that the multipath fading channel, denoted by $h_{p,q}(l)$, is constant during an OFDM block, and varies from block to block. Hence, the received signal at receive antenna q and time n can be represented as

$$r_q(n) = \sum_{p=1}^{M_T} \sum_{l=0}^{L-1} h_{p,q}(l) x_p(n-l) + \omega_q(n) \tag{3.49}$$

where $h_{p,q}(l)$ is the lth resolvable path between the pth transmit antenna and qth receive antenna, L is the number of paths of fading channels, and $\omega_q(n)$ is the additive white Gaussian noise (AWGN).

At the receiver side, the cyclic prefix is removed. Then, the OFDM symbols in the frequency

domain for the qth receive antenna and the kth subcarrier can be obtained by performing FFT

$$\begin{aligned} R_q(k) &= FFT[r_q(n)] \\ &= \sum_{n=0}^{N-1}[\sum_{p=1}^{M_T}\sum_{l=0}^{L-1} h_{p,q}(l)x_p(n-l) + \omega_q(n)]e^{-j2\pi\frac{nk}{N}} \\ &= \sum_{p=1}^{M_T} H_{p,q}(k)X_p(k) + W_q(k) \end{aligned} \tag{3.50}$$

where $W_q(k)$ is the AWGN in frequency domain, $H_{p,q}(k)$ denotes the channel state information in the frequency domain, given by

$$H_{p,q}(k) = \frac{1}{N}\sum_{l=0}^{N-1} h_{p,q}(l)e^{-j2\pi lk/N} \tag{3.51}$$

For the qth receive antenna, Eqn. 3.50 can be represented in a matrix form as

$$\mathbf{R}_q = \sum_{p=1}^{M_T} \mathbf{H}_{p,q}\mathbf{X}_p + \mathbf{W}_q \tag{3.52}$$

where $\mathbf{R}_q = [R_q(0), R_q(1), \cdots, R_q(N-1)]^T$, $\mathbf{X}_p = [x_p(0), x_p(1), \cdots, x_p(N-1)]^T$, and $\mathbf{H}_{p,q}$ is given by

$$\mathbf{H}_{p,q} = \begin{bmatrix} H_{p,q}(0) & 0 & \cdots & 0 \\ 0 & H_{p,q}(1) & \ddots & \vdots \\ \vdots & \ddots & \ddots & 0 \\ 0 & \cdots & 0 & H_{p,q}(N-1) \end{bmatrix} \tag{3.53}$$

For all M_R receive antennas, the received signals can be expressed as

$$\mathbf{R} = \mathbf{H}\mathbf{X} + \mathbf{W} \tag{3.54}$$

where $\mathbf{R} = [\mathbf{R}_1, \cdots, \mathbf{R}_{M_R}]^T$, $\mathbf{X} = [\mathbf{X}_1, \cdots, \mathbf{X}_{M_T}]^T$, and $\mathbf{W} = [\mathbf{W}_1, \cdots, \mathbf{W}_{M_R}]^T$, respectively. $\mathbf{H}$ is the channel matrix consisting of $\mathbf{H}_{p,q}$, given by

$$\mathbf{H} = \begin{pmatrix} \mathbf{H}_{1,1} & \cdots & \mathbf{H}_{M_T,1} \\ \vdots & \ddots & \vdots \\ \mathbf{H}_{1,M_R} & \cdots & \mathbf{H}_{M_T,M_R} \end{pmatrix} \tag{3.55}$$

At the receiver side, shown in Figure 3.5, the guard interval of each OFDM symbol is first removed. The demodulation of OFDM could be implemented by using FFT. Then the pilot symbols will be used to estimate the channel state information (CSI). The estimated channel will be used to update the outputs of the frequency equalizer and the parallel interference canceler iteratively. Before detecting the received signal, the intercarrier interference must be mitigated by the frequency domain equalizer. The detector provides joint soft-decision estimates of the M_T transmitted symbol sequences. Each of the detected sequences is decoded by a separate channel decoder with soft inputs/outputs. At each iteration, the decoder soft outputs are used as estimates of the transmitted signals.

An important factor that determines the complexity of the receiver is the detector. For this reason, we use a standard parallel interference canceler (PIC-STD) and its improved version known as PIC with decision statistics combiner (PIC-DSC). These detectors are chosen because they offer a good performance-complexity trade-off, particularly when the number of transmit antennas is high and the optimal joint detection and decoding becomes impractical.

3.3.1 Iterative Detection with PIC-STD

A block diagram of a PIC-STD system is shown in Figure 3.6. The convolutional codes with BPSK modulation are used in each layer. Before the received signals are transformed into the frequency domain by FFT, the cyclic prefix is removed. In the first iteration, the PIC detectors are equivalent to a bank of matched filters. The detectors provide the decision statistics of the M_T transmitted symbol sequences. The outputs of the PIC detector for antenna p, denoted by

$$\mathbf{Y}_p^1 = [Y_p^1(0), Y_p^1(1), \cdots, Y_p^1(N-1)]^T \tag{3.56}$$

are obtained from

$$\mathbf{Y}_p^1 = \mathbf{h}_p^H \mathbf{R} \tag{3.57}$$

where $\mathbf{h}_p^H$ is the pth row of matrix $\mathbf{H}^H$, which is defined as

$$\mathbf{H}^H = \begin{pmatrix} \mathbf{H}_{1,1}^H & \cdots & \mathbf{H}_{1,M_R}^H \\ \vdots & \ddots & \vdots \\ \mathbf{H}_{M_T,1}^H & \cdots & \mathbf{H}_{M_T,M_R}^H \end{pmatrix} \tag{3.58}$$

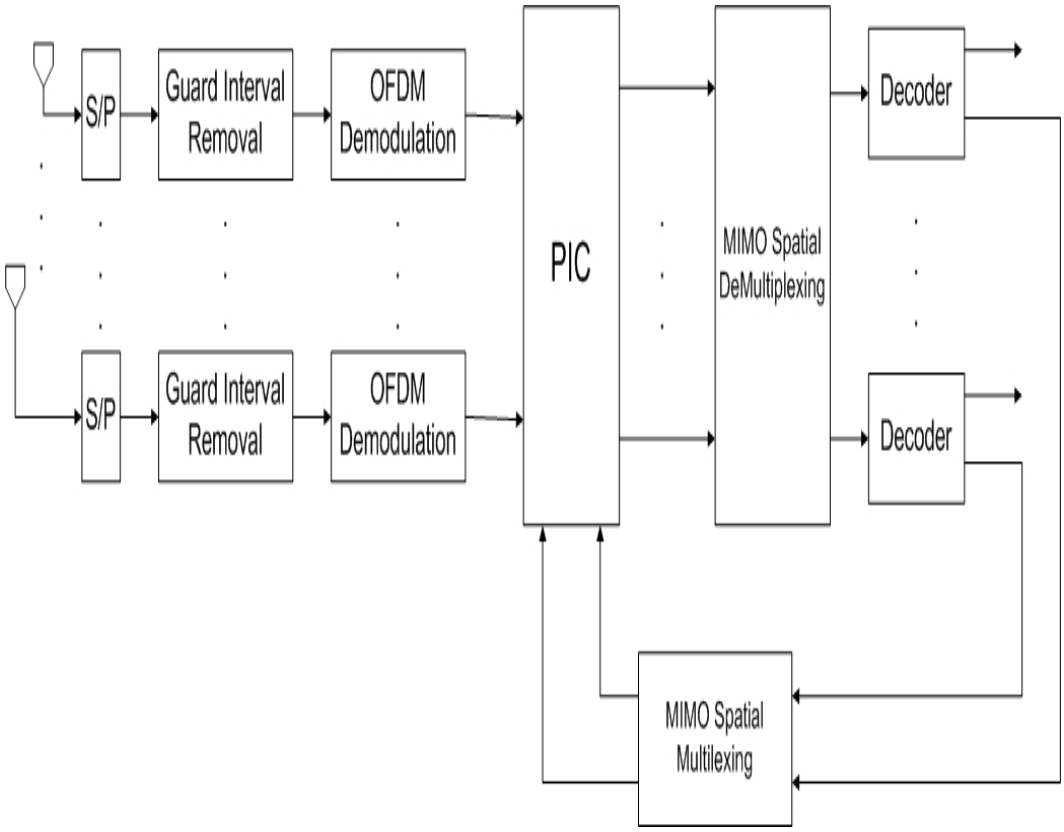

Figure 3.6: Block diagram of a MIMO-OFDM iterative receiver with PIC-STD

The decision statistics are then passed to respective decoders, which generate soft estimations of the transmitted symbols.

In the second and later iterations, the soft outputs from the decoders are used to update PIC detector with a decision statistics combiner. The decision statistics for the pth transmit antenna in the kth iteration denoted by $\mathbf{Y}_p^k$, are given by

$$\mathbf{Y}_p^k = \mathbf{h}_p^H(\mathbf{R} - \mathbf{H}\underline{\widehat{\mathbf{X}}}^{k-1}) \tag{3.59}$$

where $\underline{\widehat{\mathbf{X}}}^{k-1}$ is the transmitted symbol estimate vector in the $(k-1)$th iteration, with the elements corresponding to the pth transmit antenna set to zeros. It can be written as

$$\underline{\widehat{\mathbf{X}}}^{k-1} = [\widehat{\mathbf{X}}_1^{k-1}, \cdots, \widehat{\mathbf{X}}_{p-1}^{k-1}, \mathbf{0}, \widehat{\mathbf{X}}_{p+1}^{k-1}, \cdots, \widehat{\mathbf{X}}_{M_T}^{k-1}]^T \tag{3.60}$$

The detection outputs for the pth transmit antenna for a whole block of transmitted symbols form a vector $\mathbf{Y}_p^k$, which is interleaved and then passed to the pth decoder. The soft estimates

of the transmitted BPSK symbols are calculated at the detector output as follows

$$\hat{X}_p^k(n) = 1 \cdot P(X_p^k(n) = 1|\mathbf{Y}_p^k) + (-1) \cdot P(X_p^k(n) = -1|\mathbf{Y}_p^k) \tag{3.61}$$

where $\mathbf{Y}_p^k$ is a vector of detector outputs for the transmit antenna p and $P(X_p^k(n) = j|\mathbf{Y}_p^k)$, $j = 1, -1$, are the symbol a posteriori probabilities (APP) calculated by the decoder in the kth iteration. Let $\lambda_p^k(n)$ be the log-likelihood ratios (LLR) in the kth iteration for the transmit antenna p, at time n, defined as

$$\lambda_p^k(n) = \log \frac{P(X_p^k(n) = 1|\mathbf{Y}_p^k)}{P(X_p^k(n) = -1|\mathbf{Y}_p^k)} \tag{3.62}$$

Thus, the symbol a posteriori probabilities $P(X_p^k(n) = j|\mathbf{Y}_p^k)$, $j = 1, -1$, can then be calculated by $\lambda_p^k(n)$ as follows

$$P(X_p^k(n) = 1|\mathbf{Y}_p^k) = \frac{e^{\lambda_p^k(n)}}{1 + e^{\lambda_p^k(n)}} \tag{3.63}$$

$$P(X_p^k(n) = -1|\mathbf{Y}_p^k) = \frac{1}{1 + e^{\lambda_p^k(n)}} \tag{3.64}$$

By combining Eqn. 3.61, Eqn. 3.63 and Eqn. 3.64, the symbol estimates can be determined by

$$\hat{X}_p^k(n) = \frac{e^{\lambda_p^k(n)} - 1}{e^{\lambda_p^k(n)} + 1} \tag{3.65}$$

When the LLR is calculated on the basis of the a posteriori probabilities, it is obtained as

$$\lambda_p^k(n) = \log \frac{\sum_{m,m'=M_s-1}^{m,m'=0,X_p(n)=1} \alpha_{j-1}(m') p_n(X_p(n) = 1) exp(-\frac{\sum_{l=(j-1)d}^{jd}(Y_p^k(n) - X_p(n))^2}{2(\sigma_p^k)^2}) \beta_j(m)}{\sum_{m,m'=M_s-1}^{m,m'=0,X_p(n)=1} \alpha_{j-1}(m') p_n(X_p(n) = -1) exp(-\frac{\sum_{l=(j-1)d}^{jd}(Y_p^k(n) - X_p(n))^2}{2(\sigma_p^k)^2}) \beta_j(m)} \tag{3.66}$$

where $\lambda_p^k(n)$ denotes the LLR ratio for the pth symbol within the jth codeword transmitted at the subcarrier $n = (j-1)d + p$ and d is the code symbol length. m' and m are the pair of states connected in the trellis; $X_p(n)$ is the nth BPSK modulated symbol in a code symbol connecting the states m' and m; $Y_p^k(n)$ is the detector output in iteration k for antenna p at time n; $(\sigma_p^k)^2$ is the noise variance for transmit antenna p and iteration k; M_s is the number of states in the trellis and $\alpha(m')$ and $\beta(m)$ are the feed-forward and feedback recursive variables, defined as for LLR.

3.3.2 Iterative Interference Canceler with DSC

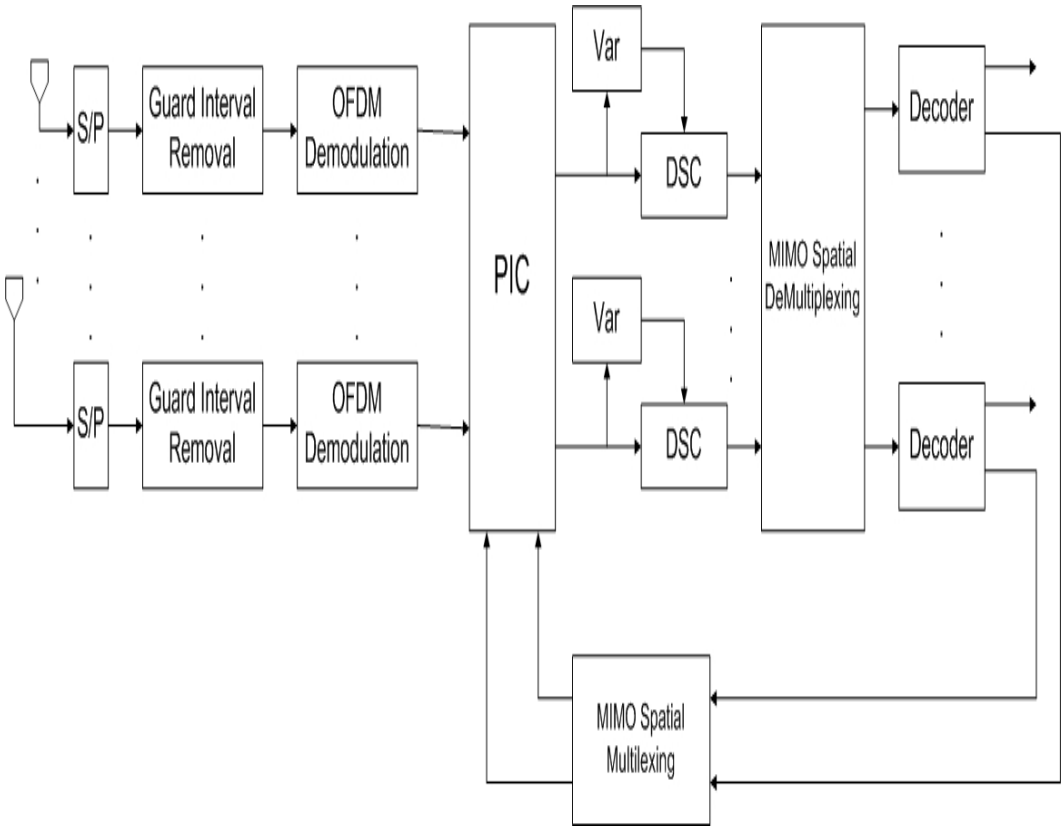

Figure 3.7: Block diagram of a MIMO-OFDM iterative receiver with PIC-DSC

In computing the LLR value in Eqn. 3.66 the decoder uses two inputs. The first input is the decision statistics $Y_p^k(n)$, which depends on the transmitted signal $X_p(n)$. The second input is the a priori probability on the transmitted signal $X_p(n)$, which computes as

$$p_n(X_p(n) = l) = \frac{1}{\sqrt{2\pi}\sigma} e^{-\frac{(Y_p^k(n) - l\mu_p)^2}{2\sigma^2}}, \quad l = 1, -1 \tag{3.67}$$

where μ_p is the mean of received amplitude after matched filtering, given by

$$\mu_p = \frac{1}{N} \sum_{n=0}^{N-1} v_p(n) \tag{3.68}$$

where $v_p(n)$ is an element in the vector $\mathbf{v}_p$, given by $\mathbf{v}_p = diag\{\mathbf{h}_p^H \mathbf{h}_p\}$. When the LLR is calculated on the basis of the APPs, the decision statistics mean value, conditional on $X_p(n)$, is biased due to the correlation of the two inputs of decoder and the bias has always a sign

opposite of $X_p(n)$. That is, the bias reduces the useful signal term and degrades the system performance. This bias is particularly significant for a large number of interferers.

The bias effect can be eliminated by estimating the mean of the transmitted symbols based on the a posteriori extrinsic information ratio (EIR) instead of LLR. The EIR does not include the metric for the symbol $X_p(n)$ that is being estimated. That is

$$\lambda_{p,e}^k(n) = \log \frac{\sum_{m,m'=M_s-1}^{m,m'=0,X_p(n)=1} \alpha_{j-1}(m')p_n(X_p(n)=1)exp(-\frac{\sum_{l=(j-1)d,l\neq t}^{jd}(Y_p^k(l)-X_p(l))^2}{2(\sigma_p^k)^2})\beta_j(m)}{\sum_{m,m'=M_s-1}^{m,m'=0,X_p(n)=1} \alpha_{j-1}(m')p_n(X_p(n)=-1)exp(-\frac{\sum_{l=(j-1)d,l\neq t}^{jd}(Y_p^k(l)-X_p(l))^2}{2(\sigma_p^k)^2})\beta_j(m)} \tag{3.69}$$

where $\lambda_{p,e}^k(n)$ denotes the EIR ratio for the pth symbol transmitted at subcarrier $n = (j-1)d + p$ and within the jth codeword, d is the code symbol length, $\alpha(m')$ and $\beta(m')$ are defined as for the LLR [30]. However, excluding the contribution of the bit of interest when estimating the mean of the transmitted symbols reduces the output SNR, leading again to a degraded system performance. A decision statistics combiner (DSC) method is effective in minimizing these effects. In the iterative parallel interference canceller with decision statistics combiner (PIC-DSC) [46], shown in Figure 3.7, a DSC module is added to the PIC-STD structure. The decision statistics of the PIC-DSC is obtained at the DSC output, generated as a weighted sum of the current PIC output and the DSC output from the previous operation. The weighting coefficients are estimated by maximizing the output signal-to-interference-plus-noise-ratio (SINR). In each stage, except in the first one, the PIC output for transmit antenna p and stage k, denoted by $Y_p^k(n)$, is passed to the DSC module. The DSC module performs recursive linear combining of the detector output in iteration k for the transmit antenna p, denoted by $Y_p^k(n)$, with the DSC output from the previous iteration for the same layer, denoted by $Y_{p,c}^{k-1}(n)$. The output of the decision statistics combiner, in iteration k and for transmit antenna p, denoted by $Y_{p,c}^k(n)$, is given by

$$Y_{p,c}^k(n) = p_1^{p,k} Y_p^k(n) + p_2^{p,k} Y_{p,c}^{k-1}(n) \tag{3.70}$$

where $p_1^{p,k}$ and $p_2^{p,k}$ are the DSC weighting coefficients in stage k, respectively. They are estimated by maximizing the signal-to-noise-plus-interference-ratio at the output of DSC in iteration k under the assumption that $Y_p^k(n)$ and $Y_{p,c}^{k-1}(n)$ are Gaussian random variables

with the conditional means μ_p^k and $\mu_{p,c}^{k-1}$, given that $X_p(n)$ is the transmitted symbol for antenna p, and variances $(\sigma_p^k)^2$ and $(\sigma_{p,c}^k)^2$, respectively. The maximization of SINR with respect to $p_1^{p,k}$ and $p_2^{p,k}$ yields linearly dependant solutions for these coefficients. Thus, these coefficients can be normalized in the following way

$$E[Y_{p,c}^k(n)] = p_1^{p,k}\mu_p^k + p_2^{p,k}\mu_{p,c}^{k-1} = 1 \tag{3.71}$$

At the first iteration, the output of the PIC-STD and PIC-DSC layer are same. That is

$$Y_{p,c}^1(n) = Y_p^1(n) \tag{3.72}$$

The SINR at the output of the DSC for transmit antenna p and in iteration k is then given by

$$SINR^{p,k} = \frac{1}{(p_1^{p,k})^2(\sigma_p^k)^2 + 2p_1^{p,k}(\frac{1-p_1^{p,k}\mu_p^k}{\mu_{p,c}^{k-1}})\rho_{k,k-1}^p\sigma_p^k\sigma_{p,c}^{k-1} + (\frac{1-p_1^{p,k}\mu_p^k}{\mu_{p,c}^{k-1}})^2(\sigma_{p,c}^{k-1})^2} \tag{3.73}$$

where $\rho_{k,k-1}^p$ is the correlation coefficient between the detector output in kth and $(k-1)$th

$$\rho_{k,k-1}^p = \frac{E[(Y_p^k(n) - \mu_p^k x_p(n))(Y_{p,c}^{k-1}(n) - \mu_{p,c}^{k-1}X_p(n))|X_p(n)]}{\sigma_p^k\sigma_{p,c}^{k-1}} \tag{3.74}$$

The optimal combining coefficient is given by

$$p_1^{p,k}{}_{opt} = \frac{\frac{\mu_p^k}{(\mu_{p,c}^{k-1})^2}(\sigma_{p,c}^{k-1})^2 - \frac{1}{\mu_{p,c}^{k-1}}\rho_{k,k-1}^p\sigma_p^k\sigma_{p,c}^{k-1}}{(\sigma_p^k)^2 - 2\frac{\mu_p^k}{\mu_{p,c}^{k-1}}\rho_{k,k-1}^p\sigma_p^k\sigma_{p,c}^{k-1} + (\frac{\mu_p^k}{(\mu_{p,c}^{k-1})^2})^2(\sigma_{p,c}^{k-1})^2} \tag{3.75}$$

The parameters required for the calculation of the optimal combining coefficients in Eqn. 3.75 are difficult to estimate, apart from the signal variances. However, in a system with a large number of interferers, which happens when the number of the transmit antennas is large relative to the number of the receive antennas, and for the APP-based symbol estimates, the DSC inputs in the first few iterations are low correlated. Thus, it is possible to combine them, in a way similar to receive diversity maximum ratio combining. Under these conditions, the weighting coefficient in this receiver can be obtained from Eqn. 3.75 by assuming that the correlation coefficient is zero and neglecting the reduction of the received signal conditional mean caused by interference. The DSC coefficient are then given by

$$p_1^{p,k} = \frac{(\sigma_{p,c}^{k-1})^2}{(\sigma_{p,c}^{k-1})^2 + (\sigma_p^k)^2} \tag{3.76}$$

The DSC output, in the second and higher iterations, with coefficients from Eqn. 3.76 can be expressed as

$$Y_{p,c}^{k}(n) = \frac{(\sigma_{p,c}^{k-1})^2}{(\sigma_{p,c}^{k-1})^2 + (\sigma_p^k)^2} Y_p^k(n) + \frac{(\sigma_p^k)^2}{(\sigma_p^k)^2 + (\sigma_{p,c}^{k-1})^2} Y_{p,c}^{k-1}(n) \quad i > 1 \tag{3.77}$$

The complexity of both PIC-STD and PIC-DSC is linear in the number of transmit antennas.

3.4 Numerical Results

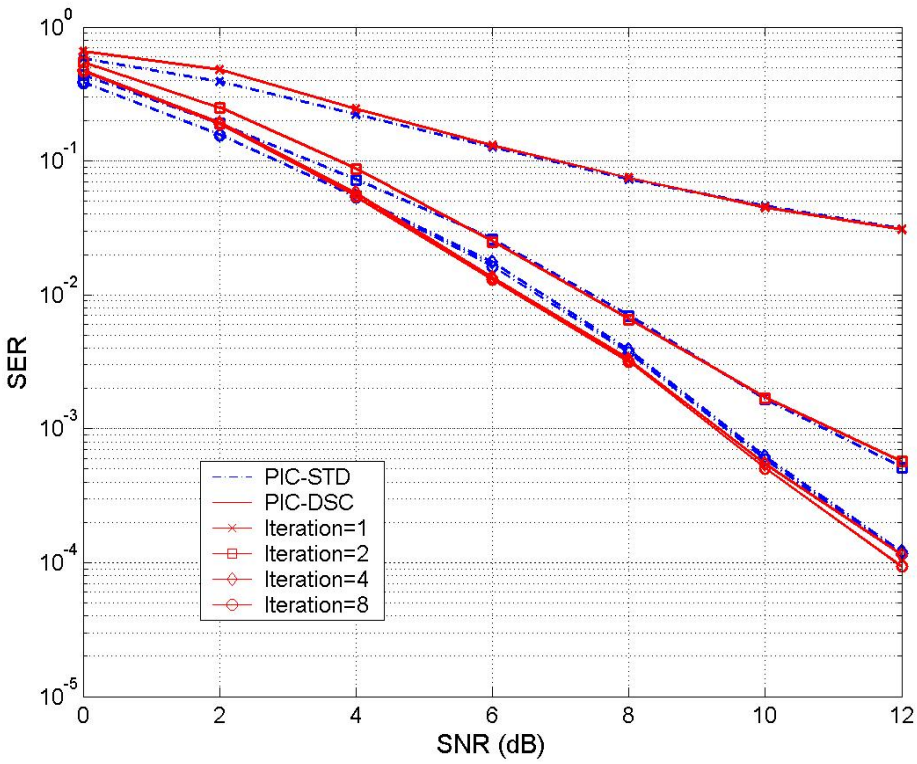

Figure 3.8: SER performance comparison of PIC-STD and PIC-DSC detection on Rayleigh fading with ($M_T = 2, M_R = 2$)

In this section, we demonstrate the system performance comparison of a proposed MIMO-OFDM iterative receiver with PIC-STD and PIC-DSC detection scheme. An $R = 1/2$, 4-state convolutional component code is chosen as the constituent code and the generator polynomial is (15,17) in octal form. The information length is $K = 130$ and block length

is $N = 256$. Before MIMO spatial multiplexing, the encoded symbols are modulated with BPSK modulation. The number of subcarrier is $N = 256$. The cyclic prefix is inserted into each OFDM symbol with length $G = \frac{1}{8}N$. The channel is modelled as a frequency-flat slow Rayleigh fading channel, which is known at the receiver. At the receiver side, the decoding is performed by a MAP algorithm. The simulation results are shown in the form of the symbol-error-rate (SER) versus signal-noise-ratio (SNR) E_b/N_0.

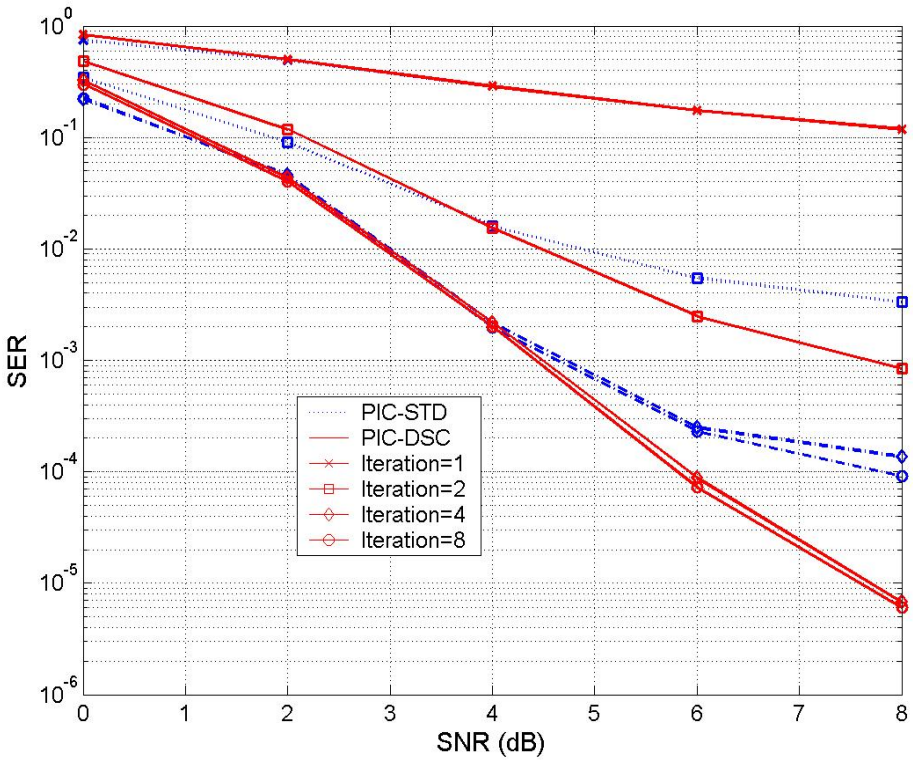

Figure 3.9: SER performance comparison of PIC-STD and PIC-DSC detection on Rayleigh fading with ($M_T = 4, M_R = 4$)

Figure 3.8 shows the SER performance between PIC-STD and PIC-DSC detection with $M_T = 2$ and $M_R = 2$. The performance of the PIC-DSC iterative receiver is slightly better than that of the PIC-STD iterative receiver after the 4th iteration.

Figure 3.9 shows the SER performance between PIC-STD and PIC-DSC detection with $M_T = 4$ transmit and $M_R = 4$ receive antennas. The performance of the PIC-DSC iterative receiver is much better than that of the PIC-STD iterative receiver after the 4th iteration when the SNR is $4dB$ or higher. With 8 iterations at SNR value of $8dB$, the error floor for

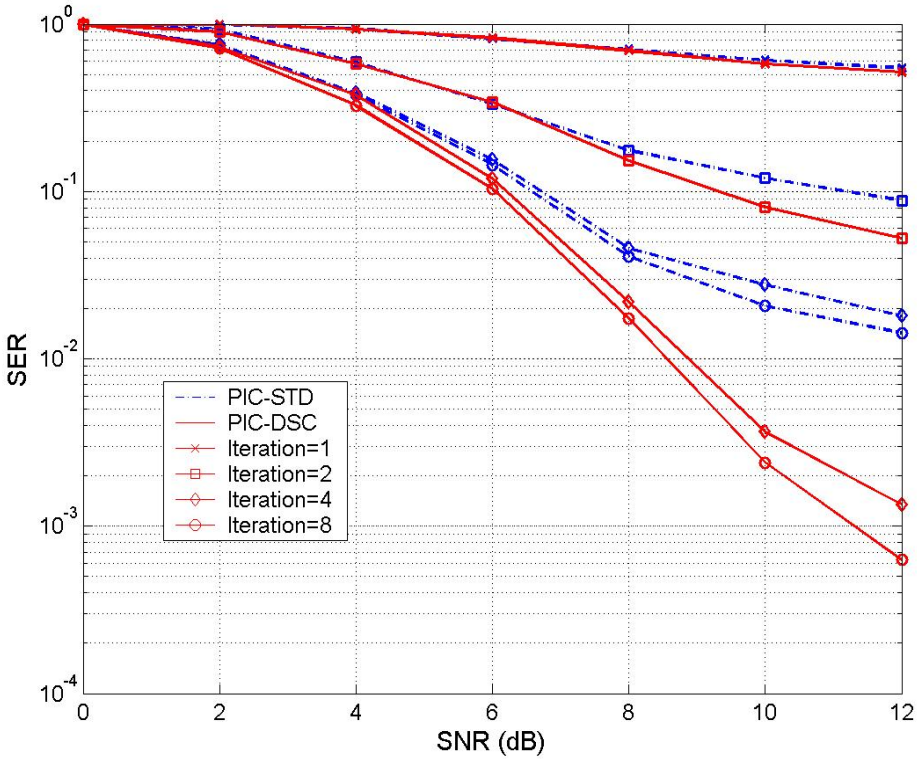

Figure 3.10: SER performance comparison of PIC-STD and PIC-DSC detection on Rayleigh fading with $(M_T = 4, M_R = 2)$

PIC-STD appears at SER of 10^{-4}. However, the PIC-DSC receiver has achieved the SER below 10^{-5}.

Figure 3.10 and Figure 3.11 compare the SER performance of PIC-STD and PIC-DSC receivers for $(M_T = 4, M_R = 2)$ and $(M_T = 6, M_R = 2)$. When the number of interferers becomes larger, the decision statistics mean value will be biased from the transmitted signals. This degrades the system performance. From these results, it is obvious that the performance of PIC-DSC receiver is much better than the performance of the PIC-STD receiver when the number of interfering layers relative to the number of receive antennas becomes higher, which means the decision statistics combining method is effective in minimizing the effect of bias.

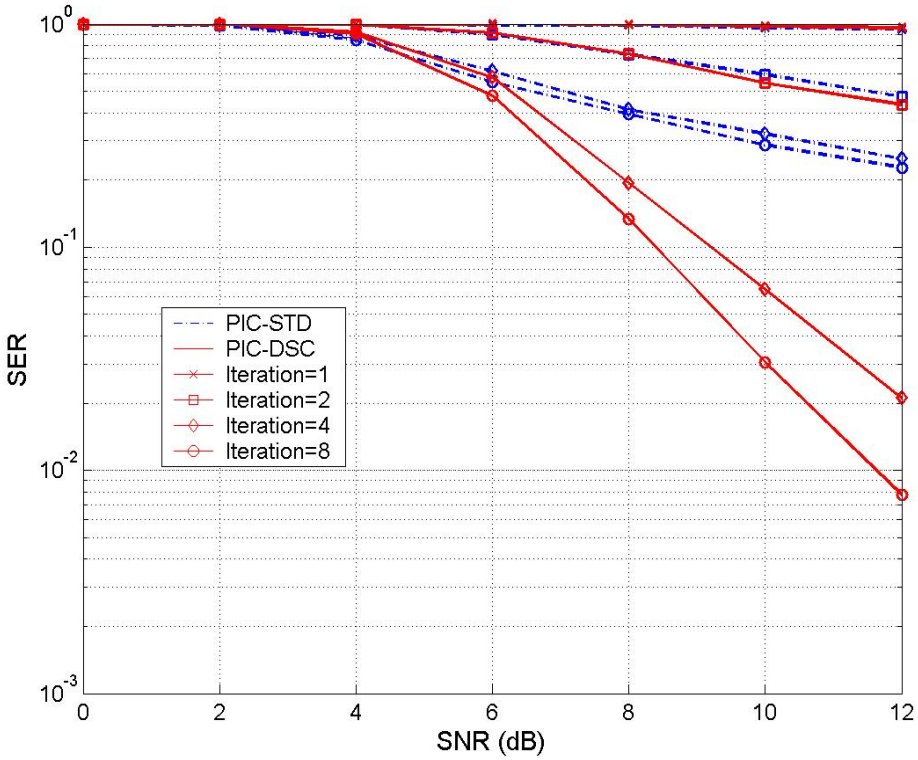

Figure 3.11: SER performance comparison of PIC-STD and PIC-DSC detection on Rayleigh fading with ($M_T = 6, M_R = 2$)

3.5 Summary

In this chapter, we first gave a brief introduction to wireless fading channel models. The principle of an OFDM system was described with a block diagram of a classic OFDM transmitter and receiver. Moreover, an OFDM system with multiple antennas, known as MIMO-OFDM system, was presented.

Then we investigated two iterative detection and decoding receivers using a convolutional code as the constituent code. A standard parallel interference canceler and an improved version of PIC with decision statistics combiner known as PIC-DSC, were used for iterative detection while maximum a posteriori probability (MAP) methods were applied for decoding. Perfect CSI was assumed known at the receiver.

Compared to the iterative receiver with PIC-STD detection, the improved PIC-DSC scheme

can dramatically improve the overall system performance when the number of interferers is larger than the number of receive antennas.

Chapter 4

Pilot-assisted Channel Estimation

4.1 Introduction

Channel state information is required in a MIMO-OFDM system for signal detection at receiver. Its accuracy directly affects the overall performance of MIMO-OFDM systems. In order to estimate the channel in high delay spread environments, pilot symbols should be inserted among subcarriers before transmission. These pilots should be placed equal-spaced in the frequency domain to minimize noise enhancement. To estimate the channel over all the subcarriers, different types of interpolators can be used. In this chapter, two interpolators are investigated: linear interpolator and trigonometric interpolator. To estimate the multipath channel, we propose a new interpolator that has a better system performance. It should be noted that the assumptions in this chapter are ideal synchronization and no mobility. The problems of intercarrier interference cancellation and channel estimation under the mobile scenarios will be discussed in the subsequent chapter.

4.2 Pilot-assisted Channel Estimation

In past years, pilot-assisted approaches have been widely used to estimate the channel properties and correct the received signal in multipath environments. Recently, the pilot tone-

and the pilot symbol-assisted transmission schemes have been proposed and attracted much attention [47–52]. In a pilot tone-assisted system, the receiver is provided with an explicit amplitude and phase reference through a pilot tone signal for data detection [47–50]. In a pilot symbol-assisted system, pilot symbols known at the receiver are inserted at the beginning of each OFDM symbol. At the receiver, these pilot symbols are used for the channel fading compensation [51, 52]. However, the receivers in these methods are required to store up data symbols before fading correction. As a result, a significant delay may be introduced by the correction process at the receiver.

For a system with only one transmit and receive antenna, known as SISO-OFDM, channel parameter estimation has been successfully used to improve the performance [27, 37, 53–56]. For systems with multiple transmit antennas, known as MIMO-OFDM, a channel estimator has been developed in [57] by exploiting the correlation of the channel parameters at different subcarrier frequencies. However, it requires the inversion of a large matrix to reduce the inter-antenna interference. Hence, a simplified channel estimator is desired to reduce the complexity.

In the rest of this chapter, we first analyze the pilot-assisted techniques that use linear and trigonometric interpolators. Then, we propose a new method of estimating multipath channels. The implementation of this method is straightforward and requires no storage at the receiver. Simulation results show that the proposed method has much better system performance compared with the other two interpolators.

4.3 Channel Estimation with Interpolators

We assume that the maximum expected length of channel delay spread is $\nu \leq G$, where G is the length of cyclic prefix. It can be shown that the number of pilot symbols required for channel estimation is $M \geq \nu + 1$ on every path from the transmitter to the receiver [58]. The total number of pilots for a MIMO-OFDM system is $M * \max\{M_T, M_R\}$, where M_T is the number of transmit antennas and M_R is the number of receive antennas. In MIMO-OFDM system, orthogonal matrix $\mathbf{P}$ can be used as pilot symbols, which is defined when

$$\mathbf{P}\mathbf{P}^T = \mathbf{I} \tag{4.1}$$

where $\mathbf{P}^T$ is the transpose of $\mathbf{P}$, and $\mathbf{I}$ is the identity matrix. Before OFDM modulation, M pilot symbols $s_{p,q}(1), s_{p,q}(2), \cdots, s_{p,q}(M)$ are inserted at the position of subcarriers $p(1), p(2), \cdots, p(M)$ for the pth transmit antenna and qth receive antenna. These M pilot tones are placed equally spaced on the frequency domain FFT grid, which is at subcarrier $p(i) = \frac{i \times N}{M}$ for $0 \leq i \leq M-1$. Then, the received pilot tones at $p(i)$ can be processed as

$$\mathbf{C}(p(i)) = \mathbf{R}(p(i))\mathbf{P}^H(\mathbf{P}\mathbf{P}^H)^{-1} \tag{4.2}$$

where $\mathbf{R}(p(i))$ is the matrix of the received signals at the $p(i)$ pilot tones, given by

$$\mathbf{R}(p(i)) = \begin{pmatrix} R_1(p(i)) & \cdots & R_1(p(i)+M_T) \\ \vdots & \vdots & \vdots \\ R_{M_R}(p(i)) & \cdots & R_{M_R}(p(i)+M_T) \end{pmatrix} \tag{4.3}$$

and $\mathbf{C}(p(i))$ is the matrix used for channel estimation

$$\mathbf{C}(p(i)) = \begin{pmatrix} C_{1,1}(p(i)) & \cdots & C_{1,M_T}(p(i)) \\ \vdots & \vdots & \vdots \\ C_{M_R,1}(p(i)) & \cdots & C_{M_R,M_T}(p(i)+M_T) \end{pmatrix} \tag{4.4}$$

For pth transmit antenna and qth receive antenna, an estimate of the channel at pilot tones can then be acquired as follows

$$\hat{H}_{p,q}(p(k)) = C_{p,q}(p(k)) = H_{p,q}(p(k)) + W_{p,q}(p(k)), \quad 0 \leq i \leq M-1 \tag{4.5}$$

where $C_{p,q}(p(k))$, $H_{p,q}(p(k))$ and $W_{p,q}(p(k))$ are the element in $\mathbf{C}(p(k))$ used for interpolation, the channel state information and the AWGN at the $p(k)$th subcarrier for the pth transmit antenna and the qth receive antenna in the frequency domain, respectively.

Some interpolators can be used to estimate the channel at subcarriers between the pilot tones. The complexity of these interpolators varies depending on the number of pilot tones used to estimate the channel at each subcarrier. In the following subsections, we will discuss two types of interpolators: linear and trigonometric interpolators. Then, we propose a new method, called the multi-tap method, to estimate multipath fading channels.

4.3.1 A Linear Interpolator

Linear interpolation, shown in Figure 4.1 can be used to estimate channels at all subcarriers. M Pilots for each transmit and receive antenna are first extracted from the received OFDM

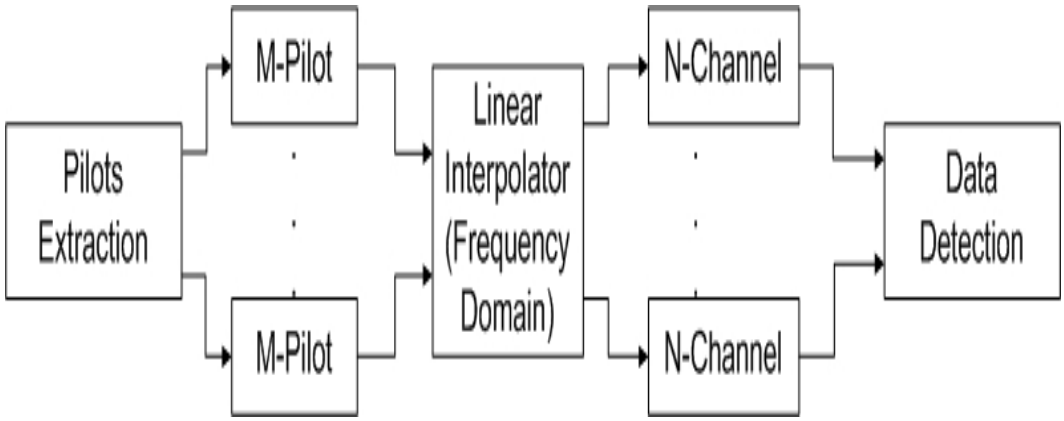

Figure 4.1: Block diagram of channel estimation with linear interpolator

symbols in the frequency domain. Then, the channel is estimated at each subcarrier by linear interpolation using only two adjacent pilots. Therefore, this interpolator has lower computational complexity compared with other interpolators in the following subsections.

The channel estimate for this interpolator can be calculated as follows

$$\hat{H}_{p,q}(m \cdot \frac{N}{M} + n) = \hat{H}_{p,q}(p(m)) + n \times \frac{\hat{H}_{p,q}(p(m+1)) - \hat{H}_{p,q}(p(m))}{N/M}$$
$$0 \leq n < \frac{N}{M}, \;\; 0 \leq m < M \tag{4.6}$$

where $\hat{H}_{p,q}(m \cdot \frac{N}{M} + n)$ is the channel estimate at the $(m \cdot \frac{N}{M} + n)$th subcarrier for the pth transmit antenna and the qth receive antenna in the frequency domain, $\hat{H}_{p,q}(p(m))$ and $\hat{H}_{p,q}(p(m+1))$ are the channel estimate at the $p(m)$th and the $p(m+1)$th subcarrier, respectively. Using these two adjacent channel estimates, the estimated channel state information $\hat{H}_{p,q}(m \cdot \frac{N}{M} + n)$ between the $p(m)$th and the $p(m+1)$th subcarriers are calculated by the linear interpolation.

4.3.2 A Trigonometric Interpolator

After pilots are extracted from the received signal in the frequency domain, IFFT on a signal block of length M is performed. The time domain channel estimate, $\hat{h}_{p,q}(n)$, is

$$\hat{h}_{p,q}(n) = \frac{1}{\sqrt{M}} \sum_{k=0}^{k=M-1} \hat{H}_{p,q}(p(k)) e^{\frac{j2\pi nk}{M}}, \qquad 0 \leq n \leq M-1 \tag{4.7}$$

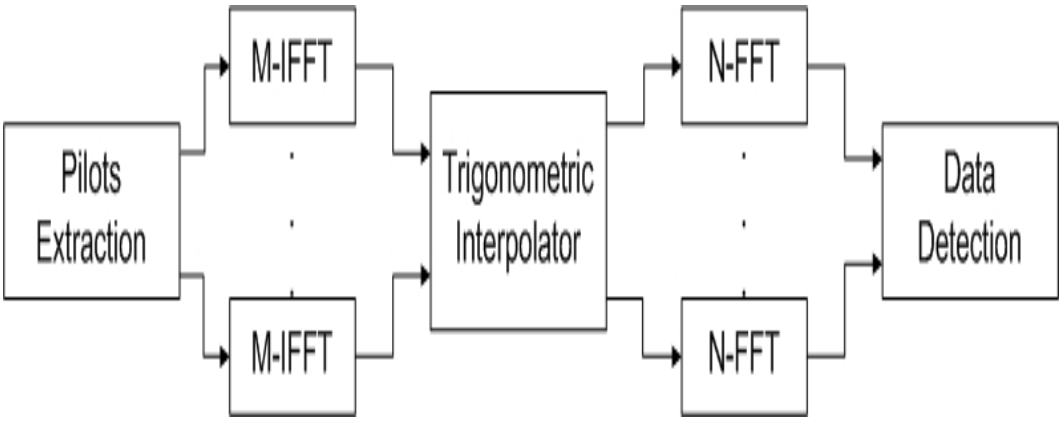

Figure 4.2: Block diagram of channel estimation with trigonometric interpolator

where $\hat{H}_{p,q}(p(k))$ is the channel estimate at the $p(k)$th subcarrier for the pth transmit antenna and the qth receive antenna in the frequency domain.

Then, $N-M$ zeros are padded after the estimated channel sequence $\hat{h}_{p,q}(n), 0 \leq n \leq M-1$. Through an FFT of signal block of length N, the estimate of the channel at all subcarriers in frequency domain can be obtained

$$\begin{aligned} \hat{H}_{p,q}(k) &= \sum_{n=0}^{N-1} \hat{h}_{p,q}(n) e^{\frac{-j2\pi nk}{N}} \\ &= \sum_{n=0}^{M-1} \hat{h}_{p,q}(n) e^{\frac{-j2\pi nk}{N}}, \qquad 0 \leq k \leq N-1 \end{aligned} \tag{4.8}$$

The channel can also be estimated directly from the pilot symbols [59]

$$\begin{aligned} \hat{H}_{p,q}(k) &= \frac{1}{\sqrt{M}} \sum_{z=0}^{M-1} \sum_{n=0}^{M-1} \hat{H}_{p,q}(p(z)) e^{-j2\pi n(\frac{k}{N} - \frac{z}{M})} \\ &= \frac{1}{\sqrt{M}} \sum_{z=0}^{M-1} \hat{H}_{p,q}(p(z)) \frac{1 - e^{-j2\pi kM/N}}{1 - e^{-j2\pi(\frac{k}{N} - \frac{z}{M})}} \\ &= \sum_{z=0}^{M-1} \frac{1 - e^{-j2\pi kM/N}}{2\sqrt{M}j} (\cot(\frac{\pi k}{N} - \frac{\pi z}{M}) + j) \times \hat{H}_{p,q}(p(z)) \end{aligned} \tag{4.9}$$

4.3.3 A Multi-tap Interpolator

Although the multipath fading channel can be estimated by the linear and trigonometric interpolators, both of them are affected by the shape of the channel, e.g. the delay spread, and the noise, resulting in the performance degradation. In this section, a new method is proposed to estimate the channel using a training block before the data transmission. The simulation results show that the proposed method achieves the better system performance compared to the other interpolators.

For packet data transmission in wireless systems, the first OFDM block of a packet is the training block that is used for initial channel parameter estimation and for time and frequency synchronization [57]. Since the transmission data for the training block are known at the receiver, we can identify the taps of the multipath fading channel, which have significant influence on the transmitted signals, and ignore the rest of taps based on the initial channel parameter estimation.

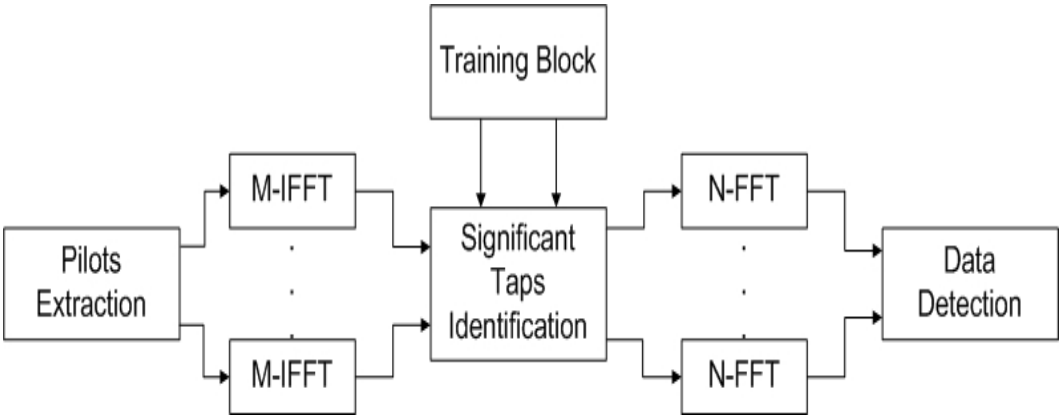

Figure 4.3: Block diagram of channel estimation with multi-tap identification

After pilots are extracted from the received signal in the frequency domain, the IFFT of a length M signal block is performed. The channel estimate in time domain $\hat{h}_{p,q}(n)$ can be obtained by performing the IFFT on the received pilot symbols

$$\hat{h}_{p,q}(n) = \frac{1}{\sqrt{M}} \sum_{k=0}^{k=M-1} \hat{H}_{p,q}(p(k)) e^{\frac{j2\pi nk}{M}}, \qquad 0 \leq n \leq M-1 \tag{4.10}$$

where $\hat{H}_{p,q}(p(k))$ is the channel estimate at the $p(k)$th subcarrier for the pth transmit antenna and the qth receive antenna in the frequency domain.

Let $\hat{h}_{p,q}(l)$ for $l = 0, 1, \cdots, L-1$ be the estimated parameters from the training block. The significant taps of the multipath fading channel can be identified by finding the l with large $|\hat{h}_{p,q(l)}|^2$ in the time domain. The number of paths L can be determined by setting a threshold on $|\hat{h}_{p,q(l)}|^2$. Then, L paths of channel estimates among the M initial channel estimates are obtained and the rest of $M - L$ channel estimates are ignored in the time domain.

Before performing the FFT of length N on the channel estimate, $N - L$ zeros are padded to $\hat{h}_{p,q}(l)$. The estimate of the channel at all subcarriers in the frequency domain can be obtained as

$$\begin{aligned} \hat{H}_{p,q}(k) &= \sum_{n=0}^{N-1} \hat{h}_{p,q}(n) e^{\frac{-j2\pi nk}{N}} \\ &= \sum_{n=0}^{L-1} \hat{h}_{p,q}(n) e^{\frac{-j2\pi nk}{N}}, \qquad 0 \le k \le N-1 \end{aligned} \tag{4.11}$$

The channel can also be estimated directly from the pilot symbols

$$\begin{aligned} \hat{H}_{p,q}(k) &= \frac{1}{\sqrt{M}} \sum_{z=0}^{M-1} \sum_{n=0}^{L-1} \hat{H}_{p,q}(p(z)) e^{-j2\pi n(\frac{k}{N} - \frac{z}{M})} \\ &= \frac{1}{\sqrt{M}} \sum_{z=0}^{M-1} \hat{H}_{p,q}(p(z)) \frac{1 - e^{-j2\pi L(\frac{k}{N} - \frac{z}{M})}}{1 - e^{-j2\pi(\frac{k}{N} - \frac{z}{M})}} \\ &= \sum_{z=0}^{M-1} \frac{1 - e^{-j2\pi L(\frac{k}{N} - \frac{z}{M})}}{2\sqrt{M} j} (\cot(\frac{\pi k}{N} - \frac{\pi z}{M}) + j) \times \hat{H}_{p,q}(p(z)) \end{aligned} \tag{4.12}$$

For the transmitted symbols at the pth transmit antenna and the qth receive antenna in the frequency domain, it is suggested to choose the number of pilot tones as a power of two, so that the efficient radix-2 FFT and IFFT algorithms can be used.

When the channel is time variant, the proposed method will not work well. The reason is the existence of the intercarrier interference caused by the Doppler spread, which affects the accuracy of the channel estimate. An ICI cancellation algorithm and a channel estimation method for time-varying channels will be discussed in the next chapter.

Table 4.1: SUI-3 Channel Model

SUI-3 Channel Model				
	Tap 1	Tap 2	Tap 3	Units
Delay	0	1.30	2.93	μ
Power-Omni Antenna	0	-5	-10	dB
90% K-Factor (omni)	0	0	0	
75% K-Factor (omni)	1	0	0	
Power-30 Antenna	0	-11	-22	dB
90% K-Factor (30 deg)	1	0	0	
75% K-Factor (30 deg)	4	0	0	

Table 4.2: SUI-4 Channel Model

SUI-4 Channel Model				
	Tap 1	Tap 2	Tap 3	Units
Delay	0	4.88	13.01	μ
Power-Omni Antenna	0	-4	-8	dB
90% K-Factor (omni)	0	0	0	
75% K-Factor (omni)	0	0	0	
Power-30 Antenna	0	-10	-20	dB
90% K-Factor (30 deg)	0	0	0	
75% K-Factor (30 deg)	2	0	0	

4.4 Numerical Results

In this section, we show the SER performance comparison for the different interpolators. The antenna configuration of a MIMO-OFDM system is $(M_T, M_R) = (2, 2)$. Since the Stanford University Interim (SUI) channel models provide the basis specifying channels for a given scenario [60], these models are used in our simulations. The parameters in these channels are related to the terrain type, delay spread, and antenna direction. It defines six channel models for different environments. Each channel model has three taps with distinct K-factor of Ricean distribution and the average power. The SUI channel models have the line-of-sight channels which are referred to as SUI-1, SUI-2 and SUI-6, and non-line-of-sight channels denoted by SUI-3, SUI-4 and SUI-5. The Table 4.1 and Table 4.2 show the SUI-3 and SUI-4 time-domain channel parameters, which are chosen to evaluate the system performance with different interpolators.

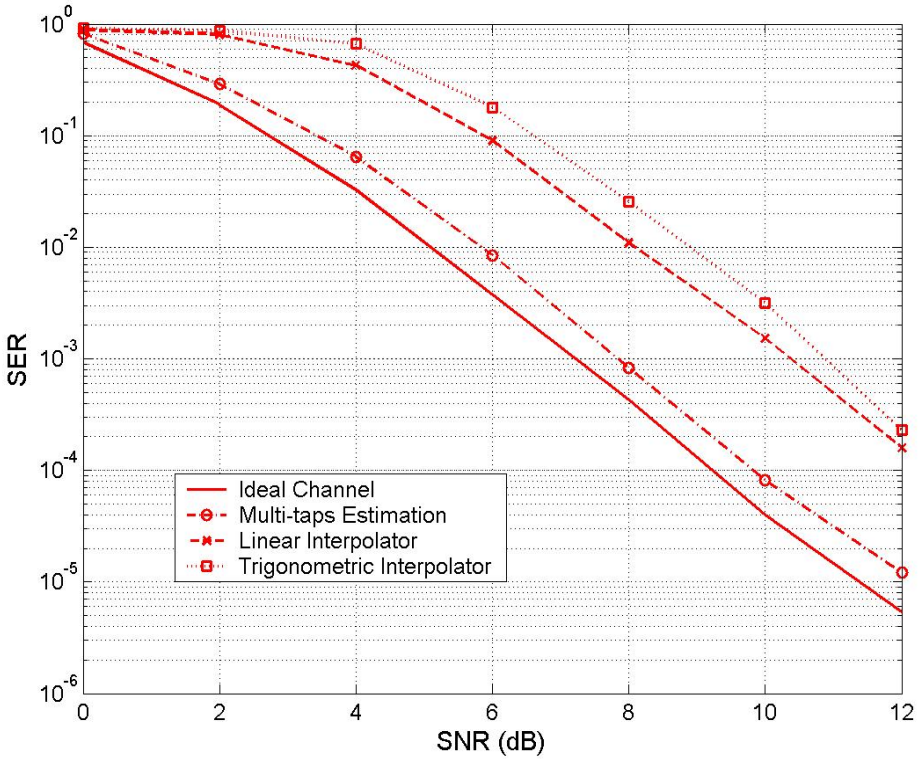

Figure 4.4: SER performance of SUI-3 channel estimation with different interpolators

In Figure 4.4, the SUI-3 channel model is used in our simulation. Since the delay spread in

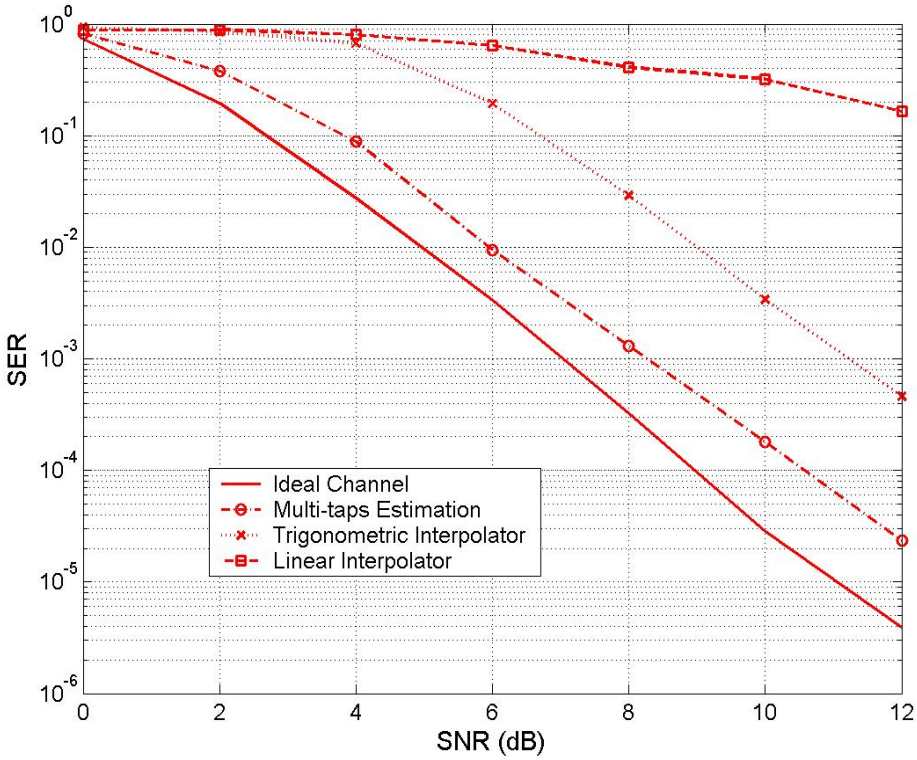

Figure 4.5: SER performance of SUI-4 channel estimation with different interpolators

this channel model is low, the SER performance of the linear interpolator is slightly better than that of the trigonometric interpolator. The multi-tap method achieves the best performance, which is $2dB$ better than those two interpolators. On the other hand, the performance of the SUI-4 channel model is shown in Figure 4.5. In the results for this scenario, the delay spread becomes the dominant factor and the values of pilot symbols are less correlated. The linear interpolator degrades considerably and has the worst SER performance due to the high delay spread. The performance of the trigonometric interpolator is also affected by the high delay spread. However, the multi-tap method stays independent of the shape of the channel and achieves high SER performance, which is no more than $1dB$ away from the system performance with ideal channel state information.

4.5 Summary

In this chapter, we demonstrated the frequency domain pilot-assisted channel estimation of a MIMO-OFDM iterative receiver. A new estimation method was proposed by identifying the significant channel taps using a training symbol in packet data transmission. The system performances of three interpolators were evaluated in simulations. As delay spread increases, we found that the performance of the linear interpolator degrades considerably. The symbol error rate of the trigonometric and multi-tap method were independent of the shape of the channel.

Chapter 5

Iterative Receiver for MIMO-OFDM Systems with Joint ICI Cancellation and Channel Estimation

5.1 Introduction

In MIMO-OFDM systems, the time-varying fading of channels can destroy the orthogonality of subcarriers. This causes serious intercarrier interference (ICI), thus leading to significant system performance degradation, which becomes more severe as the normalized Doppler frequency increases.

In references [11] and [12], the effect of ICI is analyzed and the exact expressions for the ICI of an OFDM signal resulting from time-varying channel are obtained. According to the central limit theorem for sufficient large number of subcarriers N, the ICI is modeled as a Gaussian random process under the assumption that a channel is known with a fixed number of paths. In reference [61], the further tight and universal bounds for the ICI have been derived. These bounds depend only on the product of the maximum Doppler frequency and the OFDM symbol duration.

For the OFDM systems, the issue of ICI cancellation has been widely studied. In [12]

and [13], authors use receive antenna diversity to mitigate the ICI and reduce the error floor. However, sensitivity analysis in [14] has shown that a huge performance degradation will occur for Doppler frequencies in the order of 10% of the subcarrier spacing, therefore limiting the benefits of multiple receive antennas. As normalized Doppler spread increases, the diversity equalization techniques are less effective in mitigating ICI in OFDM mobile systems.

By assuming that the channel impulse response varies in a linear fashion during an OFDM symbol period, a frequency-domain equalization technique was proposed by Jeon [15] to reduce the time-variation effect of a multipath fading channel. However, they assumed that some of the coefficients of the channel matrix are negligible, and the simulation results, showing that performance improvement under normalized Doppler spread of up to 2.72% and delay spread of $2\mu s$ for a channel that had two non-zero power-delay profile samples, indicate that the performance is improved only under low Doppler and delay spread environments. The delay spread can be much longer and normalized Doppler frequency can be as high as 10% in high mobility scenarios. This method also relies on information from adjacent OFDM symbols for channel estimation, which increases the complexity of an OFDM system.

The ICI cancellation schemes proposed in [16] and [17] are performed by modulating the same data symbol on adjacent subcarriers with different weights at the transmitter and maximal ratio combining these copies at receiver, so that the ICI can be significantly mitigated. Although these two methods have a much better signal to ICI power ratio than an ordinary OFDM system, they imply a substantial reduction of spectral efficiency and require some modifications to the traditional OFDM transmitter and receiver, making them inapplicable.

Based on the general expression of ICI power of OFDM systems, a new ICI cancellation algorithm is proposed in this chapter to reduce the effect of time-varying fading in frequency domain. In this algorithm, a two-stage parallel interference cancellation (PIC) with iterative detection and decoding is employed in the MIMO-OFDM iterative receiver. The first PIC performs as an equalizer in the frequency domain, where ICI for each OFDM symbol is mitigated in each iteration. In the second PIC, the interference resulted from neighborhood layers is suppressed by a decision statistics combining (DSC) technique. By updating the soft outputs from each decoder, the system performance is improved in each iteration. Due to the reason that the intercarrier interference for all the subcarriers are calculated in equalizer, the

iterative receiver is computational. Hence, a simplified ICI cancellation method is proposed based on the fact that most interference energy is concentrated in the neighborhood of the desired component.

Pilot-assisted approaches are widely used to estimate the channel properties and correct the received signal. For SISO-OFDM systems, authors in [58] use pilot tones to obtain channel state information, where an optimal placement of pilot tones with regard to the mean-square error (MSE) of the least squares (LS) channel estimate is proposed. Some other methods have been developed under the assumption of a low Doppler spread multipath fading channel [26, 27, 54], where the channel transfer function for the previous OFDM data block is used as the transfer function for the current data block. For MIMO-OFDM systems, optimal pilot sequences are derived in [62]. All of them require using the uniformly placed pilot tones in OFDM symbols.

In practice, a wideband wireless channel is frequency selective and time variant. The estimation of its transfer function becomes rather difficult. On the one hand, the assumption of slow fading of channels does not always hold. Thus, the transfer function of the channel might have significant changes for adjacent OFDM symbols. Therefore, it is preferable to estimate the channel based on the pilot tones in each individual OFDM data block. On the other hand, the estimates of fading channels are always corrupted by intercarrier interference due to the time-variant fading. In addition to AWGN, the accuracy of the channel estimates is strongly affected by the received pilot symbols. Therefore, it is necessary to derive the optimal pilot sequences with the non-uniform placement of pilot tones to mitigate the effects of ICI.

In this chapter, we address the challenging problem of channel estimation in a MIMO-OFDM system with Doppler spread, and we propose a promising technique based on judiciously-placed pilot tones for our system.

5.2 System Model and ICI Analysis

In this section, we consider a MIMO-OFDM system with M_T transmit antennas and M_R receive antennas, shown in Figure 5.1. With the space-time coding and spatial interleaving, each transmit antenna sends independent OFDM symbols. Let $X_p(n)$ denote the information

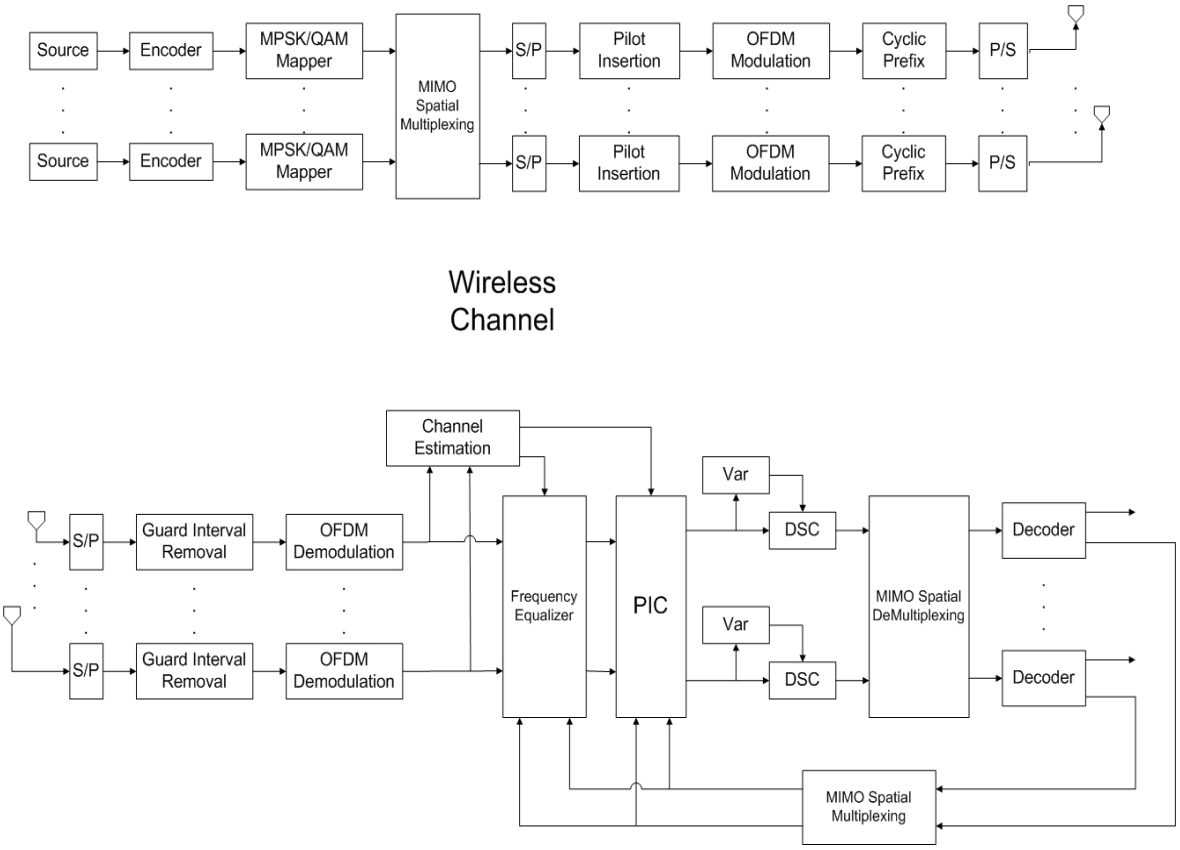

Figure 5.1: Block diagram of MIMO-OFDM transmitter and iterative receiver

symbol sent by the pth transmit antenna at the nth subcarrier, the OFDM symbol transmitted by the pth antenna is given by

$$\mathbf{X}_p = [X_p(0), X_p(1), \ldots, X_p(N-1)]^T \tag{5.1}$$

where N is the number of subcarriers for one OFDM symbol.

After performing the inverse Fast Fourier Transform (IFFT) on each transmit antenna, the modulated signal on the pth transmit antenna can be expressed as follows

$$\mathbf{x}'_p = \mathbf{F}^H \mathbf{X}_p = [x'_p(0), x'_p(1), \ldots, x'_p(N-1)]^T \tag{5.2}$$

where $\mathbf{F}$ is $N \times N$ FFT matrix, given by Eqn. 3.47.

In order to combat the multipath delay, a guard interval is inserted in each OFDM symbol, which is greater than the expected maximum time delay. The transmitted OFDM symbol with guard interval is given by Eqn. 3.48. Then, the OFDM symbols are transmitted through

time-varying frequency-selective fading channels. The received signal at receive antenna q and time n can be represented as

$$r_q(n) = \sum_{p=1}^{M_T} \sum_{l=0}^{L-1} h_{p,q}(l,n) x_p(n-l) + w_q(n) \tag{5.3}$$

where $h_{p,q}(l,n)$ is the lth resolvable path between the pth transmit antenna and qth receive antenna, L is the number of paths of fading channels, and $w_q(n)$ is the additive white Gaussian noise (AWGN).

After discarding the cyclic prefix and performing the FFT on the received signal, the symbol for the qth receive antenna and kth subcarrier in frequency domain can be expressed as

$$\begin{aligned} R_q(k) &= FFT[r_q(n)] \\ &= \sum_{n=0}^{N-1} [\sum_{p=1}^{M_T} \sum_{l=0}^{L-1} h_{p,q}(l,n) x_p(n-l) + w_q(n)] e^{-j2\pi \frac{nk}{N}} \\ &= \sum_{p=1}^{M_T} [\sum_{m=0}^{N-1} \sum_{l=0}^{L-1} H_l^{p,q}(k-m) X_p(m) e^{-j2\pi lm/N}] + W_q(k) \end{aligned} \tag{5.4}$$

where $H_l^{p,q}(k)$ is the channel state information circularly in frequency domain, $X_p(k)$ and $W_q(k)$ are the transmitted signal and the AWGN in frequency domain, respectively.

In general cases, Eqn. 5.4 can be divided into two parts as follows

$$\begin{aligned} R_q(k) = & \underbrace{\sum_{p=1}^{M_T} [\sum_{l=0}^{L-1} H_l^{p,q}(0) e^{-j2\pi lk/N}] X_p(k)}_{desired\ signal} \\ & + \underbrace{\sum_{p=1}^{M_T} [\sum_{m \neq k}^{N-1} \sum_{l=0}^{L-1} H_l^{p,q}(k-m) X_p(m) e^{-j2\pi lm/N}]}_{ICI\ component} + W_q(k) \end{aligned} \tag{5.5}$$

where $W_q(k)$ is the FFT of noise, $H_l^{p,q}(k)$ denotes the FFT of the time-varying frequency-selective channel $h_{p,q}(l,n)$

$$H_l^{p,q}(k) = \frac{1}{N} \sum_{n=0}^{N-1} h_{p,q}(l,n) e^{-j2\pi nk/N} \tag{5.6}$$

If the channel is assumed time-invariant during an OFDM symbol period, the symbol for the qth receive antenna and kth subcarrier in frequency domain can be expressed as

$$\begin{aligned} R_q(k) &= \sum_{n=0}^{N-1}[\sum_{p=1}^{M_T}\sum_{l=0}^{L-1} h_{p,q}(l,n)x_p(n-l) + w_q(n)]e^{-j2\pi\frac{nk}{N}} \\ &= \sum_{p=1}^{M_T}[\sum_{m=0}^{N-1}\sum_{l=0}^{L-1} H_l^{p,q}(k-m)X_p(m)e^{-j2\pi lm/N}] + W_q(k) \\ &= \sum_{p=1}^{M_T}[\sum_{l=0}^{L-1} H_l^{p,q}(0)e^{-j2\pi lk/N}]X_p(k) + W_q(k) \end{aligned} \tag{5.7}$$

In this equation, we can see that the ICI component contributed from neighborhood subcarriers disappears. Then, the transmitted signals can be obtained without intercarrier interference. However, in a general case with the Doppler spread, the assumption of the time-invariant channel is not true. Hence, the ICI term must be suppressed before detection.

The overall signals, after removing CP and performing the FFT on the received signals on all M_R antennas, can be represented in a matrix form

$$\mathbf{R} = \mathcal{H}\mathbf{X} + \mathbf{W} \tag{5.8}$$

where $\mathbf{X} = [\mathbf{X}_1, \cdots, \mathbf{X}_{M_T}]^T$, $\mathbf{R} = [\mathbf{R}_1, \cdots, \mathbf{R}_{M_R}]^T$ and $\mathbf{R}_q$ is received signal for the qth receive antenna: $\mathbf{R}_q = [R_q(0), R_q(1), \cdots, R_q(N-1)]^T$, $\mathcal{H}$ is the Fourier transform of the channel matrix, defined by

$$\mathcal{H} = \begin{pmatrix} \mathbf{H}^{1,1} & \mathbf{H}^{2,1} & \cdots & \mathbf{H}^{M_T,1} \\ \mathbf{H}^{1,2} & \mathbf{H}^{2,2} & \cdots & \mathbf{H}^{M_T,2} \\ \vdots & \vdots & \ddots & \vdots \\ \mathbf{H}^{1,M_R} & \mathbf{H}^{2,M_R} & \cdots & \mathbf{H}^{M_T,M_R} \end{pmatrix} \tag{5.9}$$

where

$$\mathbf{H}^{p,q} = \begin{bmatrix} \alpha_{0,0}^{p,q} & \alpha_{0,1}^{p,q} & \cdots & \alpha_{0,N-1}^{p,q} \\ \alpha_{1,0}^{p,q} & \alpha_{1,1}^{p,q} & \ddots & \vdots \\ \vdots & \ddots & \ddots & \alpha_{N-2,N-1}^{p,q} \\ \alpha_{N-1,0}^{p,q} & \cdots & \alpha_{N-1,N-2}^{p,q} & \alpha_{N-1,N-1}^{p,q} \end{bmatrix} \tag{5.10}$$

Here $\alpha_{m,n}^{p,q}$ is an ICI coefficient defined as

$$\alpha_{n,m}^{p,q} = \sum_{l=0}^{L-1} H_l^{p,q}(n-m)e^{-j2\pi lm/N}, \;\; 0 \le (n,m) \le N-1 \tag{5.11}$$

The entry $\mathbf{H}^{p,q}$ of $\mathcal{H}$ can be written as

$$\mathbf{H}^{p,q} = \mathbf{H}_D^{p,q} + \mathbf{H}_{ICI}^{p,q} \tag{5.12}$$

where $\mathbf{H}_D^{p,q}$ is a diagonal matrix, given by

$$\mathbf{H}_D^{p,q} = \begin{bmatrix} \alpha_{0,0}^{p,q} & 0 & \cdots & 0 \\ 0 & \alpha_{1,1}^{p,q} & \ddots & \vdots \\ \vdots & \ddots & \ddots & 0 \\ 0 & \cdots & 0 & \alpha_{N-1,N-1}^{p,q} \end{bmatrix} \tag{5.13}$$

and $\mathbf{H}_{ICI}^{p,q}$ is a $N \times N$ matrix with zero diagonal elements

$$\mathbf{H}_{ICI}^{p,q} = \begin{bmatrix} 0 & \alpha_{0,1}^{p,q} & \cdots & \alpha_{0,N-1}^{p,q} \\ \alpha_{1,0}^{p,q} & 0 & \ddots & \vdots \\ \vdots & \ddots & \ddots & \alpha_{N-2,N-1}^{p,q} \\ \alpha_{N-1,0}^{p,q} & \cdots & \alpha_{N-1,N-2}^{p,q} & 0 \end{bmatrix} \tag{5.14}$$

These two matrices will be used to update the output of the frequency-domain equalizer and parallel interference canceler in the proposed iterative MIMO-OFDM receiver.

5.3 Iterative receiver with frequency-domain equalization

In this section, we introduce our proposed iterative receiver with frequency-domain equalization and parallel interference cancellation with decision statistics combining techniques for the MIMO-OFDM receiver. Figure 5.1 shows the block diagram of the proposed scheme. In addition, the convolutional codes with BPSK modulation are selected for each transmit antenna. Channel parameters are estimated from received symbols and passed to the equalizer and the PIC-DSC module respectively. The effect of ICI is mitigated by the frequency-domain equalizer and then the interference from different antennas are suppressed in the following PIC-DSC module. The proposed receiver has a good performance-complexity trade-off, particularly when the number of transmit antennas is large, where the optimal joint detection and decoding becomes impractical.

The cyclic prefix is first removed from the received signals and they are transformed to the frequency domain. Then, channel estimation and equalization are performed. It should be noted that the initial derivation in this section is based on perfect channel state information. In the first iteration, the PIC detectors are equivalent to a bank of matched filters. The decision statistics for antenna p can be obtained

$$\mathbf{Y}_p^1 = \mathbf{h}_p^H \mathbf{R} \tag{5.15}$$

where $\mathbf{h}_p^H$ is the pth row of matrix $\mathcal{H}_D^H$, which is defined as

$$\mathcal{H}_D = \begin{pmatrix} \mathbf{H}_D^{1,1} & \mathbf{H}_D^{2,1} & \cdots & \mathbf{H}_D^{M_T,1} \\ \mathbf{H}_D^{1,2} & \mathbf{H}_D^{2,2} & \cdots & \mathbf{H}_D^{M_T,2} \\ \vdots & \vdots & \ddots & \vdots \\ \mathbf{H}_D^{1,M_R} & \mathbf{H}_D^{2,M_R} & \cdots & \mathbf{H}_D^{M_T,M_R} \end{pmatrix} \tag{5.16}$$

The decision statistics are then passed to respective decoders, which generate soft estimations of the transmitted symbols.

In the second and later iterations, the soft outputs from the decoders are used to update the equalizer and PIC detector with a decision statistics combiner. In the frequency-domain equalizer, the intercarrier interference, calculated from all subcarriers, is subtracted from the received signal

$$\mathbf{G}^k = \mathbf{R} - \mathcal{H}_{ICI} \widehat{\mathbf{X}}^{k-1} \tag{5.17}$$

where $\widehat{\mathbf{X}}^{k-1}$ are the soft estimates for $(k-1)$th iteration and $\mathcal{H}_{ICI}$ is interference matrix

$$\mathcal{H}_{ICI} = \begin{pmatrix} \mathbf{H}_{ICI}^{1,1} & \mathbf{H}_{ICI}^{2,1} & \cdots & \mathbf{H}_{ICI}^{M_T,1} \\ \mathbf{H}_{ICI}^{1,2} & \mathbf{H}_{ICI}^{2,2} & \cdots & \mathbf{H}_{ICI}^{M_T,2} \\ \vdots & \vdots & \ddots & \vdots \\ \mathbf{H}_{ICI}^{1,M_R} & \mathbf{H}_{ICI}^{2,M_R} & \cdots & \mathbf{H}_{ICI}^{M_T,M_R} \end{pmatrix} \tag{5.18}$$

where $\mathbf{H}_{ICI}^{p,q}$, $p = 1, \cdots, M_T$, $q = 1, \cdots, M_R$ is given in 5.14, representing the interference matrix for the pth transmit antenna and the qth receive antenna.

Here the ICI components of every subcarrier are calculated by $\mathcal{H}_{ICI}\widehat{\mathbf{X}}^{k-1}$, and then deducted from the received signal. The decision statistics for the pth transmit antenna in the kth iteration denoted by $\mathbf{Y}_p^k$, are given by

$$\mathbf{Y}_p^k = \mathbf{h}_{p,k}^H (\mathbf{G}^k - \mathcal{H}_D \underline{\widehat{\mathbf{X}}}^{k-1}) \tag{5.19}$$

where $\underline{\widehat{\mathbf{X}}}^{k-1}$ is the transmitted symbol estimate vector in $(k-1)$th iteration, with the elements corresponding to the pth transmit antenna set to zeros. It can be written as

$$\underline{\widehat{\mathbf{X}}}^{k-1} = [\widehat{\mathbf{X}}_1^{k-1}, \cdots, \widehat{\mathbf{X}}_{p-1}^{k-1}, \mathbf{0}, \widehat{\mathbf{X}}_{p+1}^{k-1}, \cdots, \widehat{\mathbf{X}}_{M_T}^{k-1}]^T \tag{5.20}$$

As discussed in Chapter 4, the decision statistics combiner gives an improved SNR as the number of iterations increases, due to the reason that the detector output in successive interations are low correlated. Thus, the decision statistics can be obtained in the DSC module as a weighted sum of the current PIC output and the DSC output from the previous operation. In each stage, except for the first one, the DSC module performs recursive linear combining on the PIC detector output for the kth iteration and the pth transmit antenna, denoted by $\mathbf{Y}_p^k$, and the DSC output from the previous iteration for the same antenna, denoted by $\mathbf{Y}_{c,p}^{k-1}$. The output of the PIC-DSC in the kth iteration and for the transmit antenna p is given by

$$\mathbf{Y}_{c,p}^k = \frac{(\sigma_{c,p}^{k-1})^2}{(\sigma_{c,p}^{k-1})^2 + (\sigma_p^k)^2}\mathbf{Y}_p^k + \frac{(\sigma_p^k)^2}{(\sigma_p^k)^2 + (\sigma_{c,p}^{k-1})^2}\mathbf{Y}_{c,p}^{k-1} \tag{5.21}$$

where $(\sigma_{c,p}^{k-1})^2$ and $(\sigma_p^k)^2$ are the variances of DSC estimates $\mathbf{Y}_{c,p}^{k-1}$ and PIC outputs $\mathbf{Y}_p^k$, respectively.

In a real system the transmitted symbols are not known at the receiver. The variance can be calculated by using the symbol estimate of the transmitted symbol from the previous decoder output

$$(\sigma_p^k)^2 = \frac{1}{N}\sum_{n=0}^{N-1}(Y_p^k(n) - \mu_p(n)\hat{X}_p^{k-1}(n))^2 \tag{5.22}$$

where $\hat{X}_p^{k-1}(n)$ is a symbol estimate of the nth subcarrier in the $(k-1)$th iteration, and μ_p is the mean of received amplitude after maximum-ratio-combining, given by

$$\mu_p = \frac{1}{N}\sum_{n=0}^{N-1} v_p(n) \tag{5.23}$$

where $v_p(n)$ is an element in the vector $\mathbf{v}_p$, given by $\mathbf{v}_p = diag\{\mathbf{h}_p^H\mathbf{h}_p\}$. The detection outputs are passed to the corresponding decoder.

In every iteration, the decoder calculates LLR for each subcarrier, which is shown by the iterative MAP algorithm in Chapter 2. Then, the soft output can be derived and given by Eqn. 3.65.

This method can be further simplified by decreasing the most computational part in Eqn. 5.17. Since the interferences from all the other subcarriers are calculated, the computational complexity of the equalizer is $O(N^2)$. Due to the fact that most interference energy is concentrated in the neighborhood of the desired component, we can restrict the interference computation to the neighboring subcarriers and ignore the ICI terms which have an insignificant influence on the desired component. Therefore, a threshold D can be set

$$\alpha_{k,m}^{p,q} = 0, \quad |k-m| > D \; and \; D \ll N \tag{5.24}$$

where D is a constant much smaller than N. Thus, the order of computational complexity is reduced from $O(N^2)$ to $O(N)$. Simulation results show that the resulting performance loss is negligible but with a significant reduction in complexity, if we use only 9 neighbors for the interference cancellation in our 256-subcarrier MIMO-OFDM system.

5.4 Pilot-assisted Channel Estimation for Time Variant Fading Channels

In last section, we have assumed that the receiver knows the exact CSI, which is not true in a real system, especially when the channel is time variant. In this section, a pilot-assisted channel estimation method is proposed under the assumption that the channel can be approximated by a linear model.

For the simplicity of analysis, we assume $(M_T, M_R) = (1, 1)$ at the first part of this section. In order to estimate channels in the time-domain $h(n,l) = [h(n,0), h(n,1), \cdots, h(n,\nu-1)]^T$, $0 \leq n \leq N-1$, in a time-varying environment, where ν is the expected maximum delay spread, $N \times \nu$ parameters are needed. Even when all OFDM subcarriers are used for pilots, only N values for the estimation of $N \times \nu$ parameters can be obtained. If a priori knowledge of channel dynamics is available at the receiver, or if the channel is constant within an OFDM block, but varying from block to block, the number of parameters can be greatly reduced. However, the assumptions is not true in real OFDM transmission environments where there is significant ICI.

Let $X(n)$ denote the information at time n, the transmitted information symbol can be given by

$$\mathbf{X} = [X(0), X(1), \cdots, X(N-1)]^T \tag{5.25}$$

After performing the IFFT, the OFDM modulated symbol can be represented as

$$\mathbf{x} = \mathbf{F}^H \mathbf{X} = [x(0), x(1), \cdots, x(N-1)]^T \tag{5.26}$$

If the length of CP is no less than the maximum channel delay spread ν, the received block after the removal of CP is

$$\mathbf{r} = \mathbf{H}\mathbf{x} + \mathbf{w} \tag{5.27}$$

where $\mathbf{w} = [w(0), w(1), \cdots, w(N-1)]^T$ denotes the vector of AWGN. $\mathbf{H}$ is an $N \times N$ circular channel matrix with elements given by

$$H(k,n) = h(k,(k-n)_N), \qquad 0 \le k \le N-1, \;\; 0 \le n \le N-1 \tag{5.28}$$

where $h(k,n)$ is the channel impulse response at the time delay n and instant k, given by

$$h(k,n) = \begin{cases} h(k,l) & 0 \le (n,l) < \nu \\ 0 & \nu \le n < N \end{cases} \tag{5.29}$$

Let $\mathbf{H}_a$ denote an $N \times N$ matrix with elements $H_a(k,n) = h_a((k-n)_N)$, $0 \le k \le N-1$, $0 \le n \le N-1$, where $h_a(n) = \frac{1}{N}\sum_{k=0}^{N-1} h(k,n)$ is the time average of $h(k,n)$ at time delay n, and $\mathbf{H}_v$ is an $N \times N$ matrix with elements $H_v(k,n) = \Delta h(k,(k-n)_N)$, where $\Delta h(k,n) = h(k,n) - h_a(n)$. The received OFDM symbol can be expressed as

$$\mathbf{r} = \mathbf{H}_a\mathbf{x} + \mathbf{H}_v\mathbf{x} + \mathbf{w} \tag{5.30}$$

where $\mathbf{H}_a$ is a time-invariant circular matrix and $\mathbf{H}_v$ is a time-variant circular matrix.

The received symbol is demodulated by performing the FFT

$$\begin{aligned} \mathbf{Y} &= \mathbf{F}\mathbf{r} \\ &= \mathbf{F}(\mathbf{H}_a\mathbf{x} + \mathbf{H}_v\mathbf{x} + \mathbf{w}) \\ &= \mathbf{F}\mathbf{H}_a\mathbf{F}^H\mathbf{X} + \mathbf{F}\mathbf{H}_v\mathbf{F}^H\mathbf{X} + \mathbf{F}\mathbf{w} \\ &= \mathbf{G}_a\mathbf{X} + \mathbf{G}_v\mathbf{X} + \mathbf{W} \end{aligned} \tag{5.31}$$

where $\mathbf{G}_a = \mathbf{F}\mathbf{H}_a\mathbf{F}^H$ is an $N \times N$ diagonal matrix with elements given by

$$G_a(k,k) = \sum_{n=0}^{\nu-1} h_a(n) e^{-j\frac{2\pi nk}{N}}, \;\; 0 \le k \le N-1 \tag{5.32}$$

where $h_a(n) = \frac{1}{N}\sum_{k=0}^{N-1} h(k,n)$ is the time average of $h(k,n)$ at time delay n, and $\mathbf{G}_v = \mathbf{F}\mathbf{H}_v\mathbf{F}^H$ is an $N \times N$ matrix with elements given by

$$G_v(k,n) = \frac{1}{N}\sum_{m=0}^{\nu-1}\sum_{r=0}^{N-1} h_v(r,m)e^{-j\frac{2\pi r(k-n)}{N}}e^{-j\frac{2\pi nm}{N}}, \;\; 0 \leq (n,k) \leq N-1 \;\; and \;\; n \neq k \tag{5.33}$$

Therefore, $\mathbf{G}_a$ is a diagonal matrix and $\mathbf{G}_v$ is an $N \times N$ matrix with zero diagonal elements.

From Eqn. 5.31, we can see that if we ignore the ICI term and only consider the isolated pilot tones placed on the FFT grid, the approach cannot produce reliable channel estimates. Consequently, channel estimation is not possible if we only look at the time-invariant part. When the ICI is not negligible, we should account for the ICI term in the process of channel estimation. Later, we will show that the OFDM system with severe ICI, the pilots should be grouped together on the equal-spaced FFT grid.

Now, we consider a system with M_T transmit antennas and M_R receive antennas. In order to construct the channel matrix in the frequency domain, channel estimation is required. To reduce the number of parameters needed for channel estimation, we make a reasonable assumption that the time-domain channel variation $h(n,l)$ can be obtained by linear interpolation. For normalized Doppler frequency less than 20%, channel variation can be approximated by a linear model [21]. Under this assumption, we can derive channel state information (CSI) in the frequency domain and estimate channel parameters.

The channel impulse response for the lth path between the pth transmit antenna and the qth receive antenna can be determined as

$$h_{p,q}(l,n) = h_{mid}^{p,q}(l) + h_{slope}^{p,q}(l) * (n - \frac{N-1}{2}) \tag{5.34}$$

where $h_{mid}^{p,q}(l)$ is the median value of channel variation, and $h_{slope}^{p,q}(l)$ denotes the slope of straight line.

Assuming that the pilot symbols are orthogonal and represented by a matrix $\mathbf{P}$ for MIMO-OFDM system. For the pth transmit antenna and qth receive antenna, M pilot symbols $s_{p,q}(1)$, $s_{p,q}(2)$, $\cdots$, $s_{p,q}(M)$ are inserted at the subcarrier $p(1)$, $p(2)$, $\cdots$, $p(M)$, $M \geq \nu$. The received signals on pilot tones can be processed as follows [63]

$$\mathbf{C}(p(i)) = \mathbf{R}(p(i))\mathbf{P}^H(\mathbf{P}\mathbf{P}^H)^{-1} \tag{5.35}$$

where $\mathbf{R}(p(i))$ is the matrix of the received signals at the $p(i)$ pilot tones, given by Eqn. 4.3, and $\mathbf{C}(p(i))$ is the matrix used for channel estimation given by Eqn. 4.4.

Insert Eqn. 5.34 and Eqn. 5.35 into Eqn. 5.5, linear equations Eqn. 5.36 for pilot symbols at frequencies $k = p(1), p(2), \cdots, p(M)$ are obtained

$$\begin{aligned} C_{p,q}(k) = &\sum_{l=0}^{\nu-1} h_{mid}^{p,q}(l) e^{-j2\pi lk/N} s_{p,q}(k) \\ &+ \sum_{m=p(1), m\neq k}^{p(M)} \frac{\sum_{l=0}^{\nu-1} h_{slope}^{p,q}(l) e^{-j2\pi lm/N}}{e^{-j2\pi n(k-m)/N} - 1} s_{p,q}(m) + w_{p,q}(k) \end{aligned} \tag{5.36}$$

Two parameters are used to simplify Eqn. 5.36: $\Phi_{p,q}$ and $\Gamma_{p,q}$, which are given by Eqn. 5.37 and Eqn. 5.39, respectively.

$$\Phi_{p,q} = [h_{mid}^{p,q}(0), \cdots, h_{mid}^{p,q}(\nu-1), h_{slope}^{p,q}(0), \cdots, h_{slope}^{p,q}(\nu-1)]^T \tag{5.37}$$

Linear equations (5.36) can be represented in a matrix form

$$\mathbf{C}_{p,q} = \Gamma_{p,q} \Phi_{p,q} + \mathbf{e}_{p,q} \tag{5.38}$$

where $\mathbf{C}_{p,q}$ is a vector defined as $\mathbf{C}_{p,q} = [C_{p,q}(p(1)), C_{p,q}(p(2)), \cdots, C_{p,q}(p(M))]^T$, $\mathbf{e}_{p,q}$ is the approximation error given in Eqn. 5.42, $\Gamma_{p,q}$ defined in Eqn. 5.39 can be precalculated and stored in the receiver when the placement of pilots symbols is fixed in OFDM symbols before transmission.

$$\Gamma_{p,q} = \begin{bmatrix} s_{p,q}(p(1)) & \cdots & s_{p,q}(p(M)) \\ \vdots & \ddots & \vdots \\ s_{p,q}(p(1)) e^{-j2\pi p(1)(\nu-1)/N} & \cdots & s_{p,q}(p(M)) e^{-j2\pi p(M)(\nu-1)/N} \\ \sum_{m=p(1), m\neq p(1)}^{p(M)} \frac{s_{p,q}(m)}{e^{-j2\pi(p(1)-m)/N}-1} & \cdots & \sum_{m=p(1), m\neq p(M)}^{p(M)} \frac{s_{p,q}(m)}{e^{-j2\pi(p(M)-m)/N}-1} \\ \vdots & \ddots & \vdots \\ \sum_{m=p(1), m\neq p(1)}^{p(M)} \frac{s_{p,q}(m) e^{-j2\pi m(\nu-1)/N}}{e^{-j2\pi(p(1)-m)/N}-1} & \cdots & \sum_{m=p(1), m\neq p(M)}^{p(M)} \frac{s_{p,q}(m) e^{-j2\pi m(\nu-1)/N}}{e^{-j2\pi(p(M)-m)/N}-1} \end{bmatrix}^T \tag{5.39}$$

We assume that the pilot sequence is designed such that the matrix $\Gamma_{p,q}$ is full column rank. The Moore-Penrose pseudo-inverse [64] of $\Gamma_{p,q}$ can thus be written as $\Gamma_{p,q}^{\dagger} = (\Gamma_{p,q}^H \Gamma_{p,q})^{-1} \Gamma_{p,q}^H$.

Now we can obtain the estimation of the channel vector

$$\widehat{\Phi_{p,q}} = \Gamma_{p,q}^{\dagger}\mathbf{C}_{p,q} \tag{5.40}$$

where $\widehat{\Phi_{p,q}}$ can be represented by the estimates of the median value of channel variation $\hat{h}_{mid}^{p,q}(n)$ and the estimates of the slope of channel variation $\hat{h}_{slope}^{p,q}(n)$

$$\widehat{\Phi_{p,q}} = [\hat{h}_{mid}^{p,q}(0), \cdots, \hat{h}_{mid}^{p,q}(\nu-1), \hat{h}_{slope}^{p,q}(0), \cdots, \hat{h}_{slope}^{p,q}(\nu-1)]^T \tag{5.41}$$

Unlike the time-invariant multipath channel, pilot symbols should be placed equally spaced on the FFT grid [58]. For time-varying frequency-selective fading channels, the placement of pilot tones has a significant impact on the quality of the channel estimates. The scheme of pilot placement can be obtained by minimizing $\mathbf{E}\{\|\mathbf{e}_{p,q}\|^2\}$ for specific pilot position. Assuming transmitted symbols are i.i.d. with $\mathbf{E}\{\|\mathbf{X}\|^2\} = 1$, we obtain

$$\mathbf{E}\{\|\mathbf{e}_{p,q}\|^2\} = (\sum_{k \neq p(m)} \Gamma_{p,q}\mathbf{R}_{\Phi}^{p,q}\Gamma_{p,q}^{H}) + \sigma_{p,q}^2, \quad 1 \leq m \leq M \tag{5.42}$$

where $\mathbf{R}_{\Phi}^{p,q} = \mathbf{E}\{\Phi_{p,q}\Phi_{p,q}^{H}\}$ and $\sigma_{p,q}^2$ is the variance of the channel noise. Consider that $\Gamma_{p,q}\mathbf{R}_{\Phi}^{p,q}\Gamma_{p,q}^{H}$ is a decreasing function of $(k - p(m))_N$ [19], $\mathbf{E}\{\|\mathbf{e}_{p,q}\|^2\}$ is minimized when pilots at frequencies $k \neq p(m)$ are placed as close to $p(m)$ as possible. Therefore, it is much better to group the pilots together on the equally spaced FFT grid [62], as shown in Figure 5.2.

Figure 5.2: The placement of pilot tones in an OFDM symbol

5.5 Simulation Results

In this section, we evaluate the performance of OFDM systems using proposed ICI cancellation and channel estimation method. The simulation programs are all written in C language.

We consider a 256-subcarrier OFDM system with BPSK modulation. The total number of OFDM symbols in the simulations is 1500000. The guard interval with 22 cyclic prefix

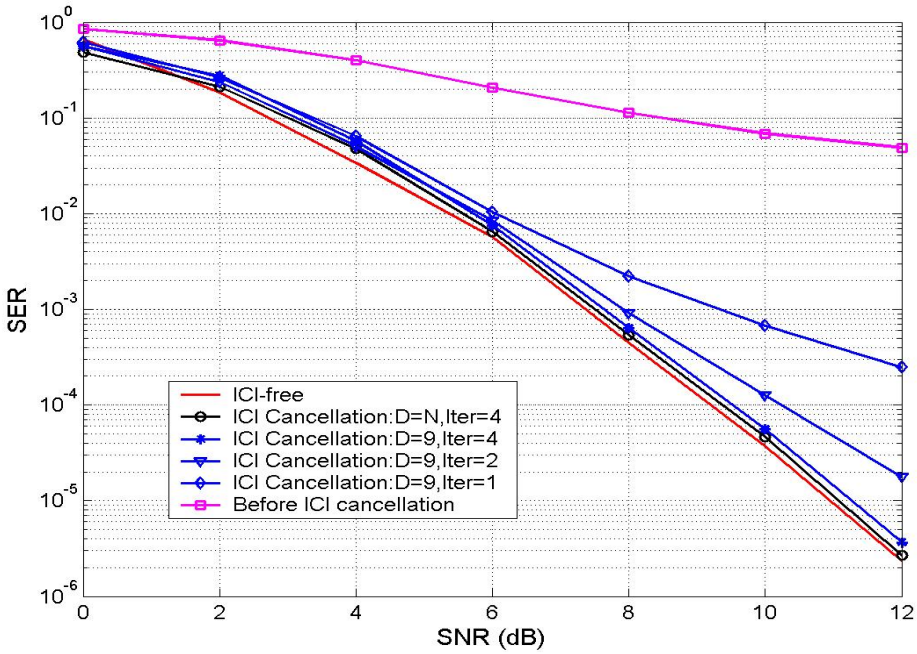

Figure 5.3: SER performance with perfect channel when normalized Doppler frequency is 0.1, $(M_T, M_R) = (2, 2)$

and 10 postfix symbols are used to prevent inter-symbol interference caused by channel multipath delay spread. Hadamard matrix is used as the orthogonal pilot symbols' matrix in our simulation. The non-line-of-sight SUI-3 channel model with Ricean fading is used to represent the mobile environment with the maximum time delay of 2.93μs [60]. For each channel, a Doppler spread is generated by Jakes' model. Its correlation function can be written as [40]

$$r_h(k) = \sigma_h^2 J_0(2\pi f_d T_s k) \tag{5.43}$$

where σ_h^2 is the channel power, $J_0(\cdot)$is the zeroth-order Bessel function, T_s is the OFDM symbol duration, and f_d is the Doppler spread.

Figure 5.3 and Figure 5.4 show the system performance of the proposed ICI equalization method with different antenna configurations, under the condition that the normalized Doppler frequency is 0.1. The results are generated after the 4th iteration. As mentioned above, the channel variation can be approximated by a linear model. When the perfect channel information is utilized in both frequency-domain equalization and PIC-DSC, our approach with full size channel interference matrix and a limited number of neighborhood subcarriers in-

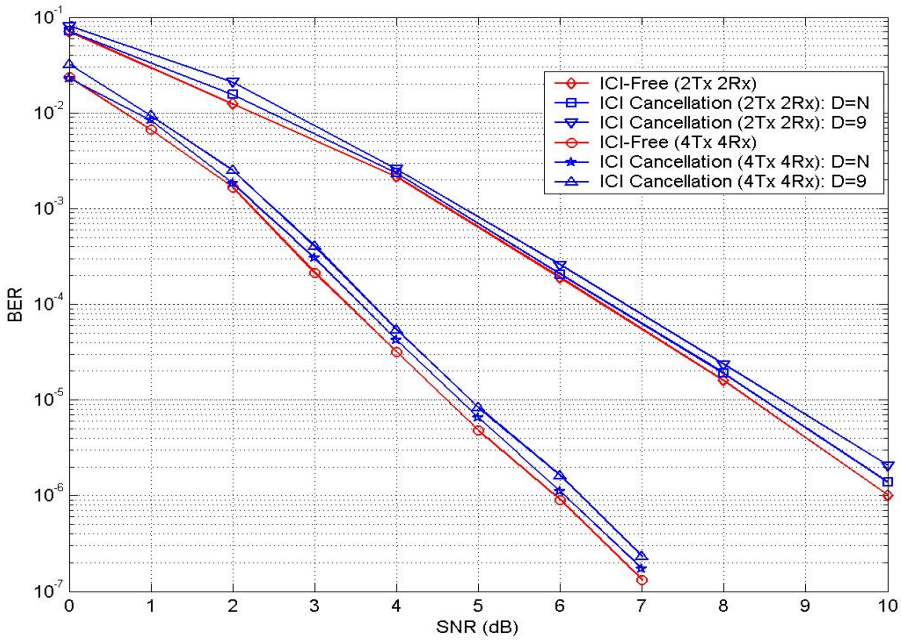

Figure 5.4: SER performance with perfect channel when normalized Doppler frequency is 0.1, $(M_T, M_R) = (2, 2)\ \ and\ \ (4, 4)$

terference matrix ($D = 9$), is very close to the ideal ICI-free curve for which the channel is assumed constant during a block period. This means the interference due to the time-varying and frequency-selective fading channel is almost completely suppressed.

For the estimated channel shown in Figure 5.5, the results with both the full size interference matrix and the limited number of neighborhood subcarriers interference matrix ($D = 9$) also show large improvement compared to the result without ICI cancellation. A significant reduction of system complexity is achieved by restricting the number of interference subcarriers at the cost of a very small performance degradation. The SER performance loss for real channel estimation compared to the perfect channel estimation is less than $3dB$.

In Figures 5.6 and 5.7, we simulate the proposed ICI method with ideal channel state information and the different channel subcarrier interference matrices when the normalized Doppler frequency is 0.3. Here the assumption that the channel varies in a linear fashion during a block period no longer holds as the normalized Doppler frequency is relatively high. However, the proposed equalization method with perfect CSI still offers a great improvement after four iterations. Even with small number of adjacent subcarriers ($D = 9$), our

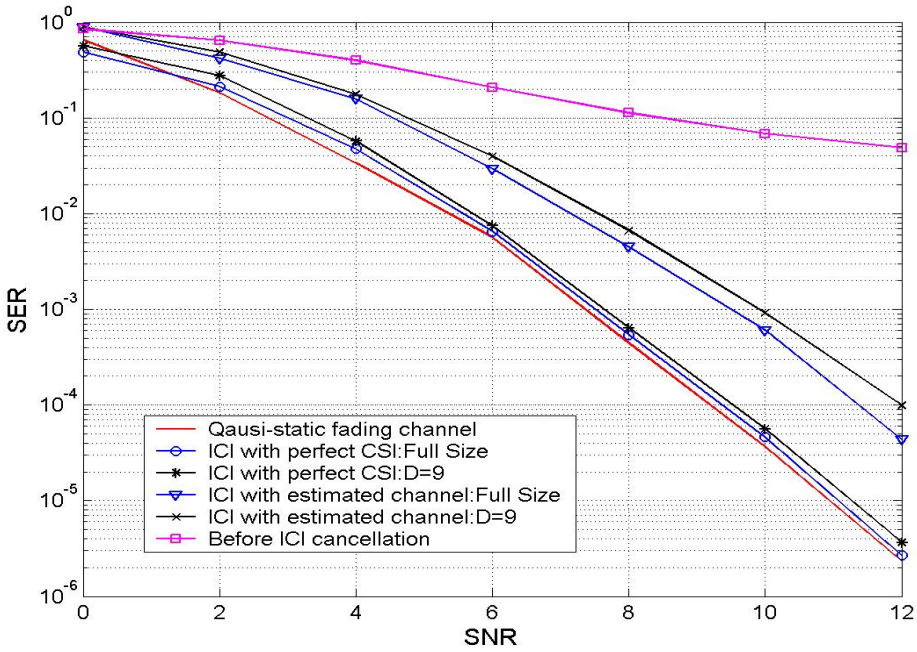

Figure 5.5: SER performance with estimated channel and normalized Doppler frequency is 0.1, $(M_T, M_R) = (2, 2)$

proposed equalizer is effective in compensating for the distortion caused by the time-varying channel. For a higher normalized Doppler frequency, more iterations are needed to achieve better SER performance.

5.6 Summary

In this chapter, we presented an iterative receiver for the MIMO-OFDM system with joint ICI cancellation and channel estimation. The intercarrier interference caused by time-varying channel was compensated by the frequency-domain equalizer, and then the interference from different antennas was suppressed by the PIC-DSC technique. The decision statistics of each stage were updated by soft outputs generated from decoders. The complexity of equalization was significantly reduced by limiting the number of neighboring interference subcarriers.

A pilot-assisted channel estimation technique for this MIMO-OFDM system was proposed to compensate for channel variation over time-varying frequency-selective channels. For

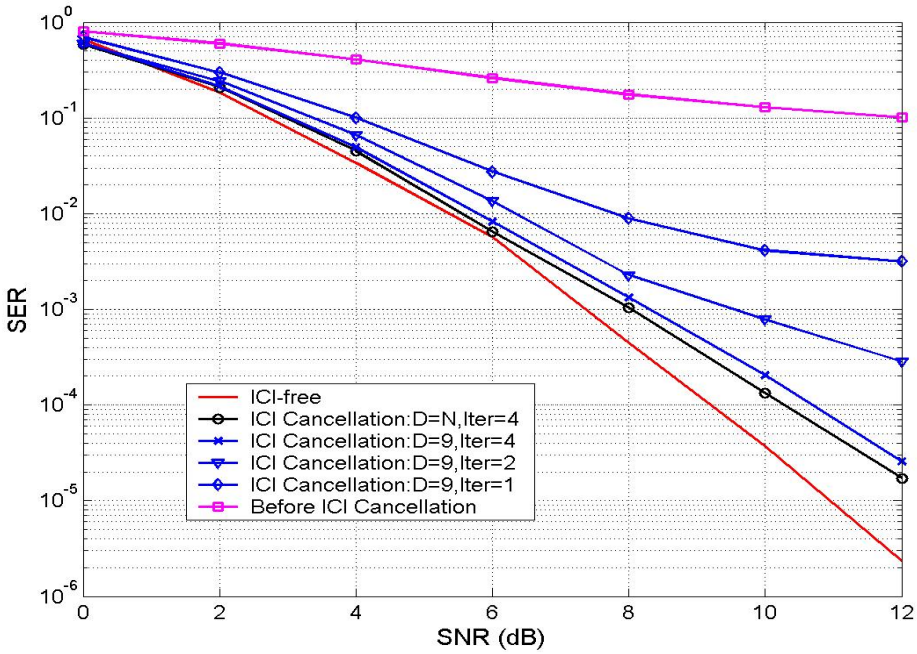

Figure 5.6: SER performance with perfect channel when normalized Doppler frequency is 0.3, $(M_T, M_R) = (2, 2)$

the mobile transmission scenarios, simulation results show that the proposed methods can effectively compensate for the effect of intercarrier interference and can approach ICI-free performance.

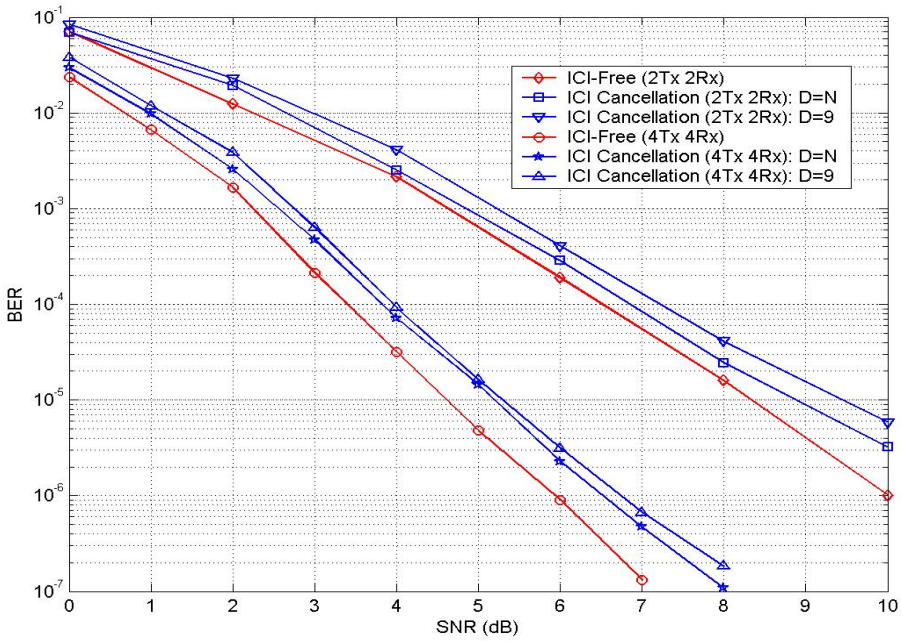

Figure 5.7: SER performance with perfect channel when normalized Doppler frequency is 0.3, $(M_T, M_R) = (2, 2)\ \ and\ \ (4, 4)$

Chapter 6

Conclusions

In this thesis, we proposed an iterative receiver for MIMO-OFDM systems. Based on this receiver, solutions to two of the most important problems in OFDM systems have been provided, namely, intercarrier interference cancellation and channel estimation over time-varying frequency-selective fading channels.

6.1 Thesis Summary

Chapter 1 described motivation as an introduction to our research. Two research problems of MIMO-OFDM systems design over time-varying multipath fading channels were described.

Chapter 2 introduced the iterative receiver model, and briefly reviewed the various decoding principles of forward error correcting codes. Particularly, we discussed optimal decoding of convolutional codes and the maximum a posteriori probability (MAP) iterative decoding algorithm. Furthermore, the principles of turbo codes were introduced and illustrated by an example.

The fundamental techniques of OFDM systems were given in Chapter 3, including the use of cyclic prefix, modulation, equalization and channel estimation. An important factor that determined the complexity of the receiver was the detector. For this reason, we considered a standard parallel interference canceler (PIC-STD) and its improved version known as PIC

with decision statistics combiner (PIC-DSC). These detectors were chosen because they offered a good performance-complexity trade-off, particularly when the number of transmit antennas was high and the optimal joint detection and decoding became impractical. The simulation results showed that, after the 4th iteration, the performance of the PIC-DSC iterative receiver is slightly better than that of the PIC-STD iterative receiver when the number of transmit and receive antennas is $(M_T, M_R) = (2, 2)$. However, when the number of transmit and/or receive antennas is increased to ($M_T = 4, M_R = 4$), the PIC-DSC iterative receiver performed much better that PIC-STD iterative receiver, especially when the SNR is $4dB$ or higher. Furthermore, when the number of interfering layers relative to the number of receive antennas becomes larger, e.g. ($M_T = 4, M_R = 2$) and ($M_T = 6, M_R = 2$), the decision statistics combining technique can still minimize the bias of the mean value from the transmitted signals effectively.

Pilot-assisted channel estimation for the MIMO-OFDM system over time-invariant multi-path channels has been discussed in Chapter 4. Two frequency-domain interpolators were analyzed: a linear interpolator and a trigonometric interpolator. To estimate the time invariant multi-path channel, a new algorithm called multi-tap method has been proposed by sending training block. Since the transmission data of the training block is known at the receiver, the significant taps from the initial channel parameter estimation can be identified, and the taps, which have insignificant influence on the accuracy of channel estimation, are ignored in order to reduce the complexity of computation. In the simulation results with SUI-3 channel model, the performance of the proposed method is $2dB$ better than that of the linear interpolator and the trigonometric interpolator. Even in a high delay spread scenario, the proposed method achieves considerable SER performance improvement compared to the other two interpolators, and is no more than $1dB$ away from the system performance with ideal channel state information.

Chapter 5 extended the scope of Chapter 4 to a more general case. In this part of thesis, we proposed an intercarrier interference cancellation algorithm in the frequency domain to reduce the effect of time-varying fading, based on the general expression of ICI power for MIMO-OFDM systems. The iterative MIMO-OFDM receiver in our algorithm consists of a two-stage parallel interference cancellation with iterative detection and decoding. In the frequency domain equalizer, the channel matrix and the intercarrier interference matrix are calculated based on the general expression of the received symbols, and then the ICI is subtracted from received OFDM symbols. At the second stage of interference cancellation,

the parallel interference canceler and decision statistics combining technique are used to mitigate the interference from different antennas. The decision statistics of each stage are updated by soft outputs generated from each corresponding decoder and used to improve the system performance in the next iteration. Furthermore, a simplified ICI cancellation method is proposed based on the fact that most interference energy is concentrated in the neighborhood of the desired component. Hence, by restricting the interference computation to the limited number of neighboring subcarriers and ignoring the ICI terms that have insignificant influence on the desired component, the computational complexity of our proposed receiver is greatly reduced from $O(N^2)$ to $O(N)$. When the normalized Doppler frequencies is 0.1 and 0.3, simulation results have shown that our approaches with the full size channel interference matrix $(D = N)$ and the simplified channel interference matrix $(D = 9)$, are very close to the ideal ICI-free curve for which channel is assumed constant during a block period. A significant reduction of complexity was achieved with a negligible loss of system performance.

Another challenging problem of channel estimation approaches was discussed. Because the estimates of fading channels are always corrupted by intercarrier interference and additive white Gaussian noise from the time-variant fading channel, the placement of pilot tones has a significant impact on the quality of the channel estimates. For normalized Doppler frequency less than 20%, channel variation can be approximated by a linear model. Under this assumption, we can derive channel state information (CSI) in the frequency domain and estimate channel parameters. As a result, the optimal pilot sequences with the non-uniform placement of pilot tones have been used to mitigate the effects of ICI and update the parallel interference canceler and the frequency-domain equalizer. The simulation results show that the SER performance of the iterative receiver between the estimated channel and the ideal channel is less than $3dB$.

6.2 Future Work

The MIMO-OFDM system is a promising technique in high data rate wireless communications. In this thesis, two challenging techniques for ICI cancellation and time-varying channel estimation have been proposed to improve the system performance. There are still many issues for MIMO-OFDM systems that need to be investigated.

The algorithm of channel estimation proposed in Chapter 5 has been proven effective for estimating a time-varying multipath channel. However, it was based on the assumption that channel variation can be approximated by a linear model, which could be a limit on Doppler spread. For the higher normalized Doppler shifts, it is a challenge to develop robust channel estimation algorithms based on higher-order approximations for channel variations.

It must be noted that OFDM systems are sensitive to frequency offset and phase noise, which are also the causes of the ICI problem. The design of robust frequency offset and phase noise mitigation algorithm without using additional training symbols will be a challenge. Although the interference suppression scheme and the channel parameter estimation scheme proposed in this thesis can be applied to ICI cancellation effectively for MIMO-OFDM systems, a detailed implementation strategy to mitigate frequency offset and phase noise still needs investigation.

Bibliography

[1] G. Foschini and M. J. Gans, "On limits of wireless communications in a fading environment when using multiple antennas," *Wireless Personal Communications*, vol. 6, pp. 311 – 355, Mar. 1998.

[2] I. E. Telatar, "Capacity of multi-antenna Gaussian channels," *Technical Report, AT&T-Bell Labs*, Jun. 1995.

[3] B. Saltzberg, "Performance of an efficient parallel data transmission system," *IEEE Trans. Commun.*, vol. 15, no. 6, pp. 805 – 811, Dec 1967.

[4] S. B. Weinstein and P. M. Ebert, "Data transmission by frequency-division multiplexing using the discrete Fourier transform," *IEEE Trans. Commun.*, vol. 19, no. 5, pp. 628 – 634, Oct. 1971.

[5] "Radio broadcasting systems: Digital audio broadcasting (DAB) to mobile, portable and fixed receivers," *ETSI-European Telecommunications Standards Institute Std. EN 300 401 Rev.1.3.3*, May 2001.

[6] "Digital video broadcasting (DAB): Framing structure, channel coding and modulation for digital terrestrial television," *ETSI-European Telecommunications Standards Institute Std. EN 300 744 Rev.1.4.1*, Jan. 2001.

[7] "Asymmetric digital subscriber line (ADSL)," *ANSI American National Standards Institute Std. T1.413*, 1995.

[8] "Broadband radio access networks (BRAN): HIPERLAN type 2, physical (PHY) layer," *ETSI-European Telecommunications Standards Institute Std. TS 101 475 Rev.1.3.1*, Dec. 2001.

[9] "Supplement to IEEE standard for information technology telecommunications and information exchange systems between local and metropolitan area networks - specific requirements. part 11: wireless LAN medium access control (MAC) and physical layer (PHY) specifications: high-speed physical layer in the 5 ghz band," *The Institute of Electrical and Electronics Engineering, Inc. Std. IEEE 802.11a*, Sep. 1999.

[10] K. Sathananthan and C. Tellambura, "Performance analysis of an OFDM system with carrier frequency offset and phase noise," *IEEE Veh. Technol. Conf.*, vol. 4, pp. 2329 – 2332, Oct. 2001.

[11] P. Robertson and S. Kaiser, "The effects of doppler spreads in OFDM(A) mobile radio systems," in *Proc. IEEE Vehicular Technology Conf.*, Fall 1999, pp. 329 – 333.

[12] M. Russell and G. Stuber, "Interchannel interference analysis of OFDM in a mobile environment," in *Proc. IEEE Vehicular Technology Conf.*, July 1995, pp. 820 – 824.

[13] S. Sung and D. Brady, "Spectral spatial equalization for OFDM in time-varying frequency-selective multipath channels," *Sensor Array and Multichannel Signal Processing Workshop 2000 Proc.*, pp. 434 – 438, Mar. 2000.

[14] A. Hutter, E. Carvalho, and J. Cioffi, "On the impact of channel estimation for multiple antenna diversity reception in mobile OFDM systems," *Thirty-Fourth Asilomar Conference on Signals, Systems and Computers*, vol. 2, pp. 1820 – 1824, Oct.29th-Nov.1st 2000.

[15] W. G. Jeon, K. Chang, and Y. S. Cho, "An equalization technique for orthogonal frequency-division multiplexing systems in time-variant multipath channels," *IEEE Trans. Commun.*, vol. 47, no. 1, pp. 27 – 32, Jan. 1999.

[16] Y. Zhao and S. G. Haggman, "Intercarrier interference self-cancellation scheme for OFDM mobile communication systems," *IEEE Trans. Commu.*, vol. 49, no. 7, pp. 1185 – 1191, Jul. 2001.

[17] J. Armstrong, P. M. Grant, and G. Povey, "Polynomial cancellation coding of OFDM to reduce intercarrier interference due to Doppler spread," *IEEE Global Telecommunications Conference*, vol. 5, pp. 2771 – 2776, Nov. 1998.

[18] Y.-S. Choi, P. J. Voltz, and F. A. Cassara, "On channel estimation and detection for multicarrier signals in fast and selective Rayleigh fading channels," *IEEE Trans. Commun.*, vol. 49, no. 8, pp. 1375 – 1387, Aug. 2001.

[19] A. Stamoulis, S. N. Diggavi, and N. Al-Dhahir, "Intercarrier interference in MIMO OFDM," *IEEE Trans. on Signal Processing*, vol. 50, no. 10, pp. 2451 – 2464, Oct. 2002.

[20] J.-P. M. G. Linnartz and A. Gorokhov, "New equalization approach for OFDM over dispersive and rapidly time varying channel," *IEEE Personal, Indoor and Mobile Radio Communications 2000*, vol. 2, pp. 1375 – 1379, Sep. 2000.

[21] Y. Mostofi and C. Cox, "ICI mitigation for pilot-aided OFDM mobile systems," *IEEE Trans. on Wireless Commun.*, vol. 4, no. 2, pp. 765 – 774, 2005.

[22] M. K. Tsatsanis and Z. Xu, "Pilot symbol assisted modulation in frequency selective fading wireless channels," *IEEE Trans. on Signal Processing*, vol. 48, no. 6, pp. 2353 – 2365, Aug. 2000.

[23] C. Tepedelenlioglu and G. B. Giannakis, "Transmitter redundancy for blind estimation and equalization of time- and frequency-selective channels," *IEEE Trans. on Signal Processing*, vol. 48, pp. 2029 – 2043, Jul. 2000.

[24] H. Cheon and D. Hong, "Effect of channel estimation error in OFDM-based WLAN," *IEEE Commun. Lett.*, vol. 6, no. 5, pp. 190 – 192, May 2002.

[25] S. Colieri, M. Ergen, A. Puri, and A. Bahai, "A study of channel estimation in OFDM systems," *IEEE 56th Vehicular Technology Conference 2002 Proceedings.*, vol. 2, pp. 894 – 898, Sept. 2002.

[26] J.-J. van de Beek, O. Edfors, M. Sandell, S. K. Wilson, and P. O. Borjesson, "On channel estimation in OFDM systems," *IEEE 45th Vehicular Technology Conference*, vol. 2, pp. 815 – 819, Jul. 1999.

[27] O. Edfors, M. Sandell, S. K. Wilson, and P. O. Borjesson, "OFDM channel estimation by singular value decomposition," *IEEE Trans. Commun.*, vol. 46, no. 7, pp. 931 – 939, Jul. 1998.

[28] M.-H. Hsieh and C.-H. Wei, "Channel estimation for OFDM systems based on comb-type pilot arrangement in frequency selective fading channels," *IEEE Trans. on Consumer Electronics*, vol. 44, no. 1, pp. 217 – 225, Feb. 1998.

[29] R. Steele, *Mobile Radio Communications*. Pentech Press Limited, London, 1992.

[30] B. Vucetic and J. Yuan, *Turbo Coding: Principles and Applications*. Kluwer Academic Publishers, May 2001.

[31] L. H. C. Lee, *Convolutional Coding: Fundamentals and Applications*. Artech House, May 1997.

[32] S. Lin and D. J. Costello, *Error Control Coding: Fundamentals and Applications*. NJ. Prentice Hall, May 1983.

[33] B. Vucetic and J. Yuan, *Space-Time Coding*. John Wiley, April 2003.

[34] J. G. Proakis, *Digital Communications 4th Ed*. McGraw-Hill, New York, 2001.

[35] T. S. Rappaport, *Wireless Communications: Principles and Practice Second Edition*. Prentice Hall, 2002.

[36] Y. Gong and K. B. Letaief, "Performance evaluation and analysis of space-time coding in unequalized multipath fading links," *IEEE Trans. Commun.*, vol. 48, no. 11, pp. 1778 – 1782, Nov. 2000.

[37] Y. G. Li, L. J. Cimini, and N. R. Sollenberger, "Robust channel estimation for OFDM systems with rapid dispersive fading channels," *IEEE Trans. Commun.*, vol. 46, pp. 902 – 915, Jul. 1998.

[38] H. Meyr, M. Moeneclaey, and S. A. Fechtel, *Digital Communication Receivers : Synchronization, Channel Estimation and Signal Processing*. Wiley NY, 1998.

[39] R. H. Clark, "A statistical theory of mobile-radio reception," *Bell Syst. Tech. J.*, pp. 957 – 1000, Jul. - Aug. 1968.

[40] W. Jakes, *Microwave Mobile Communications*. Piscataway, NJ, 1974.

[41] R. W. Chang, "Synthesis of band-limited orthogonal signals for multichannel data transmission," *Bell Syst. Tech. J.*, vol. 46, pp. 1775 – 1796, Dec. 1966.

[42] A. Peled and A. Ruiz, "Frequency domain data transmission using reduced computational complexity algorithms," *IEEE International Conference on ICASSP '80.*, vol. 5, pp. 964 – 967, Apr. 1980.

[43] B. Hirosaki, "An analysis of automatic equalizers for orthogonally multiplexed QAM systems," *IEEE Trans. Commun.*, vol. 28, pp. 73 – 83, Jan. 1980.

[44] L. J. Cimini, "Analysis and simulation of a digital mobile channel using orthogonal frequency division multiplexing," *IEEE Trans. Commun.*, vol. COM-33, no. 7, pp. 665 – 675, Jul. 1985.

[45] I. Kalet, "The multitone channel," *IEEE Trans. Commun.*, vol. 37, pp. 119 – 124, Feb. 1989.

[46] S. Marinkovic, B. Vucetic, and A. Ushirokawa, "Space-time iterative and multistage receiver structures for CDMA mobile communication systems," *IEEE J. on Select Areas in Communications*, vol. 19, no. 8, pp. 1594 – 1604, Aug. 2001.

[47] J. P. McGeehan and A. J. Bateman, "Phase locked transparent tone-in-band (TTIB): A new spectrum configuration particularly suited to the transmission of data over SSB mobile radio networks," *IEEE Trans. Commun.*, vol. 32, pp. 81 – 87, Jan. 1984.

[48] F. Davarian, "Mobile digital communications via tone calibration," *IEEE Trans. on Vehicular Technology*, vol. 36, no. 2, pp. 55 – 62, May 1987.

[49] M. L. Moher and J. H. Lodge, "TCMP - a modulation and coding strategy for Rician fading channel," *IEEE J. on Select Areas in Communications*, vol. 7, pp. 1347 – 1355, Dec. 1989.

[50] H. W.-H. Li and J. K. Cavers, "An adaptive filtering technique for pilot-aided transmission systems," *IEEE Trans. on Vehicular Technology*, vol. 40, pp. 532 – 545, Aug. 1991.

[51] J. K. Cavers, "An analysis of pilot symbol assisted modulation for Rayleigh fading channels," *IEEE Trans. on Vehicular Technology*, vol. 40, pp. 686 – 693, Nov. 1991.

[52] S. Sampei and T. Sunaga, "Rayleigh fading compensation for QAM in land mobile radio communicaitons," *IEEE Trans. on Vehicular Technology*, vol. 42, pp. 137 – 147, May 1993.

[53] P. Hoeher, S. Kaiser, and P. Robertson, "Two-dimensional pilot-symbol-aided channel estimation by Wiener filtering," *Proc. 1997 IEEE Int. Conf. Acoustics, Speech, and Signal Processing*, pp. 1845 – 1848, Apr. 1997.

[54] V. Mignone and A. Morello, "CD3-OFDM: a novel demodulation scheme for fixed and mobile receivers," *IEEE Trans. Commun.*, vol. 44, pp. 1144 – 1151, Sep. 1996.

[55] Y. G. Li and N. R. Sollenberger, "Adaptive antenna arrays for OFDM systems with co-channel interference," *IEEE Trans. Commun.*, vol. 47, pp. 217 – 229, Feb. 1999.

[56] Y. G. Li, "Pilot-symbol-aided channel estimation for OFDM in wireless systems," *IEEE Trans. on Vehicular Technology*, vol. 49, pp. 1207 – 1215, Jul. 2000.

[57] Y. G. Li, N. Seshadri, and S. Ariyavisitakul, "Channel estimation for OFDM systems with transmitter diversity in mobile wireless channels," *IEEE Trans. on J. Select. Areas Commun.*, vol. 17, pp. 461 – 471, Mar. 1999.

[58] R. Negi and J. Cioffi, "Pilot tone selection for channel estimation in a mobile OFDM system," *IEEE Trans. on Consumer Electronics*, vol. 44, no. 3, pp. 1122 – 1128, Aug. 1998.

[59] C. W. Therrien, *Discrete Random Signal and Statistical Signal Processing*. Prentice Hall NJ, 1992.

[60] "Channel models for fixed wireless applications," *IEEE 802.163c.01/29r4*, Jun. 2001.

[61] Y. G. Li and L. J. Cimini, "Bounds on the interchannel interference of OFDM in time-varying inpairments," *IEEE Trans. Commun.*, vol. 49, no. 3, pp. 401 – 404, Mar. 2001.

[62] I. Barhumi and M. Moonen, "Optimal training design for MIMO OFDM systems in mobile wireless channels," *IEEE Trans. on Signal Processing*, vol. 51, no. 6, pp. 1615 – 1624, Jun. 2003.

[63] S. Haykin, *Adaptive Filter Theory 4th Edition*. Prentice-Hall, New Jersey, 2001.

[64] A. Albert, *Regression and the Moore-Penrose Pseudoinverse*. Academic Press, New York, 1972.